DEPARTMENT OF MECHANICAL ENGINEERING

MASTER THESIS

Full analysis of suspension geometry and chassis performance of Formula Student racing car

AUTHOR:
Miłosz Kowalik

SUPERVISION:
Fernando Jose Ferreira

PORTO 2014

TABLE OF CONTENT

TABLE OF FIGURES

1. INTRODUCTION

1.1 BACKGROUND

Formula Student events gather engineering students, who compete, designing, building and racing single-seater cars. The team of ISEP is working on its first car that soon will take part in this competition. This work aims to analyze the current design's chassis, focusing on suspension geometry and frame's performance. After analyzing results of the tests planned suggestions, that can be taken into consideration during design process of next cars will be presented. As the car has not been tested yet this work can also be helpful to explain its performance on the track later.

Fig. 1.1 presents the car's state in the beginning of June 2014 and the model that was delivered for virtual tests in February the same year. The car was later undergoing adjustments even on the last days before the practical experiments. All the changes were taken into consideration and the results presented refer to the state of the car actual for the day of the papers presentation.

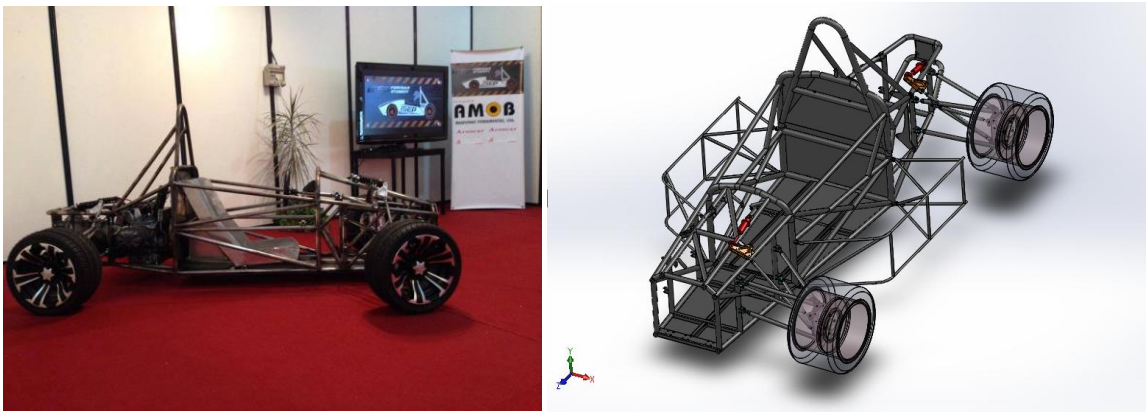

Fig. 1.1 The car in June 2014 and the virtual model actual in February 2014.

Correct geometry of suspension is necessary to provide good handling of a car. The requirement for correct behavior of suspension however is also a well designed frame. If it does not ensure enough rigidity and does not support suspension correctly, it disturbs its correct functioning. It is therefore important to make sure both these systems work properly.

This work will propose design goals that, if met, ensure good kinematic behavior of the suspension. Later virtual tests will be prepared and performed in order to compare their results with the goals set. To verify the results of chassis stiffness tests additional laboratory experiments will be run.

1.2 GOALS

The goals of this work therefore are set as follows:

- Set design targets for suspension geometry and frame
- Analyze suspension geometry of the car, using Lotus Suspension Analysis software
- Analyze frame behavior, using Finite Elements Method
- Verify virtual tests of frame by running laboratory experiments
- Compare the results with goals set and propose improvements

2. DOUBLE WISHBONE SUSPENSION (SLA)

The suspension used in analyzed vehicle can be classified as Short Long Arm suspension with push rod. This type of suspension is very commonly used because it allows to design-in demanded kinematic features, that are the topic of this paper, with less compromise in comparison with other types. The usage of push rod and placing shock absorbers onboard decreases unsprung mass.

The suspension system (Fig. 2.1) consists of two A-shaped control arms (upper 1 and lower 2) of different length in front view of the vehicle, which determine upright 3 path and position in suspension travel. Steering rod 4 is an element of steering system, which determines upright position with steering rack 5 travel. Push rod 6 is attached to upright and through rocker 7 transfers suspension movements on shock absorber 8 (spring and damper).

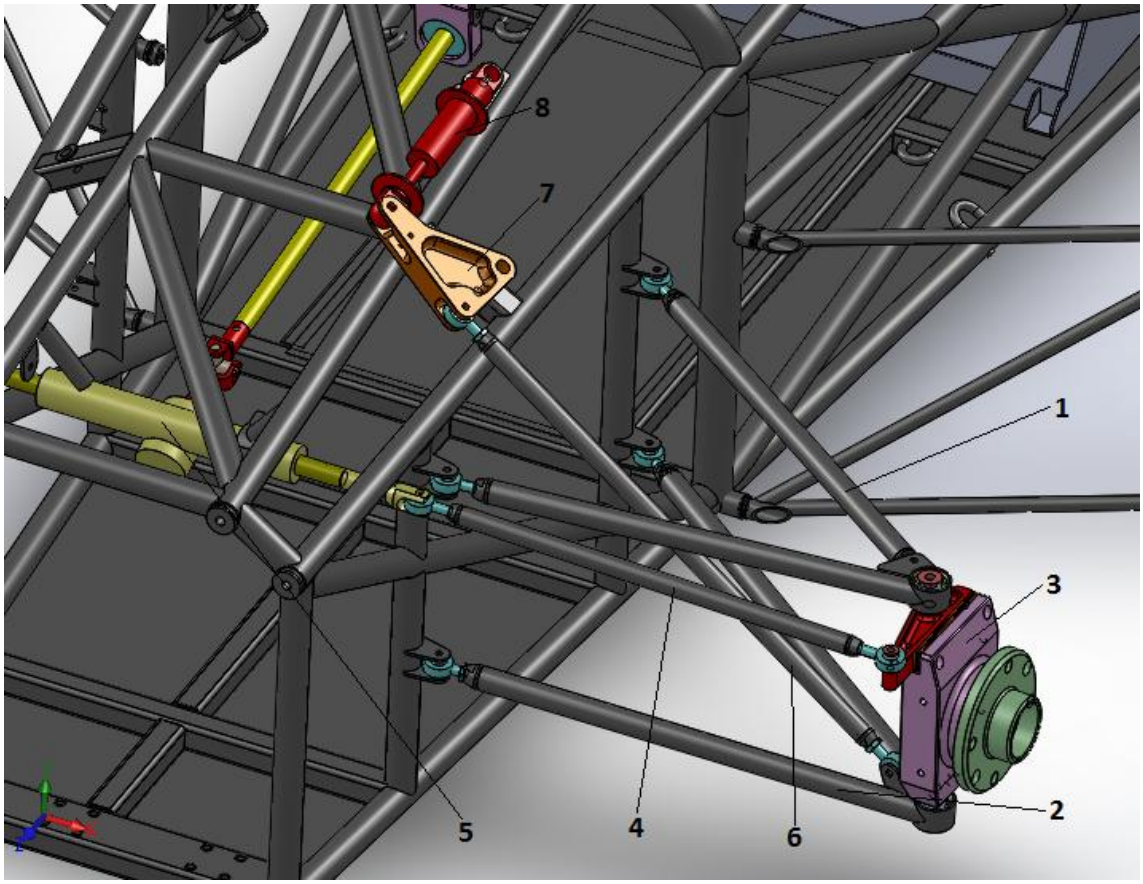

Fig. 2.1. Short Long Arm suspension with push rod of analyzed vehicle. Control arms: upper – 1, lower – 2, upright – 3, steering rod – 4, steering rack – 5, push rod – 6, rocker – 7, shock absorber – 8.

3. SUSPENSION GEOMETRY PARAMETERS

The following chapter defines and explains all the parameters, dimensions and features that are crucial for suspension system design and vehicle behavior, that the following part of this paper refers to. It aims mostly to get the reader acquainted with them, while considerations about specific values and their influence on sport vehicle are mostly presented with analysis of results of virtual test in other chapters. The exception here are only camber and roll centers, that required introducing to the reader additional, more complex questions related to tire behavior and load transfer.

This chapter can also be referred to as the theoretical basis, that justifies the conclusions and advices included in analysis of virtual tests' results.

3.1. WHEELBASE AND TRACK WIDTH

Wheelbase is defined as distance between centers of contact patches of front and rear axis tire in side view (Fig. 3.1). Long wheelbase decreases vehicle pitch (longitudinal inclination) while short ensures better maneuverability.

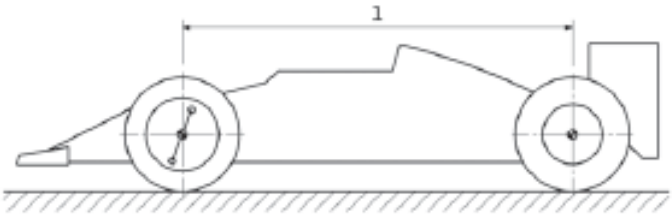

Fig. 3.1. Wheelbase [1]

Track width (Fig. 3.2) is the distance between centers of contact patches of left and right tire of the same axis in front view. Wider track width reduces body roll. Its value can be different for front and rear axis.

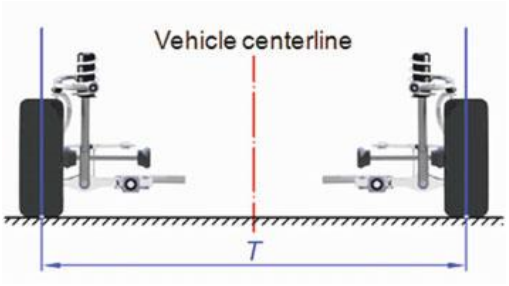

Fig. 3.2. Track width [2]

Both wheelbase and track width may change with wheel travel and suspension movements related to its elasticity (Fig. 3.3). As there were no reasons found for wheelbase changes being included in design goals of a sport vehicle, it is not analyzed in following part of this paper.

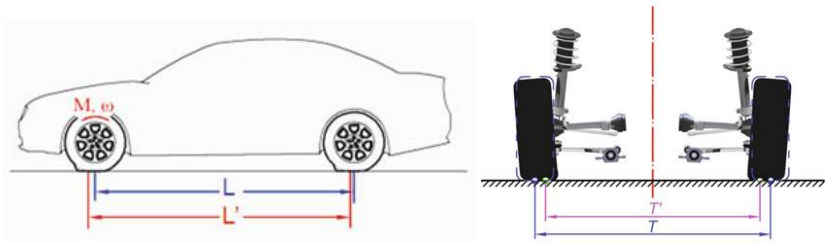

Fig. 3.3. Wheelbase and track width changes with wheel travel.[2]

The changes of track width depend on the location of instant center of rotation of suspension in front view (Fig. 3.4; explanations about instant center in chapter about camber). The closer to ground it is located, the smaller these changes will be.

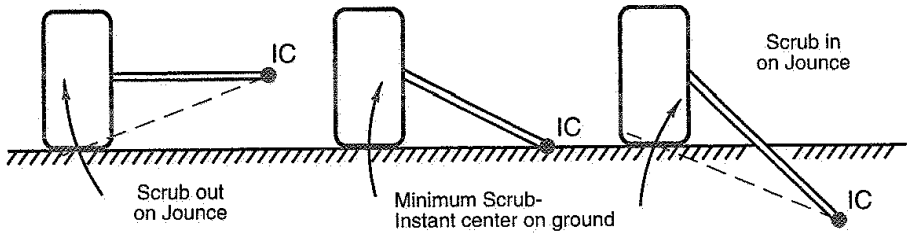

Fig. 3.4. Relation between track width changes (scrub changes) and IC location [[3]

3.2. KINGPIN INCLINATION ANGLE AND OFFSET

Kingpin inclination is an angle between steering axis and line normal to the road surface in front view of the car (Fig. 3.5). The distance between points where those two lines intersect ground surface is called scrub radius or kingpin offset.

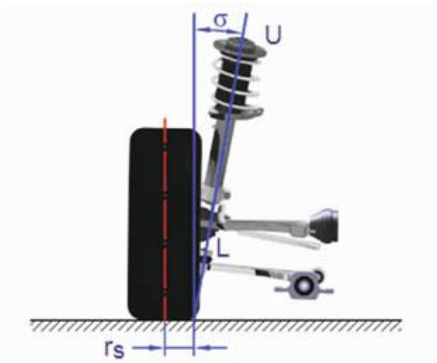

Fig. 3.5. Kingpin inclination and scrub radius (both are positive in this example) [2]

Kingpin inclination is positive when the top of steering axis is closer to the centerline of the vehicle and scrub radius is positive if the steering axis intersects the ground more inboard than the wheel's central plane.

Kingpin inclination causes both wheels to drop relatively to body when steering, which lifts the front of the car, generating force, that sets the wheels back to straight forward position. Kingpin inclination also causes the wheels to change camber while steering – outer wheel towards positive values (loose camber) and inner towards negative values.

Scrub radius is a lever which produces steering torque related to longitudinal forces from road on tire.

The values of kingpin inclination and scrub radius are correlated in such way, that decreasing one increases the other. In order to avoid this kind of compromise changes in packaging of brakes and upright or a selection of rim with different wheel offset are required.

3.3. CASTER AND CASTER TRAIL

Caster is an angle that steering axis creates with line perpendicular to ground in the side view of a car (Fig. 3.6). The distance between the point where steering axis intersects the ground and projection of wheel's axis on the ground is referred to as caster trail or caster offset.

Although caster angle and offset are related to each other it is possible to obtain any combination of these values by offsetting wheel axis from steering axis (in side view) in upright design. The distance between wheel axis and steering axis along ground level is called spindle offset.

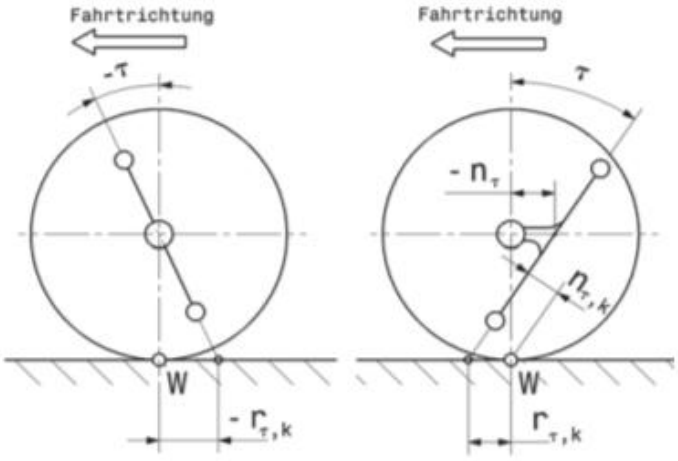

Fig. 3.6. Negative caster angle and caster offset with 0 spindle offset (left) and positive camber angle and offset with negative spindle offset. [1]

Caster angle is positive when the top of steering axis is leaned backwards (towards rear of the car). With zero spindle offset it generates positive caster trail (steering axis intersects ground in front of wheel's axis projection on the ground). The spindle offset is considered positive if the steering axis crosses the wheel axis' level in front of the wheel's axis.

While steering positive caster angle causes the inner wheel to drop and outer wheel to raise relatively to body. That is a reason for car's front's roll that generates forces setting wheels back in straight forward position, contributing to kingpin inclination's similar effect. When it comes to camber changes though positive caster causes both wheels to lean in the turn (camber values change towards negative values).

When the wheels are steered, caster trail generates steering torque, caused by lateral forces acting on the tires' contact patch, that sets the wheels back to straight forward position.

3.4. ROLL CENTERS AND ROLL AXIS

Roll center is a point in a front view of a car which the body rolls around. The line connecting front and rear axis' roll centers is the roll axis (Fig. 3.7).

In order to draw roll center of an axis lines connecting center of tire contact patch and IC of an upright have to be drawn for both – left and right – wheels. The point where these lines intersect is the roll center (Fig. 3.8). If the suspension is symmetric and no roll is present the roll center is located on the centerline of the car.

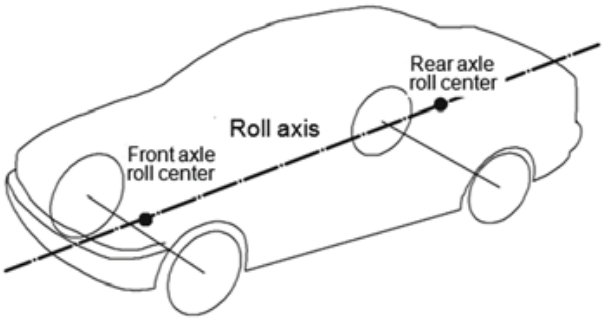

Fig. 3.7. Roll center and roll axis [2]

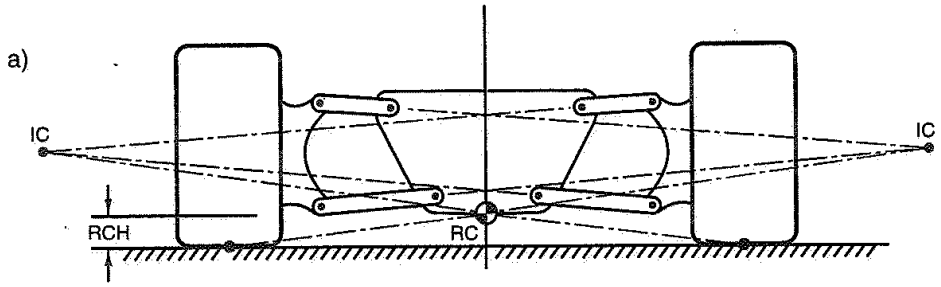

Fig. 3.8. Determining roll center (RCH – roll center height) [3]

As roll center is an instant center of rotation, its location changes with roll and suspension travel.

If the CG of the vehicle is subjected to any side forces (ex. centrifugal force while cornering) a torque around roll axis is generated. This torque's value depends on the force and the distance between CG and the roll axis.

Roll center is also related to horizontal-vertical coupling effect of lateral forces acting on tires. This is often called "jacking effect" and the forces causing it – "jacking forces". Fig. 3.9 explains how lateral forces generate torque around suspensions' front view instant center (whose location is correlated with roll center's location Fig. 3.8). A lateral force on a tire's contact patch with a ground has to act on a line connecting the patch's center with the IC. It has to have the vertical force component then and, in case of roll center located above ground, push the wheel down, under the body and lift the sprung mass.

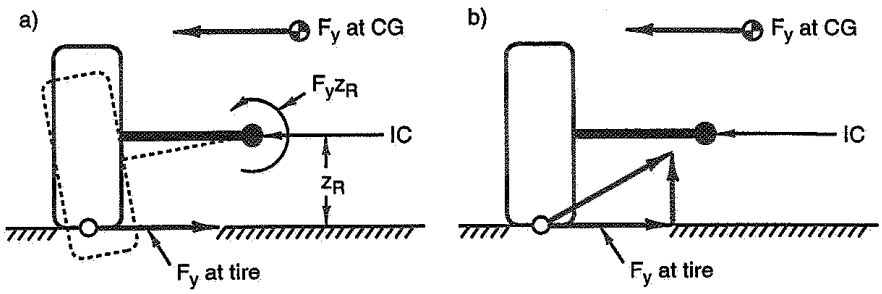

Fig. 3.9. Jacking effect [3]

3.5. TIRES SIDE FORCES DISTRIBUTION

In order to present the influence that the roll centers' location has on handling of the vehicle it is necessary to discuss more profoundly tires' and suspension's behavior in cornering, explaining phenomena of slip angle and lateral load transfer.

3.5.1. Slip angle

Slip angle is defined as the angle between tire's direction of heading (or in practice wheel center plane) and its actual direction of travel (Fig. 3.10). The reason for discrepancy of these two directions is the fact that any side force generated by the tire, that is needed to keep the car in turn, requires it to deform elastically at the contact patch with ground, causing the change of travel direction.

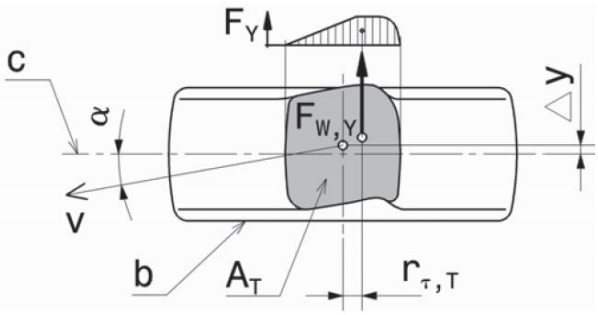

Fig. 3.10. Slip angle and tire's deformation at contact patch with road. [1]

That means that for each tire with certain inflation pressure and vertical load a curve of relation between side force generated and slip angle can be plotted (Fig. 3.11). For changing vertical load however the side force generated at the same slip angle will be changing too as it is presented on Fig. 3.12.

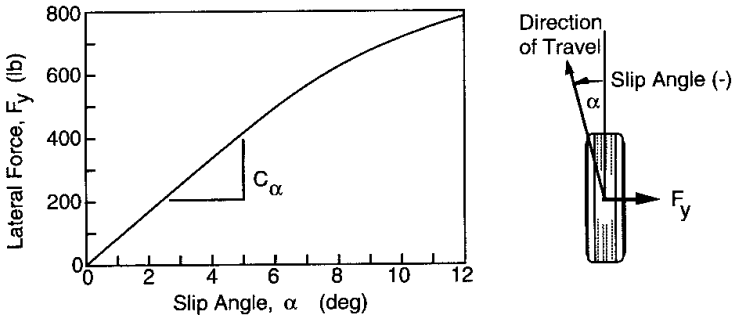

Fig. 3.11. Example relation between lateral force and slip angle [4]

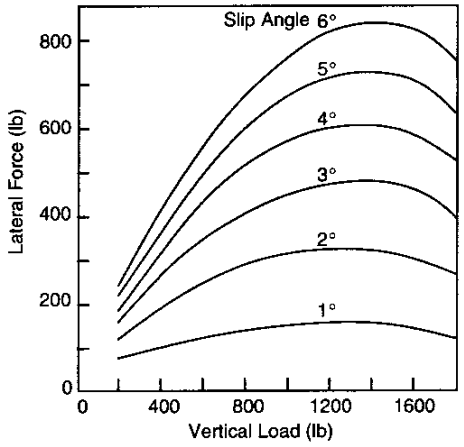

Fig. 3.12. Lateral force and vertical load relation for different slip angles [4]

From an example relation between vertical load on tires and the lateral force they generate with constant slip angle (Fig. 3.13) a conclusion can be drawn, that if the vertical load is distributed equally between tires they generate more lateral force (760lb each in example) than when a difference between inner and outer tire occurs (680lb per tire on average). In other words more slip angle is required to generate the same amount of lateral force.

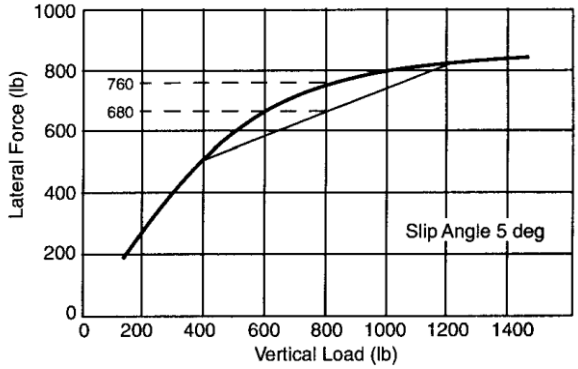

Fig. 3.13. Example relation between vertical load on tire and lateral force generated with 5° slip angle. Two tires with distribution of loads 400lb on one and 1200lb on the other generate on average 680lb lateral force while tire loaded with 800lb generates 760lb. [4]

3.5.2. Lateral load transfer

Whenever a car is cornering a centrifugal force directed to the center of the cornering curve must appear. Being attached to the center of gravity, it causes a moment around roll axis and makes the car body roll around it. Analysis of this situation is presented in Fig. 3.14. Assuming small values of ϕ and ε (cos ϕ = cos ε = 1 and sin ϕ = ϕ) the roll angle may be calculated as [4]:

$$\phi = \frac{W h_1 V^2}{(K_{\phi f} + K_{\phi r} - W h_1) R g} \qquad \text{(Eq. 3.1)}$$

where K_ϕ is roll stiffness of an axis, defined as amount of counteracting moment generated by an axis with 1rad of body roll.

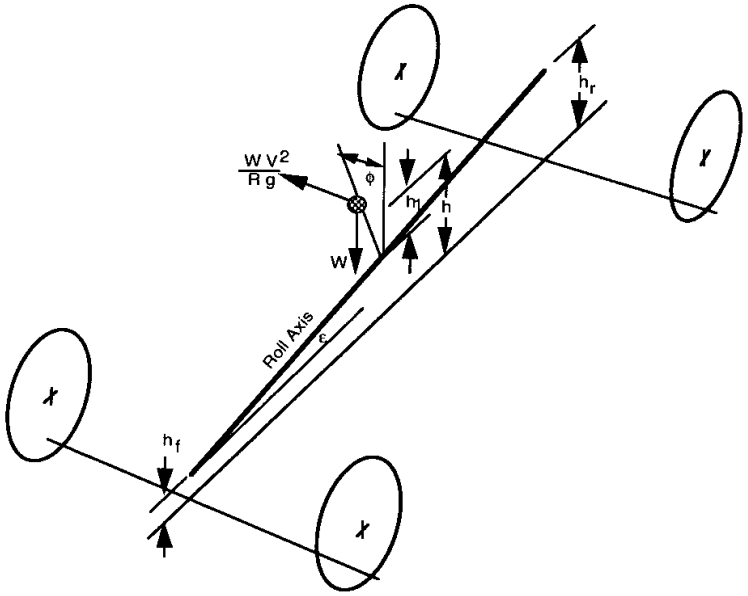

Fig. 3.14.Roll of a car in cornering. Force analysis. [4]

Except for determining car body roll it is important to analyze force diagram on front and rear axis separately, as it significantly influences lateral load distribution between tires. As any kind of suspension can be presented as set of two springs, simple diagram of rigid axis suspension from Fig. 3.15 can be applied in this case for calculations of independent suspension too (as long as roll stiffness is already given and does not have to be calculated with respect to the diagram). An equation for equilibrium of moments around roll center can be solved for the difference between vertical forces on outside and inside tire:

$$F_{zo} - F_{zi} = \frac{2F_y h_r}{t} + \frac{2K_\phi \phi}{t} \qquad \text{(Eq. 3.2)}$$

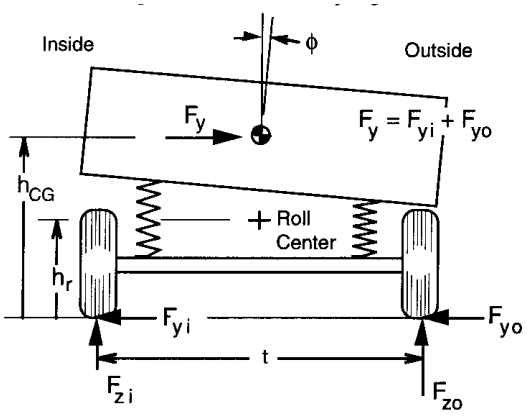

Fig. 3.15. Single axis force analysis.[4]

It can be noticed that there are two mechanisms that are responsible for load transfer while cornering. First is related to side forces generating moment around roll center and therefore its influence on increase of load being transferred grows with roll center height. The other one, caused by centrifugal force, depends on axis roll stiffness and roll angle, or in other words on summary roll stiffness of both axis, as it determines roll angle, and its distribution between front and rear.

3.6. CAMBER

Camber is defined as the angle between wheel's center plane and a plane perpendicular to the ground (Fig. 3.16). It is considered positive when the top of the wheel is leaned outboard and negative, when it is leaned inboard.

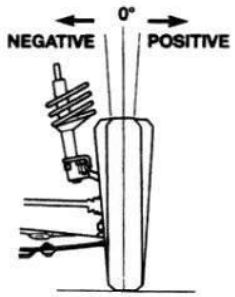

Fig. 3.16. Positive and negative camber.

Camber changes with body roll, suspension travel and steer travel. These changes have to be taken into consideration during design of suspension system, so that camber has demanded values within all range of vehicle behavior.

The general approach to design of camber changes is that gains related to suspension and steer travel should compensates for loss related to body roll.

Camber gain rate with suspension travel depends on control arms configuration in front view. At any given moment the upright rotates around instantaneous center IC, located where elongations of arms intersect (Fig. 3.17). The position of IC however constantly changes when arms change their position.

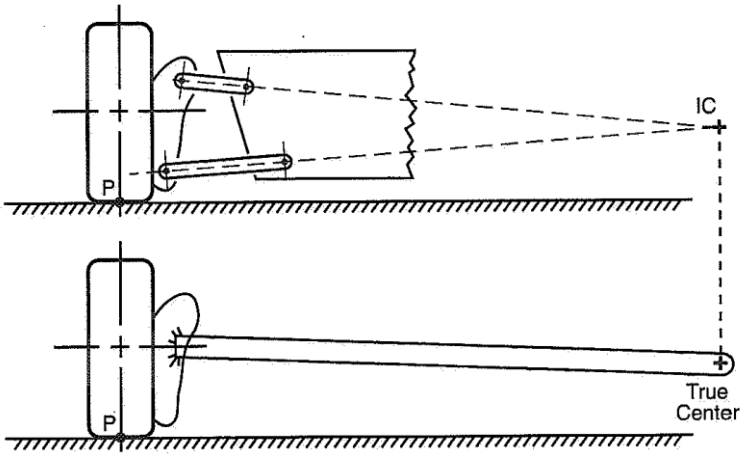

Fig. 3.17. Concept of instant center.[3]

The camber change rate depends on the distance between IC and center of the wheel in front view (fvsa length – front view swing arm length) according to the following equation [3]:

$$camber\ change\ rate\ = \arctan\left(\frac{1}{fvsa\ length}\right) \qquad \text{(Eq. 3.3)}$$

It can be concluded that suspensions with front view IC located close to wheels have higher camber gain rates (Fig. 3.18).

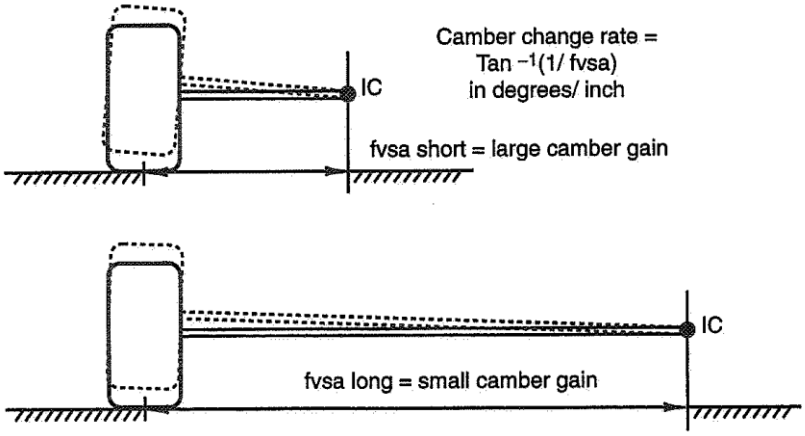

Fig. 3.18. Relation between camber change rate and fvsa length. [3]

As IC travels with changing position of control arms, camber change rate values also vary with wheel travel. This fact can be used to design demanded shape of camber gain curve. Shortening upper arm in relation to lower arm causes camber to grow faster in jounce of suspension and slower in rebound.

Camber changes related to steer travel depend on kingpin positioning and for this reason are mentioned in following chapters.

3.7. CAMBER THRUST

Camber contributes to lateral tire forces due to mechanism presented on Fig. 3.19. Inclined wheel behaves like a part of a cone rolling on the ground and tends to generate force directed to the peak of the cone (positive camber outboard and negative camber inboard force). The side force generated by camber is called camber thrust.

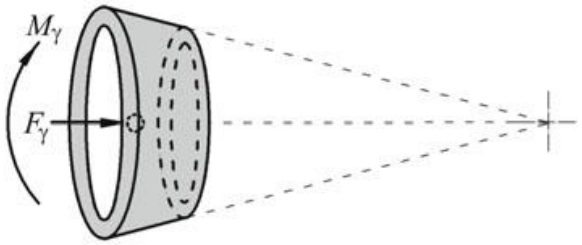

Fig. 3.19. Mechanism of camber generating lateral force [2].

Although mechanism of camber thrust for radial tires (or wide bias-ply tires) is not well understood it is probably caused by distortions in tire's tread pattern and side walls and can be compared to mechanism observed in narrower bias-ply tires (Fig. 3.20). Center line of a contact patch of a static, cambered tire is curved. When it rolls, however the path of a point entering the contact patch goes straight along the direction of motion. The sum of the forces from road causing this kind of tire deformation result in camber thrust.

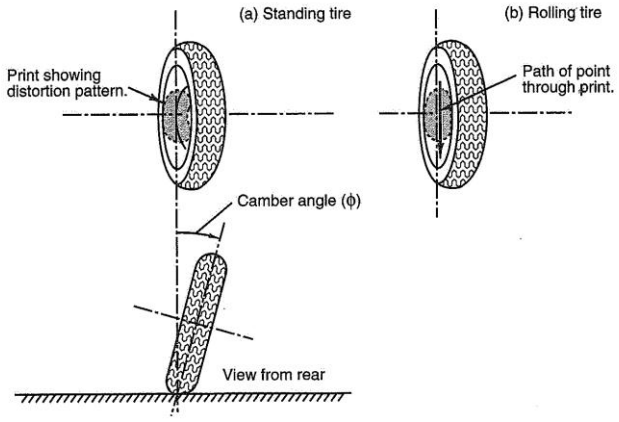

Fig. 3.20. Cambered bias-ply tire contact patch distortion. [3]

Camber thrust can be generally treated as a separate mechanism, additive with slip angle generating side force (Fig. 3.21). For higher values of slip angle however the camber thrust "rolls-off", which means its additive effect decreases. Nevertheless it causes the maximum side force generated by tire to grow.

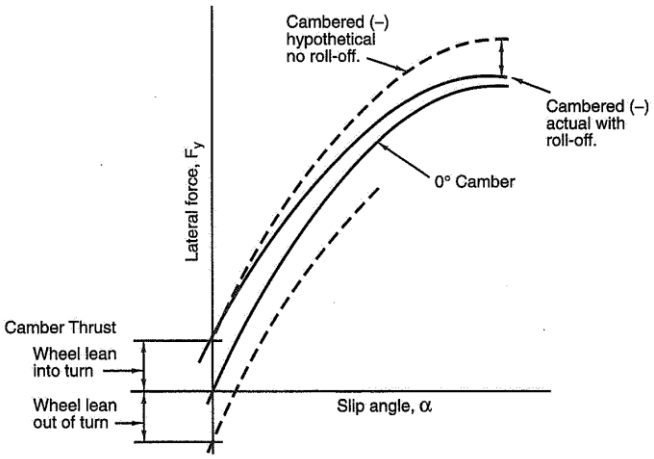

Fig. 3.21. Effect of camber on lateral force – slip angle relation. [3]

Tests of tires can indicate the optimum camber value, for which a specific tire model reaches the best maximum side force. For racing tires it is usually less than 5°. The tests proved also, that the optimum camber value grows with tire's vertical load (Fig. 3.22). This relation is untrue only for lower load values, which the results are probably less reliable for.

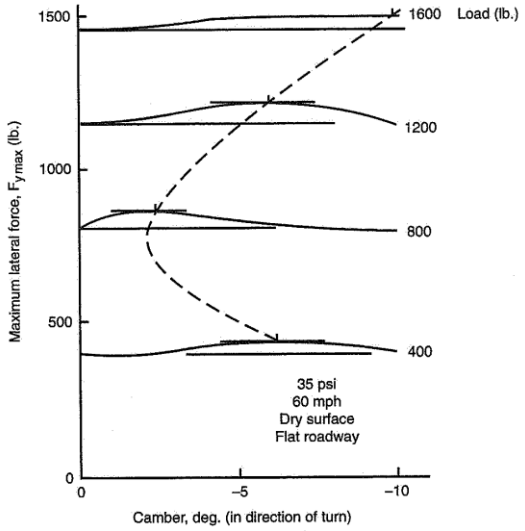

Fig. 3.22. Peak lateral force vs. camber, P225/70R15 tire. [3]

3.8. TOE ANGLE

Toe angle is an angle between wheel's central plane and centerline of the vehicle in top view (Fig. 3.23). It is called toe-in when the forward distance between wheels is smaller than the aft distance. In the opposite situation it is called toe-out.

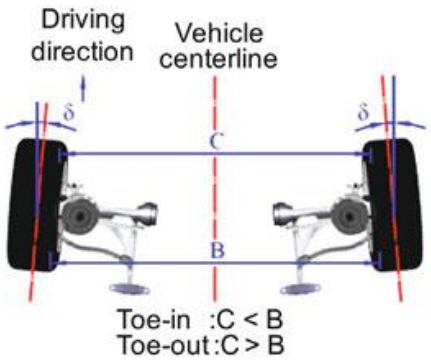

Fig. 3.23. Toe-in and toe-out [2]

Some toe angle is introduced in neutral position in order to compensate for steering system elasticity effects and keep the wheels in straight forward position, reducing rolling resistance. Toe angle changes with bump travel, depending on steering rod location.

3.9. ANTI-DIVE AND ANTI-SQUAT

Control arms configuration in side view can provide that some portion of force counteracting weight transfer during accelerating and braking is provided by suspension linkage and not by springs. That results in less deflection and elongation of springs and reduction of pitch. These features are called anti-squat (for acceleration) and anti-dive (for braking). Their values are expressed as percentage that the force delivered by linkage constitutes in whole force counteracting weight transfer.

Anti features depend on IC of control arms position in side view and therefore their demanded values have to be considered when this IC is located. Solving free body diagram from Fig. 3.24 the following equations [3] relating IC position ($tan\phi_F = \frac{svsa\ height}{svsa\ length}$, where svsa is side view swing arm; l – distance between center of tire patch and CG along horizontal axis; h – CG's height above ground) and anti-dive can be obtained:

$$\%\ anti-dive\ front = (\%\ front\ braking)(tan\phi_F)\frac{l}{h} \qquad \text{(Eq. 3.4)}$$

And analogically for rear:

$$\%\ anti-dive\ rear = (\%\ rear\ braking)(tan\phi_R)\frac{l}{h} \qquad \text{(Eq. 3.5)}$$

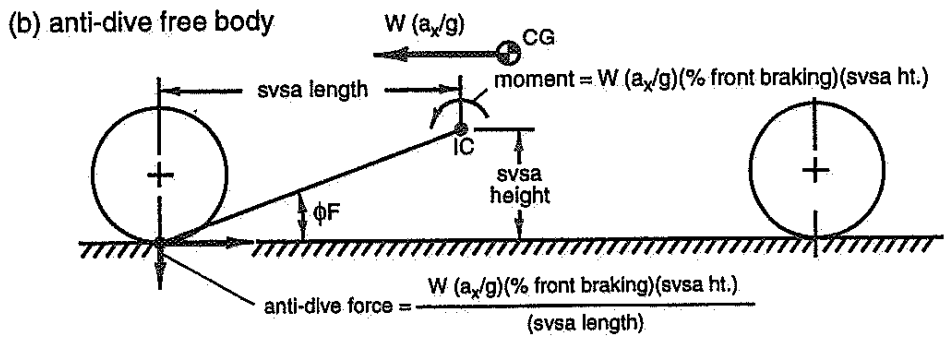

Fig. 3.24. Free body diagram for calculation of anti-dive [3]

In case of anti-squat however two facts have to be paid attention to. First of all anti-squat can only be considered for driven axis, in this case rear, as while accelerating the front axis does not generate any horizontal force that could counteract weight transfer. Second of all for independent suspension torque reaction is not transferred through suspension linkage and a different free body diagram (Fig. 3.25) should be considered. The resulting equation [3] is as follows:

$$\%\, anti - squat = 100\%\, (tan\theta_R)\, \frac{l}{h} \qquad \text{(Eq. 3.6)}$$

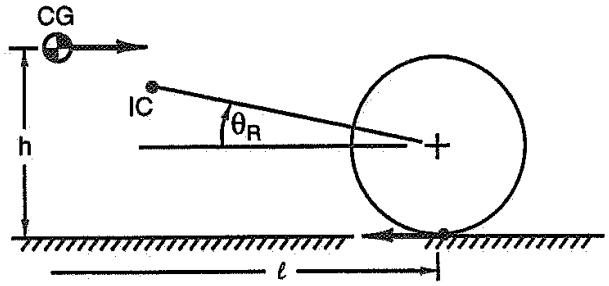

Fig. 3.25. Free body diagram for calculating anti-squat of independent rear suspension [3]

4. SUSPENSION GEOMETRY DESIGN PROCESS

The following chapter presents the process of suspension geometry design presented in [3]. It focuses mostly on the order of the decisions about dimensions that have to be defined, while considerations about their specific values and way to calculate or draw them are included in other parts of that paper.

First general packaging parameters (related to car body size), wheelbase and track width should be determined. Later on a designer is allowed to proceed with wheel packaging. This should start with choosing tire size and rim diameter. As the next step a brake caliper should be located in such way, that enough clearance is maintained between inner surface of the rim. That automatically determines position of brake rotor. At this point a lower ball joint should be placed. In order to obtain desired (low) values of kingpin inclination and scrub radius in following step this joint should be placed possibly outboard. It is generally also advised because of structural reasons to place it possibly low with, of course, maintaining minimum clearance with ground and rim.

At that moment values of kingpin inclination and scrub radius are determined (Fig. 4.1). For rear-wheel-drive cars, as those values are correlated, a low kingpin inclination is set and the resulting scrub radius has to accepted.

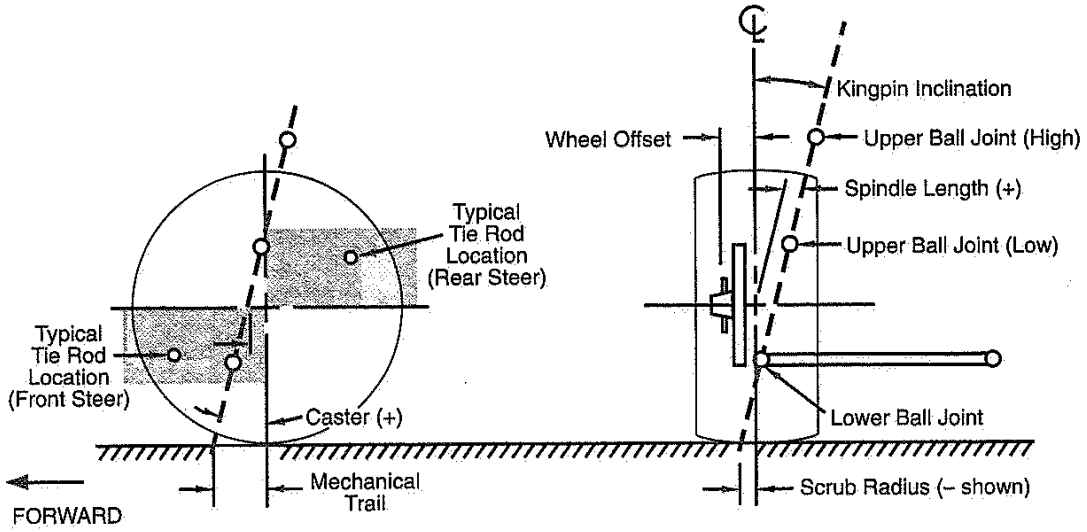

Fig. 4.1. Wheel packaging [3]

A steering rack can be located then. Packaging constraints should be considered and design of steering system geometry too. Due to compliance effects while cornering it is required to place the steering rack in front of wheel axis if it is low-mounted and behind it if it is high-mounted. If so the elasticity related steer angle will cause understeer rather than dangerous oversteer.

Next step is defining control arms configurations, starting with determining roll center height and then camber ratio and calculating front view swing arm length as it is described in previous chapters. This values together with outer ball joints location determine lines on which control arms are located (Fig. 4.2).

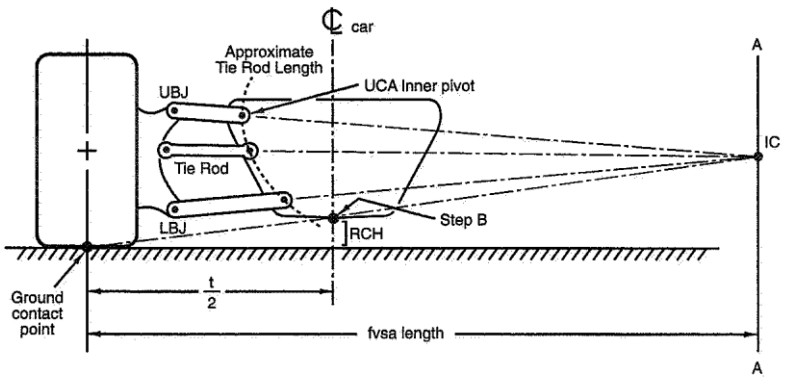

Step A—Establish front view swing arm length (line A-A)
Step B—Establish roll center location and project from ground contact point through RC to line A-A, establishing IC
Step C—Project lines from outer ball joints to IC
Step D—Choose control arm lengths to get inner pivot locations
Step E—Connect tie rod outer pivot to IC
Step F—Establish tie rod length.

Fig. 4.2. Front view control arms configuration design process [3]

Later usually the lower control arm is designed as long as packaging constraints let and the upper one's length is shortened until the demanded camber curve is obtained (compare with chapter 3.6). Designing push rod and rocker should result with spring ratio close to 1:1, which ensures good stiffness with low weight of design.

The following task is designing side view geometry. Instant centers should be established first. They should result from decision about demanded anti features, which according to Eq. 3.4, Eq. 3.5 and Eq. 3.6 determine ϕ, and decision about the shortest acceptable svsa length (Fig. 4.3). As for rear axis it may be impossible to obtain demanded anti-squat, anti-dive and svsa length some kind of compromise may be required.

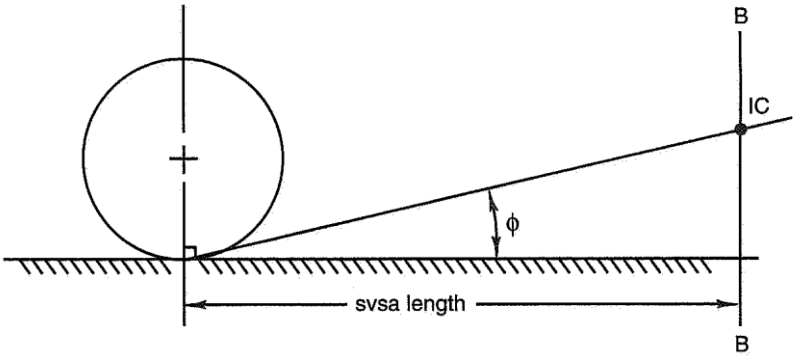

Step A—Angle ϕ establishes anti-dive
Step B—svsa length gives line B-B
Side view IC is the intersection of steps A and B.

Fig. 4.3. Process of side view IC location [3]

Position of ball joints of upright in side view should be determined too, establishing demanded caster angle and caster trail.

When both front and side view geometries are ready, what still has to be done is determining positions of inner ball joints of control arms, as at that moment control arms are only

presented as single lines. That requires applying descriptive geometry to combine front and side view, ensuring that all the features designed-in until this point will be maintained in final drawing too.

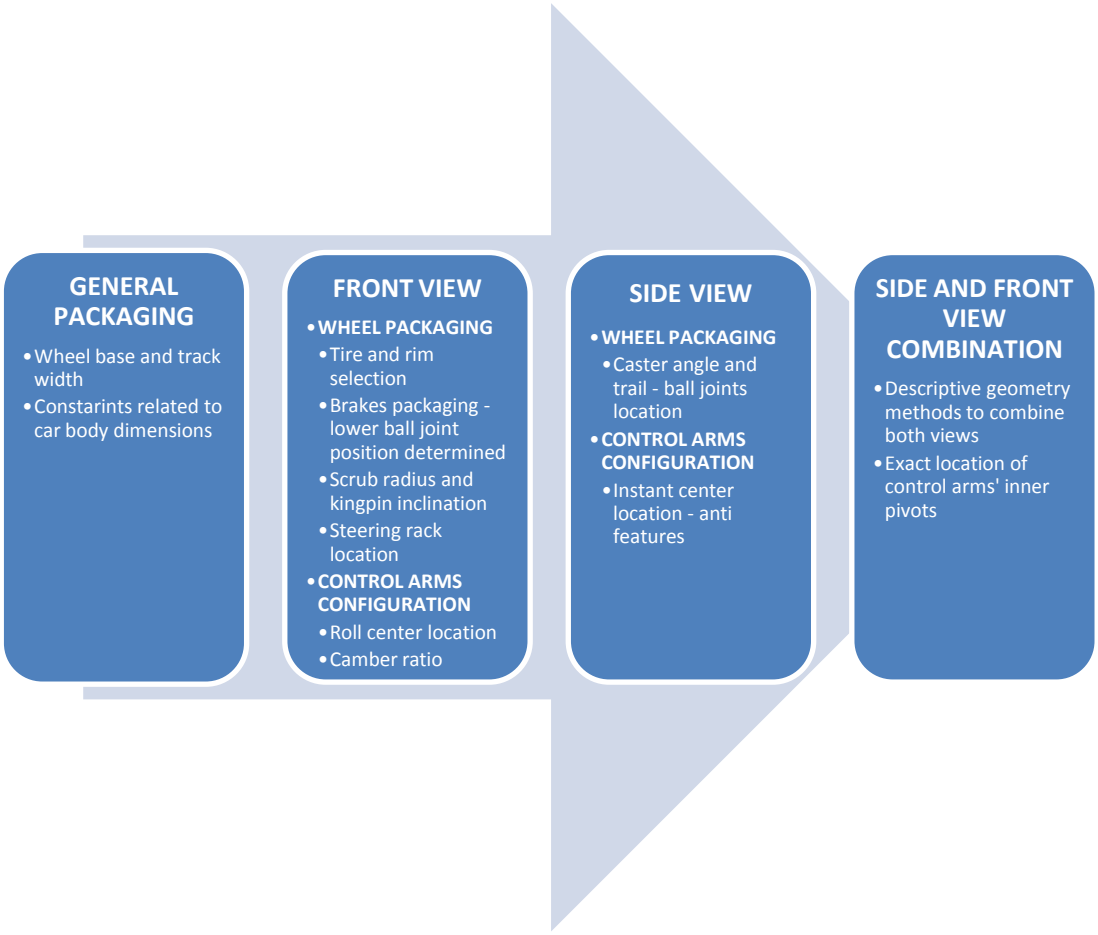

Fig. 4.4. Suspension geometry design process.

5. VIRTUAL MODEL FOR SUSPENSION ANALYSIS

Lotus Suspension Analysis (LSA) is a software that allows users to easily design three dimensional models of vehicle suspensions by introducing coordinates of points, that define its geometry and perform virtual tests, which include among others kinematic tests for: bump travel, steer travel and body roll. Output data demanded in that analysis is comprised of:

- Bump travel
  - Roll centers height change relatively to ground
  - Camber gain
  - Half track change (track width change)
  - Toe angle change (bump steering)
  - Ant-dive and anti-squat values change
- Body roll
  - Roll centers migration in YZ plane
  - Camber change
- Steering rack travel
  - Camber change

After selecting correct suspension type (Double wishbone with push rod) all the points required to define suspension's geometry (listed in Table 5.1 and Table 5.2 and presented on Fig. 5.6 and Fig. 5.7) that had been collected from SolidWorks 3D model were introduced. Fig. 5.1 – Fig. 5.5 compare models in LSA and SolidWorks.

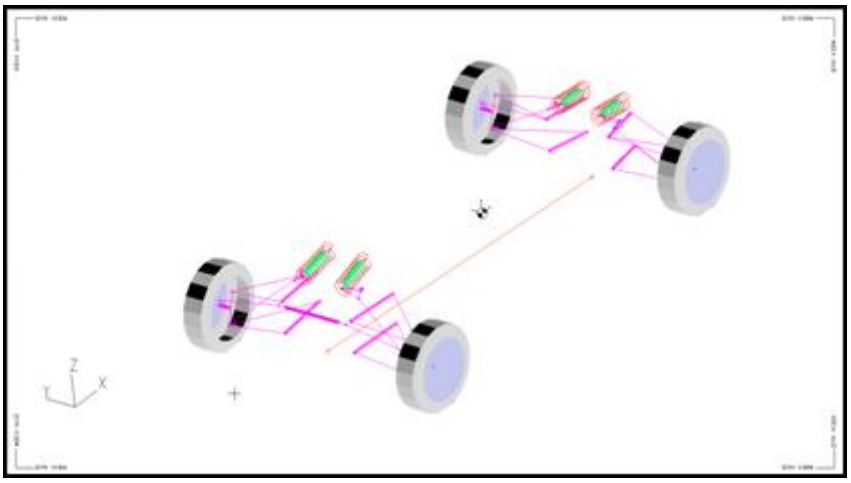

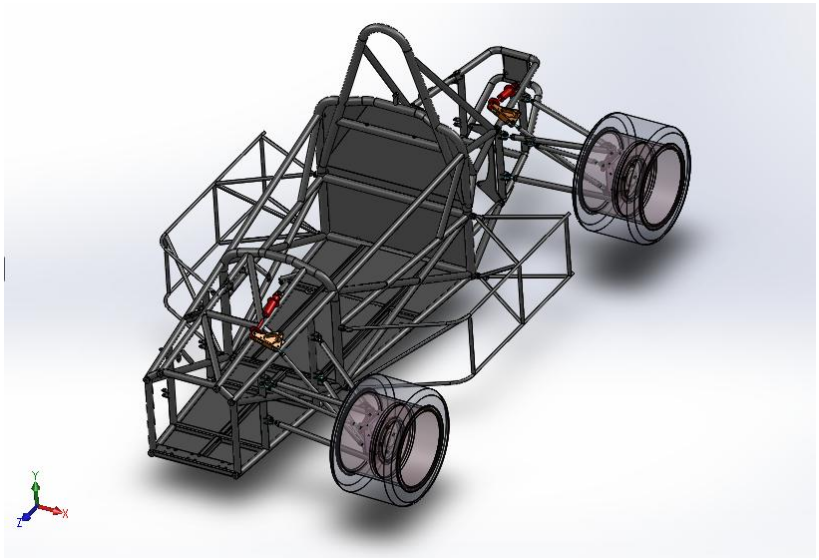

Fig. 5.1. Full suspension model in LSA and SolidWorks. Components other than those of frame and suspension subsystems were hidden in SolidWorks assembly.

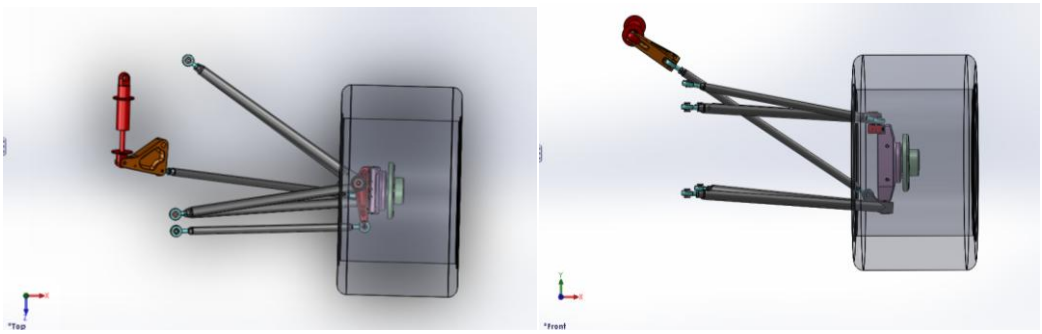

Fig. 5.2. Top and front view of front suspension. SolidWorks model.

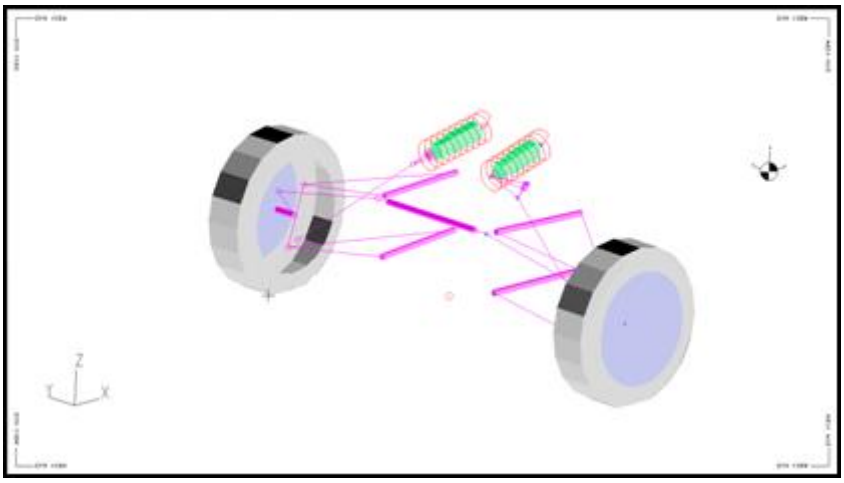

Fig. 5.3. Front suspension model in LSA.

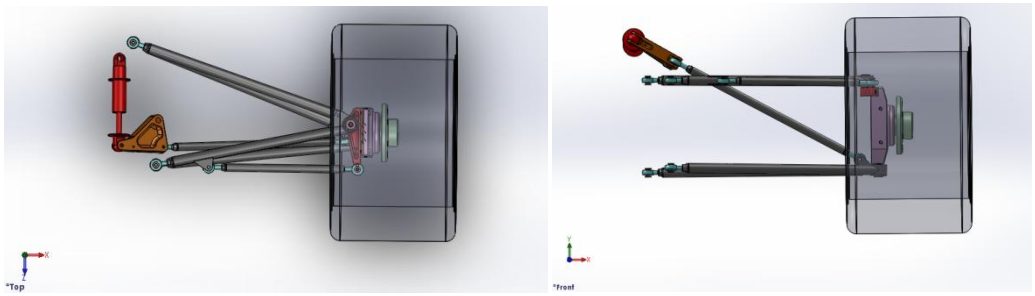

Fig. 5.4. Top and front view of rear suspension. SolidWorks model.

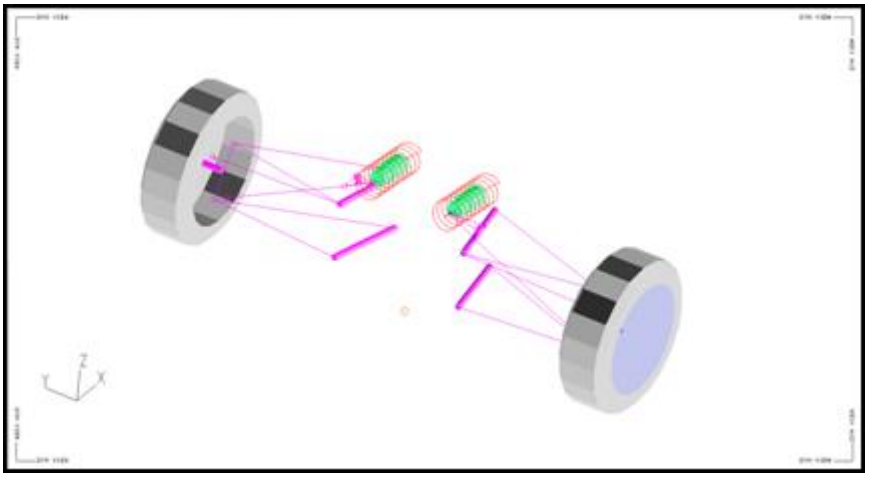

Fig. 5.5. Rear suspension model in LSA.

The coordinate system in SolidWorks model however was not compatibile with the one used in LSA. Those two systems can be compared in Fig. 5.1. In order to transform coordinates collected from SolidWorks model following operations were performed:

- LSA X values = negative SolidWorks Z values (+ 3000mm in order to obtain positive values for both axis, which does not influence results)
- LSA Y values = SolidWorks X values
- LSA Z values = SolidWorks Y values

Moreover coordinate system center in SolidWorks was not placed in vehicle's central plane, so it was crucial to calculate points' positions in relation to another point, that met this requirement. A point placed in the middle of one of frame's pipes (-341,46; -459,14; -965,65 in SolidWorks coordinate system) was chosen.

As the model from SoildWorks was not set in the vehicle's ride height it was necessary to define it according to designers' preference after introducing point coordinates in LSA.

Table 5.1. Coordinates of points defining front suspension geometry in SolidWorks and LSA.

FRONT SUSPENSION

	SolidWorks*			LSA - introduced			LSA - adjusted ride height		
	X	Y	Z	X	Y	Z	X	Y	Z
1. Lower wishbone - front pivot	226,54	-75,00	2279,51	720,49	226,54	-75,00	720,49	226,54	-75,00
2. Lower wishbone - rear pivot	254,23	-65,00	1949,50	1050,50	254,23	-65,00	1050,50	254,23	-65,00
3. Lower wishbone - outer ball joint	641,69	-152,59	2241,37	758,63	641,69	-152,59	758,63	641,69	-152,59
4. Upper wishbone - front pivot	226,54	105,00	2279,51	720,49	226,54	105,00	720,49	226,54	105,00
5. Upper wishbone - rear pivot	254,23	105,00	1949,50	1050,50	254,23	105,00	1050,50	254,23	105,00
6. Upper wishbone - outer ball joint	616,49	33,83	2212,26	787,74	616,49	33,83	787,74	616,49	33,83
7. Push rod - wishbone end	608,00	-123,02	2237,12	762,88	608,00	-123,02	762,88	608,00	-123,02
8. Push rod - rocker end	212,22	183,44	2178,34	821,66	212,22	183,44	821,66	212,22	183,44
9. Steering rod - outer ball joint	628,67	28,01	2305,59	694,41	628,67	28,01	694,41	628,67	28,01
10. Steering rod - inner ball joint	222,00	104,99	2315,00	685,00	222,00	104,99	685,00	222,00	104,99
11. Damper - body point	116,16	280,99	1986,84	1013,17	116,16	280,99	1013,17	116,16	280,99
12. Damper - rocker point	129,29	232,88	2204,40	795,61	129,29	232,88	795,61	129,29	232,88
13. Wheel - spindle point	636,55	-59,38	2226,50	773,50	636,55	-59,38	773,50	636,55	-59,38
14. Wheel - center point	705,03	-59,41	2228,22	771,78	705,03	-59,41	771,78	705,03	-59,41
15. Rocker axis - first point	187,99	194,04	2127,20	872,80	187,99	194,04	872,80	187,99	194,04
16. Rocker axis - second point	200,97	213,90	2130,82	869,18	200,97	213,90	869,18	200,97	213,90

*in relation to point (-341,46; -459,14; -965,65)

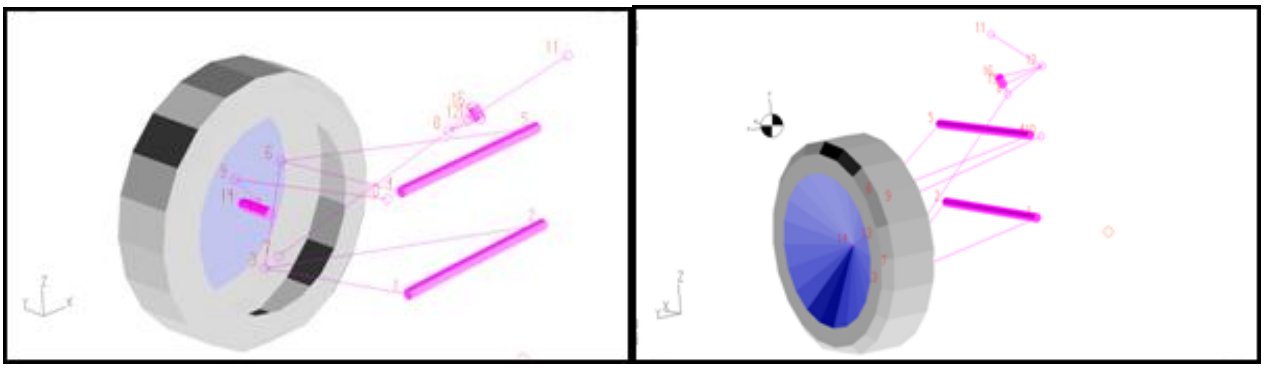

Fig. 5.6. Front suspension model in LSA with points numbered in accordance with Table 5.1

Table 5.2. Coordinates of points defining rear suspension geometry in SolidWorks and LSA

REAR SUSPENSION

	SolidWorks*			LSA - introduced			LSA - adjusted ride height		
	X	Y	Z	X	Y	Z	X	Y	Z
1. Lower wishbone - front pivot	206,76	-93,40	454,13	2545,87	206,76	-93,40	2547,33	206,76	-92,82
2. Lower wishbone - rear pivot	159,42	-103,40	200,01	2799,99	159,42	-103,40	2801,45	159,42	-102,82
3. Lower wishbone - outer ball joint	638,95	-98,36	404,49	2595,51	638,95	-98,36	2593,94	634,79	-155,26
4. Upper wishbone - front pivot	206,18	88,60	454,24	2545,76	206,18	88,60	2547,22	206,18	89,18
5. Upper wishbone - rear pivot	158,80	88,60	200,12	2799,88	158,80	88,60	2801,34	158,80	89,18
6. Upper wishbone - outer ball joint	611,65	86,90	370,35	2629,65	611,65	86,90	2630,32	607,41	29,56
7. Push rod - wishbone end	600,18	-75,52	406,05	2593,95	600,18	-75,52	2593,18	599,32	-127,54
8. Push rod - rocker end	216,46	126,91	417,77	2582,23	216,46	126,91	2595,90	238,60	113,77
9. Steering rod - outer ball joint	625,90	83,98	463,53	2536,47	625,90	83,98	2537,07	621,38	27,74
10. Steering rod - inner ball joint	315,96	88,16	458,90	2541,10	315,96	88,16	2547,22	206,18	89,18
11. Damper - body point	130,45	156,68	233,86	2766,14	130,45	156,68	2767,60	130,45	157,26
12. Damper - rocker point	129,27	175,77	414,47	2585,53	129,27	175,77	2549,59	163,51	160,86
13. Wheel - spindle point	632,75	-5,68	386,98	2613,02	632,75	-5,68	2612,55	628,55	-62,80
14. Wheel - center point	701,25	-5,10	387,55	2612,45	701,25	-5,10	2611,78	697,05	-62,14
15. Rocker axis - first point	211,08	138,08	361,56	2638,44	211,08	138,08	2639,90	211,08	138,66
16. Rocker axis - second point	199,34	117,25	363,68	2636,32	199,34	117,25	2637,78	199,34	117,83

*in relation to point (-341,46; -459,14; -965,65)

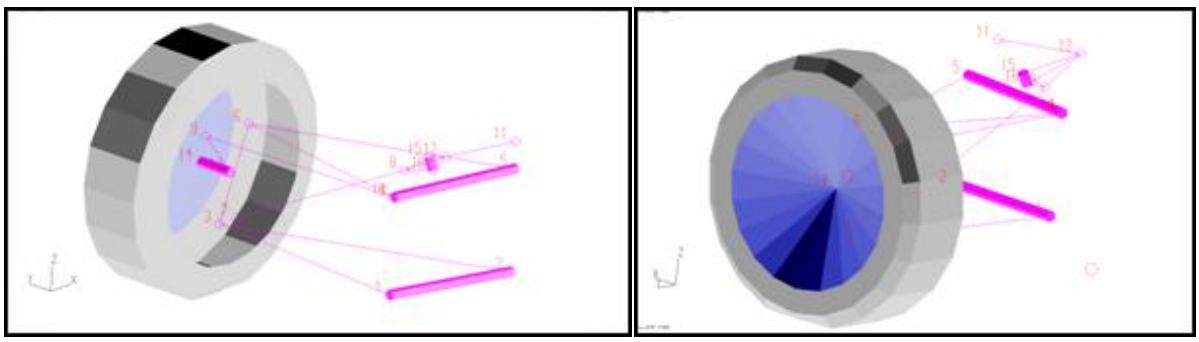

Fig. 5.7. Rear suspension model in LSA with points numbered in accordance with Table 5.2

6. SUSPENSION GEOMETRY GOALS CONSIDERATIONS AND RESULTS ANALYSIS

The following chapters present considerations about what are the demanded values, dimensions and features related to the analyzed vehicle's suspension geometry. They are based on included in literature conclusions about their influence on vehicle behavior, normally accepted limits and example values. Where it was especially needed due to lack of precise information in literature and the fact that preferred values may be different for Formula Student vehicle and for other types of race cars, benchmarking based on online research for other Formula Student designs was carried out. It is important to underline that only those parameters, that have significant influence on race car performance and can be set as design goals were taken into consideration. Others were not mentioned.

These considerations are then followed by analysis of results obtained with LSA, conclusions resulting from comparison of these two and suggestions of what changes could be introduced in the car in following seasons. Please note that at the moment of writing this paper the vehicle was not tested yet and no feedback from track was delivered.

6.1. KINGPIN POSITIONING ANALYSIS

6.1.1. Caster and kingpin inclination

Caster ensures directional stability of the vehicle but increases the steering torque reaction too due to related to it caster offset (trail).

Positive caster causes also increase of camber towards negative values on the outer wheel while cornering. This is primarily advantageous phenomenon, but can lead to nonlinear understeering. Thus a balance between caster and roll related changes of camber should be found. Caster values are between 2° and 6° usually [1].

Caster angle changes with bump travel do not influence vehicle behavior in any important way and are only a result of side view geometry design. Growing caster on outside wheel however increases camber gains while cornering, but it also makes it more difficult to maintain toe angle changes with bump travel linear.

Example of acceptable caster changes in bump travel and camber changes with steering are presented in Fig. 6.1.

Kingpin inclination values lay normally between 0° and around 7° [1], but lower are preferred, as this angle increases disadvantageous changes of camber (in positive side for outer wheel) while steering. On the other hand for race cars a positive, but possibly low kingpin offset (scrub radius) is demanded in order to ensure correct feedback for the driver. Example for Formula Student designs value of scrub radius usually does not exceed 10mm [5[6]. Some positive kingpin inclination also helps to center the steered wheels in low speed of vehicle.

Summing up the goals for caster and kingpin inclination should be formed as follows:

- Caster between 2°-6°, with camber changes related to it balanced with camber gain in bump travel
- Caster trail ensuring directional stability, but not causing too strong reactions while steering
- Possibly low kingpin inclination between 0° and 7°
- Possibly low, positive kingpin offset, 0mm to 10mm

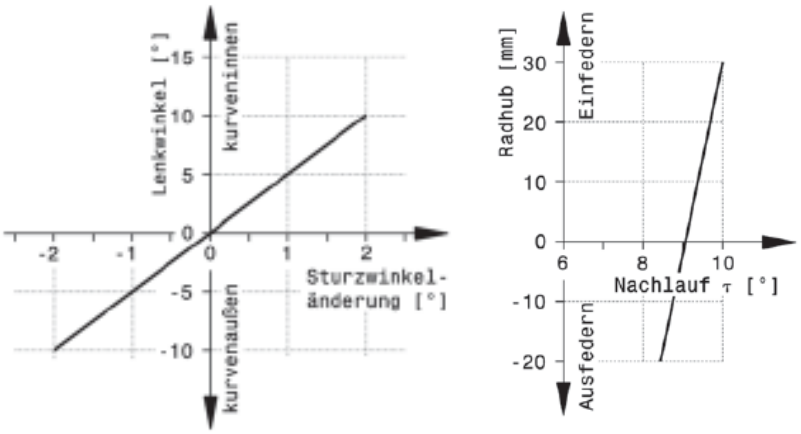

Fig. 6.1. Example of acceptable camber gains with steering (left) and caster gains with bump travel. [1]

6.1.2. Results analysis

The values of caster change from 8,6° to 9,2° with bump travel with 8,9° for ride height. Kingpin inclination grows from 7,6° to 7,8° and its value for ride height is 7,7°. These values appear to be a little higher than recommended ones and those applied in other designs mentioned in benchmarking. The values of castor offset (trail) – 33,31mm – is within acceptable limits while kingpin offset – 45,80mm - is high too. This might cause strong steering torque reactions.

Table 6.1. Castor angle/offset and kingpin angle/offset for ride height.

Castor angle	8,9°
Castor offset	33,31mm
Kingpin inclination	7,7°
Kingpin offset	45,80mm

Despite high value of caster, camber gain while turning – around 2° per 15° turning angle - is lower than suggested in literature - 2° per 10° turning angle (Fig. 6.2). The reason for that situation is high kingpin inclination, which causes exactly opposite changes in camber. As camber loss related to body roll (analyzed in following chapter) is very high it can be concluded that steering related gains will not be able to compensate for them.

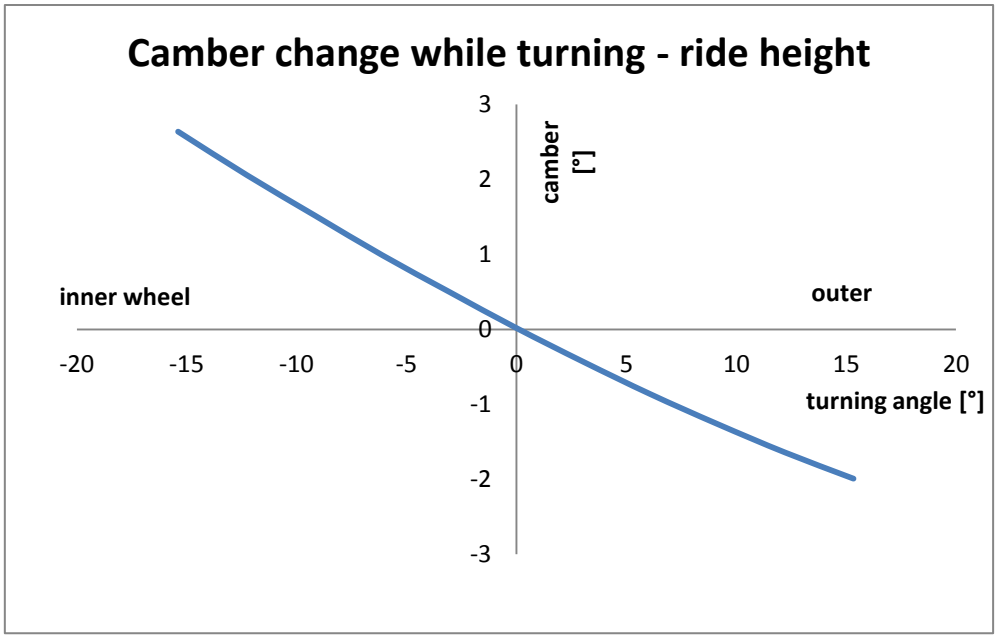

Fig. 6.2. Camber changes while turning for analyzed vehicle.

6.1.3. Conclusions

First of all it is recommended to decrease kingpin inclination and offset, values of which are too high in comparison with suggestions from literature and benchmarking. It should be also underlined that these geometrical parameters have mostly negative influence on vehicle performance.

As decreasing kingpin inclination increases kingpin offset the only solution for the problem being analyzed is different packaging of components localized inside the wheel and changes in upright design in order to move them closer to wheel's central plane (as far outboard as possible) or selection of a different wheel.

It was found out that in order to meet budget requirements the design team decided to purchase wheels and tires designated for quad instead of those normally used in Formula Student competitions. Later it turned out that the mounting holes of the rims do not match those on hub's disc and an additional adapter had to be applied, which resulted in extra millimeters of kingpin offset. It implies that changing selection of rims would make a significant and demanded difference.

Remembering that changes in kingpin inclination influence camber gain related to turning, which should be balanced with camber gain in bump (suggested to be changed in following part), the final decision about caster angle, that also takes part in camber control, can be made later (in side view design). It is however suggested to decrease its value below 7° as with changes that has just been mentioned it should still ensure enough camber gain. Adjusting caster offset during design is relatively easy as it can be done by offsetting wheel axis in upright (spindle offset), without influencing other parameters, as it is presented in chapter 3.3.

With some limitations these changes – caster angle and offset - can be also implemented without changing upright design, because current design includes three different positions of mounting lower control arm to upright (Fig. 6.3).

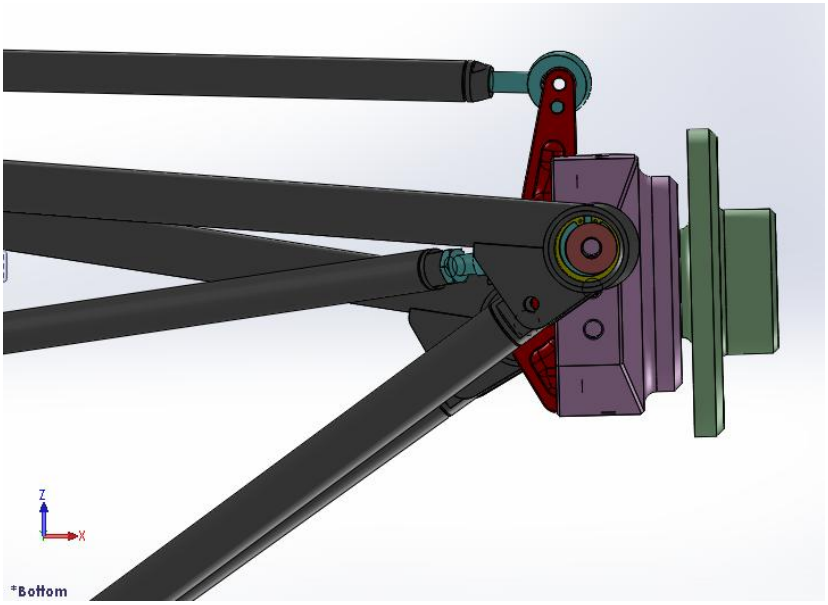

Fig. 6.3. Bottom view of lower control arm mounted to upright. Three different holes for this connection are available in the upright.

6.2.1. Roll centers

While cornering the car body pivots around roll axis, determined by front and rear roll centers. As it is preferred that the maximum roll is possibly low the distance between roll axis and vehicle's center of gravity should be small, so the rolling torque related to it is low too (Eq. 3.1). On the other hand that would require roll centers to be placed relatively high. According to Eq.3.2 both roll angle and roll center height influence growth of difference between vertical forces on inside and outside wheel in cornering and drop of side forces generated (chapter 3.5.1). High roll centers also increase jacking forces, causing the suspension to drop relatively to body (for roll centers above ground or raise for roll centers below the ground), what limits bump travel related camber compensation. Therefore keeping roll centers close to the ground is advised.

Table 6.2 present roll center heights for different types of vehicles. The roll center heights of analyzed vehicle can be also compared to those of other teams taking part in Formula Student competition. These roll center heights normally do not exceed 50mm [[5[6].

Table 6.2. Roll center heights for different kinds of vehicles (values for front axis in the line above and for rear below). Race cars (all other than Pkw – passenger car) have roll centers placed close to the ground – from -26mm (below ground level) to 40mm (above ground level).[1]

Fahrzeug	Pkw[1)]	Indy Car[2)]	IMSA GTS[2)]	Formel Ford[2)]	Sportprototyp
$h_{Ro,f}$ [mm]	30 bis 100	15	−2,5	−26	15
$h_{Ro,r}$ [mm]	60 bis 130	18	12,5	26,6	40

Important part of suspension geometry analysis is also roll centers migration. While rolling it is required that roll centers follow relatively linear path. If that requirement is not met unpredictable changes of jacking forces and overturning moment may occur, making handling more difficult. With bump travel roll centers' locations should not move significantly relatively to vehicle's body's center of gravity (Fig. 6.4) [1].

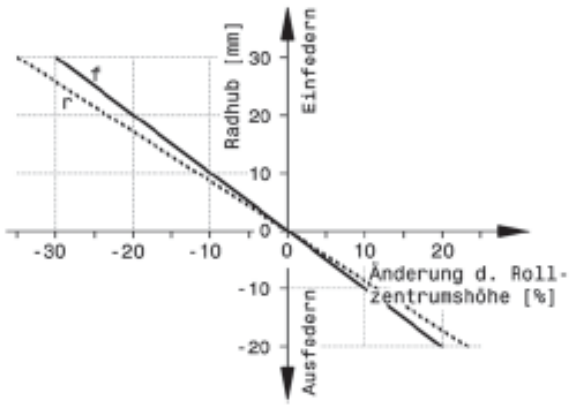

Fig. 6.4. Example of acceptable roll center heights changes relatively to ground with bump travel (f – front, r – rear axis).It can be concluded that roll centers heights do not change their position relatively to car body significantly.[1]

It is also preferred to design rear roll center a little higher than the front one. Typical values of roll axis inclination are between 0° and 6° [2].

6.2.2. Results analysis – roll centers

In the design of analyzed vehicle roll centers are placed high above the ground comparing to other vehicles mentioned before. 137,14mm for front axis and 93,08mm for rear. The roll axis is therefore inclined towards rear of the car (Fig. 6.5).

Roll centers migrating while car body rolls follow a path presented in Fig. 6.6, that should not cause any unexpected changes to jacking forces or overturning torque. From the Fig. 6.7 however it can be concluded that roll centers change location relatively to body's center of gravity, which implies that changes in overturning torque occur.

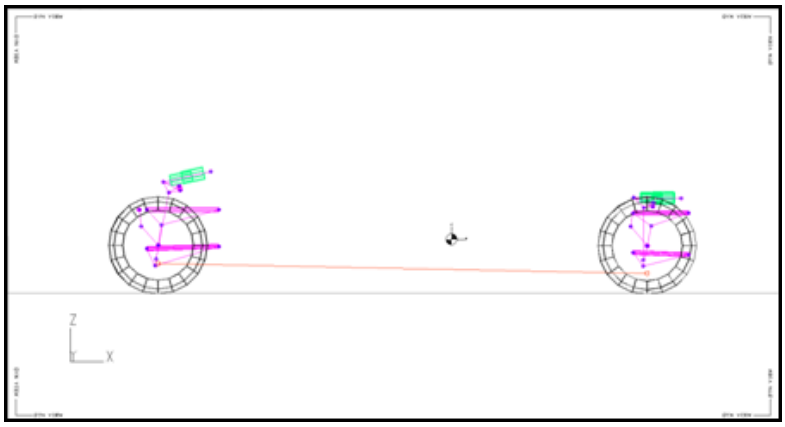

Fig. 6.5. Roll axis in side view. Front roll center (left) is placed higher above the ground than the rear.

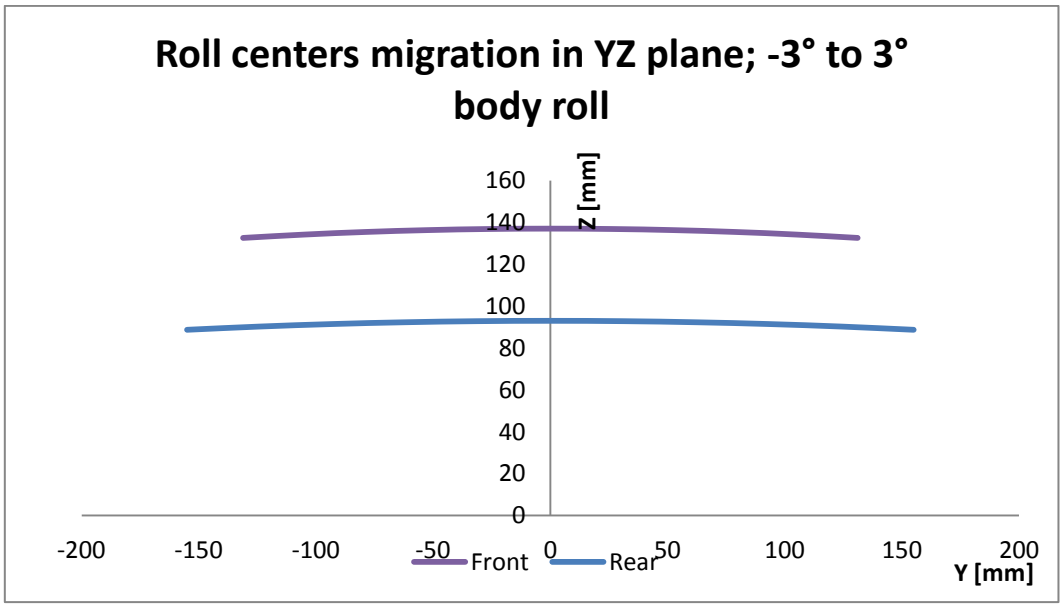

Fig. 6.6. Roll centers' migration with roll of the vehicle's body.

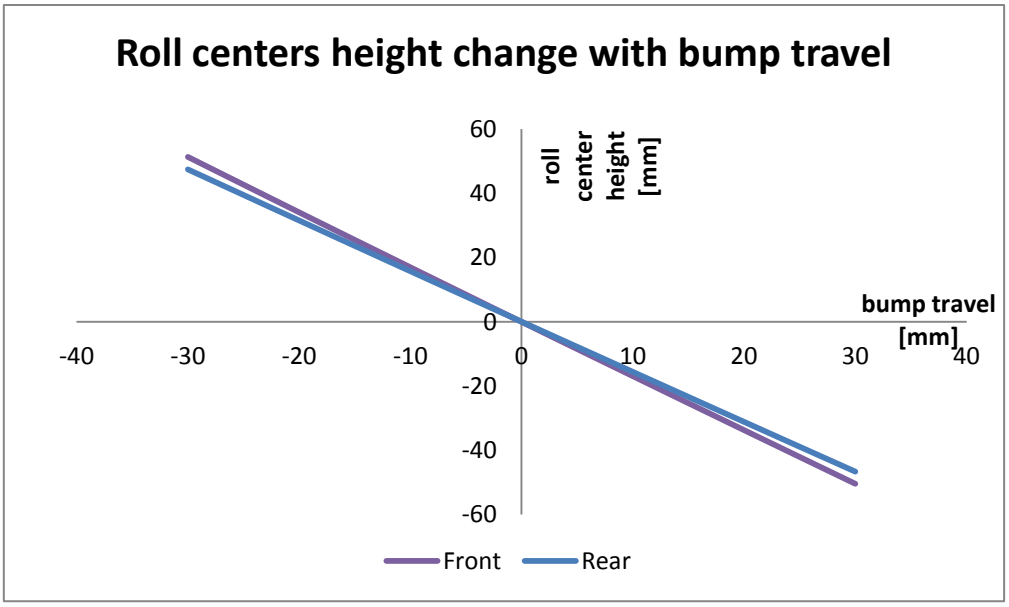

Fig. 6.7. Roll centers height change with bump travel. As roll centers' height changes faster than bump travel it can be concluded that their location changes relatively to body's center of gravity.

6.2.3. Camber gain

The allowable values of camber angle depend on the tire requirements, the power to weight ratio, usage on driven or non-driven axis and the aerodynamic properties. This however can be controlled by adjusting static camber.

The camber angle should be changing with bump travel, growing to the negative side. That tendency compensates for changes related to roll movements of the body. Moreover as the outer wheels while cornering carry more load and therefore their tires are submitted to significant side deformations, the increasing camber is supposed to compensate those deformations too, ensuring better contact conditions between the tire and road. Analyzing diagrams form Fig. 3.22 it can be concluded that adding negative camber to strongly loaded tire results in very beneficial grow of cornering force. If there is no exact data for the tires chosen available, it can be assumed that camber values below 5° are the optimum [3].

The inner wheel, being in rebound, should remain normal to the road (camber=0°) or gain low positive value. Higher values of camber, positive or negative, could cause side of the tire to be lifted, which would decrease side forces generated.

Example curve of camber changes in bump travel is presented in Fig. 6.8.

Taking into consideration advices from literature and benchmarking the following design goals for camber can be formulated:

- Camber change should remain less than 1° per 1° roll angle of the car body and about 25 mm wheel travel [1]. Can be 0,2°-0,3° per 1° roll for front axis and 0,5°-0,8° per 1° roll for rear axis, that is not affected by steer related camber gain [6].
- It is preferred for the wheel in rebound not to change camber and remain 0° or reach low positive values [1].

- Due to different conditions of particular competitions static camber has to be easily adjustable from 0° to 4°.

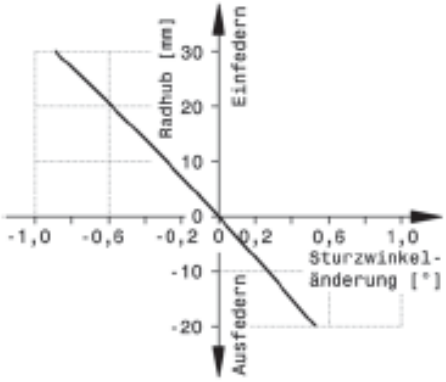

Fig. 6.8. Examples of acceptable relation between camber gain and bump travel

6.2.4. Results analysis – camber gain

The following diagrams (Fig. 6.9 - Fig. 6.11) present analyzed vehicle's suspension properties, that can be used to verify whether the design goals pointed in previous chapter are met: Camber gain with bump travel for front (Fig. 6.9) and rear axis (Fig. 6.10) and camber loss for body roll (Fig. 6.11).

It can be noticed, that the camber gain with bump travel for front axis is very low (0,06° per 30mm bump travel from ride height) while for the rear axis camber grows slightly to positive values (camber loss). As a result camber compensation related to bump travel practically cannot be observed in body roll. In Fig. 6.11, presenting camber changes with body roll the plotted lines stand for linear relation between camber values and angle of body roll with ~1° camber loss per 1° body roll. This situation is even more disadvantageous for rear axis, which does not have compensating camber changes related to steering analyzed in following chapter.

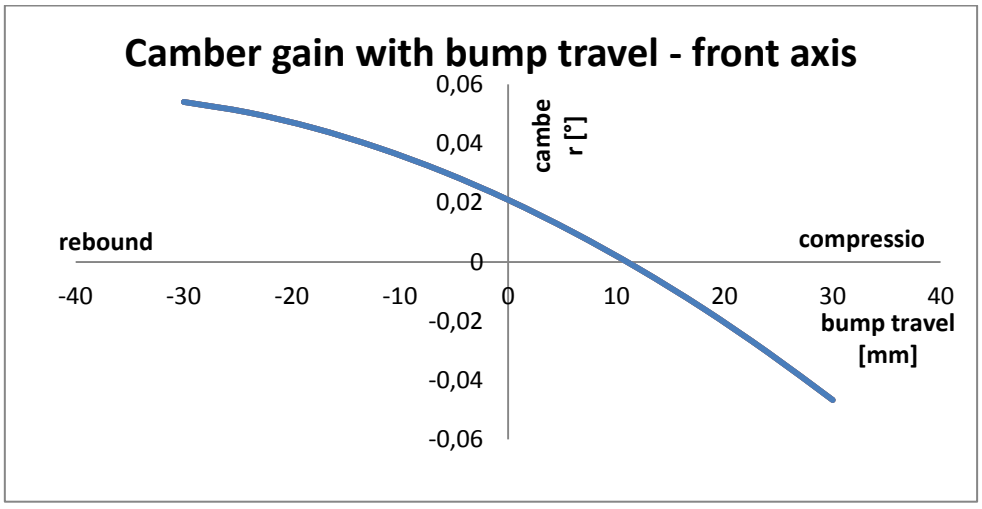

Fig. 6.9. Camber gain with bump travel for front axis. Camber values grow towards negative values with bump travel, gaining however only 0,06° per 30mm bump travel from ride height.

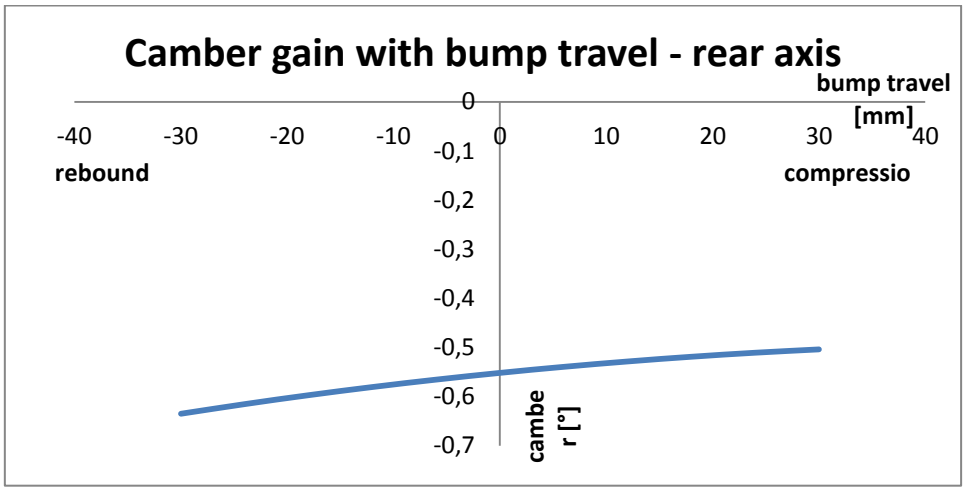

Fig. 6.10. Camber gain with bump travel for rear axis. Camber values slightly grow towards positive values –camber loss.

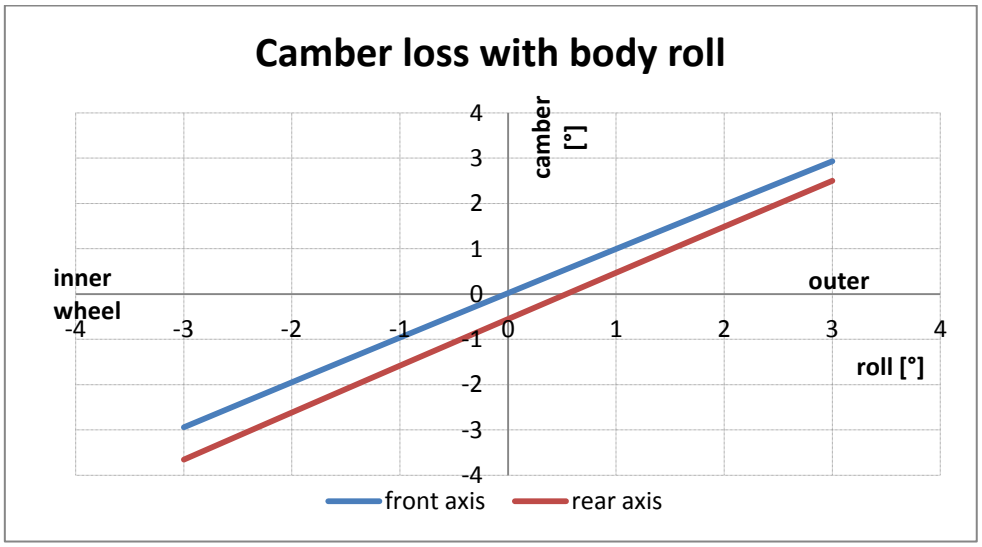

Fig. 6.11. Camber loss with body roll for front and rear axis. Camber changes are practically equal to angle of body roll - ~1° camber loss per 1° body roll.

6.2.5. Track width change and bump steering

Another characteristic related to front view geometry analysis that should be taken into consideration is track width change with bump travel. As it can laterally disturb the car and increase rolling resistance, these changes should be diminished. According to [2] track change should not be more than 20mm (for street cars).

Similar effects on the car can be also caused by toe angle changes related to bump travel and these should be as low as possible too. Despite being related rather to steering system geometry, this phenomenon is analyzed in this report for the reason of being easily analyzed with LSA and because of suspension travel being one of the causes of these changes.

Especially bad influence on the car behavior in the turn is the one of nonlinear toe angle (Fig. 6.14). Bump travel curve, while linear, directed to understeer (Fig. 6.13) in roll can be even favorable as they imply compensation to compliance effects in the steering system.

Examples of acceptable characteristics of track width and toe angle changes with bump travel are presented on Fig. 6.12 and Fig. 6.15 respectively.

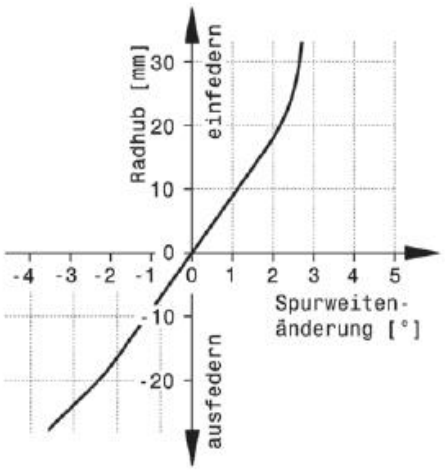

Fig. 6.12. Example of acceptable track width change with bump travel.[1]

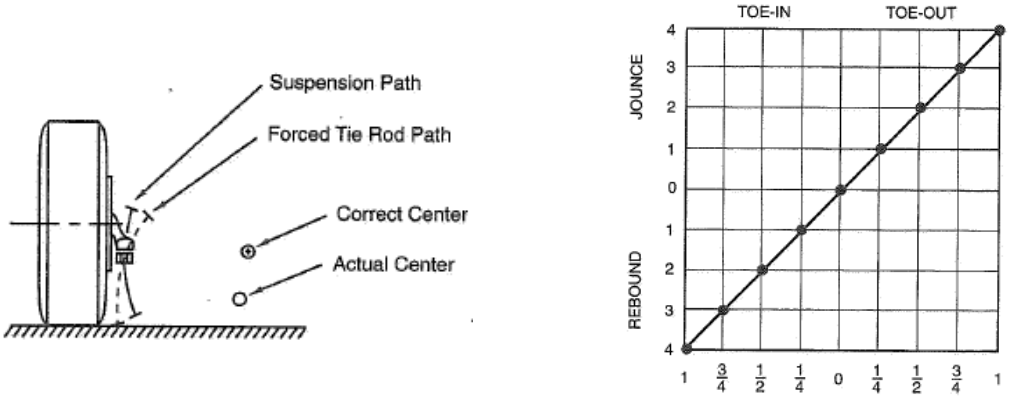

Fig. 6.13. Example of wheel that tends to toe-out with jounce and toe-in in rebound. The curve suggest correct length of the steering rod (linear relation), but incorrect position of ball joints – inner too low, or outer too high. [3]

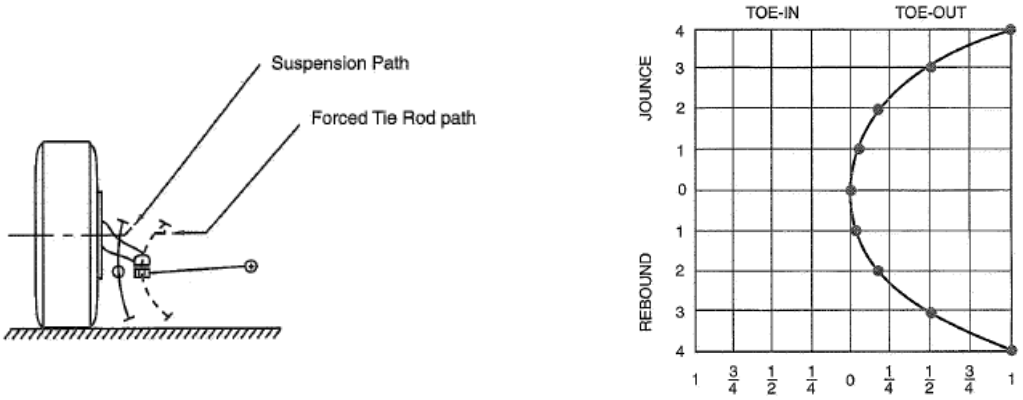

Fig. 6.14. Example of wheel that tends to toe-out both in jounce and rebound, passing through initial position in ride height. The curve suggest that the ball joints of the steering rod are placed in the correct height, but it is too short. [3]

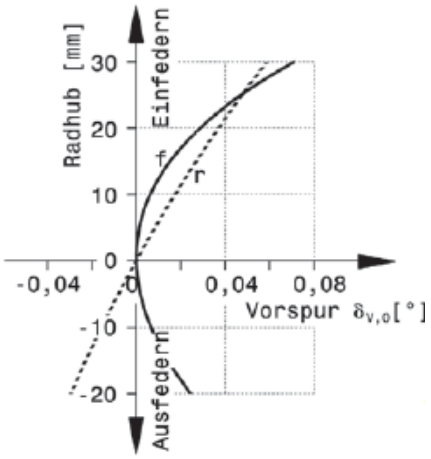

Fig. 6.15. Example of acceptable toe angle change with bump travel. [1]

6.2.6. Results analysis - track width change and bump steering

Both diagrams obtained from analysis in LSA present that changes of (half) track width (Fig. 6.16) and toe angle (Fig. 6.17) are more rapid than those presented as an example above. With 30mm rise of suspension width track grows over 4mm for rear axis and 8mm for front (half track over 2mm and 4mm respectively). Literature suggests however even 30mm scrub change as acceptable, but for street cars (and with much longer bump travel typical for that kind of cars), while example typical for race cars suggests only 3mm growth. Toe angle changes even 0,15° for front axis, comparing to less than 0,08° suggested before. Only toe angle change for rear axis stays within accepted boundaries.

As the relation between steer angle and bump travel is almost linear, it can be concluded that it is more important to apply changes in steering rod's location rather than its length.

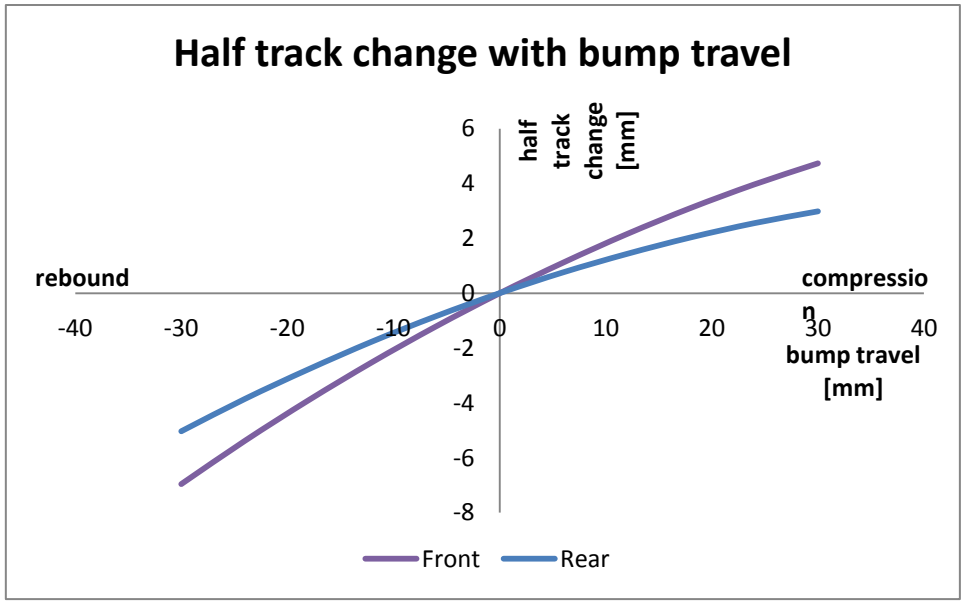

Fig. 6.16. Half track change with bump travel for analyzed vehicle.

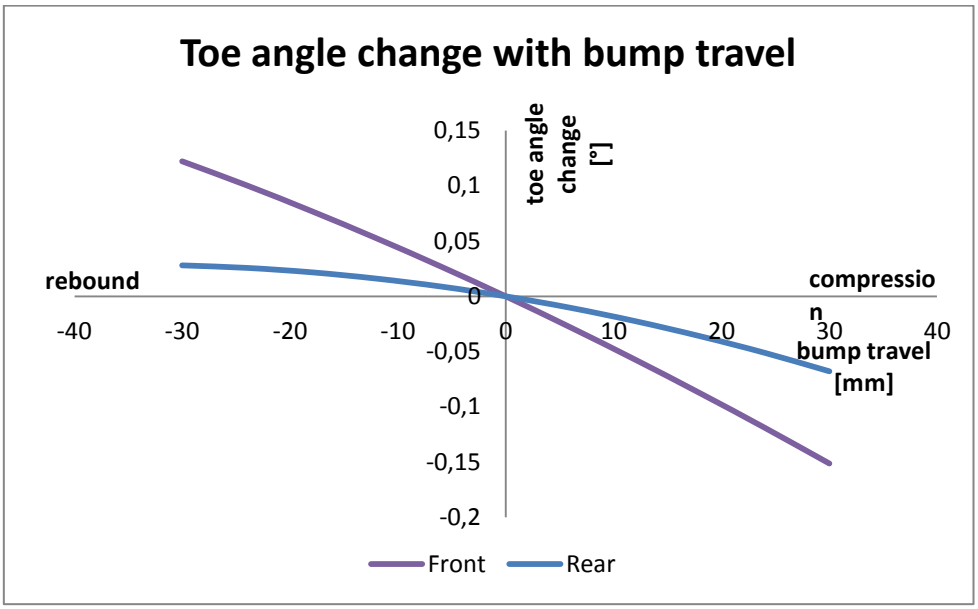

Fig. 6.17. Toe angle change with bump travel for analyzed vehicle.

6.2.7. Conclusions

It can be concluded that the suspension does not meet all of the design goals set, related to front view geometry. It is advised to manipulate control arms configuration in order to obtain higher camber gains with bump travel compensating for camber loss related to body roll. The desired relation should be non linear with more rapid changes for compression than for rebound, resulting in maintaining camber of inner wheel low over 0° and outer wheel growing to negative values while roll.

These changes of camber value should be a little bigger for rear axis while those for front axis must be balanced with changes related to caster and kingpin inclination analyzed in previous chapter.

The above can be obtained in the following process according to literature [3]

- Set demanded values for camber gain for front and rear axis. For example 0,3° camber gain relatively to ground per 1° body roll for front axis and 0,7° for rear axis.
- Calculate fvsa length for ride height according to Eq. 3.3, getting, following the example camber gain values,

$$fvsa_{front} = \frac{1410{,}05mm}{2(1-0{,}3)} = 1007{,}18mm \quad \text{(Eq. 6.1)}$$

for front axis and

$$fvsa_{rear} = \frac{1394{,}09mm}{2(1-0{,}6)} = 2323{,}48mm \quad \text{(Eq. 6.2)}$$

for rear axis.

- After deciding on roll center heights (advices in following paragraph of this chapter), which together with fvsa length determine instant centers for front view geometry, design lower control arm as long as packaging restraints allow (ball joints on upright should be already placed) and manipulate upper control arm's length until demanded relation between camber and roll is obtained. LSA should be a really helpful tool in that case as it can automatically plot diagram of this relation in real time, while changes are being made.

Roll centers should be placed lower. Their height, according to benchmarking, shouldn't be more than 40mm with lower value in the front. As their height (together with fvsa) is first to be decided in the design process, this change is very easy to make.

Lowering roll centers and what follows moving instant centers closer to ground level according to Fig. 3.4 will result in favorable decrease in track width changes too.

When it comes to the phenomenon of bump steering (toe angle change with bump travel) a slight change of steering rack location is suggested. Due to compliance effects however it is better to move it down, close to lower control arm as in Fig. 4.1 (placing it behind the axle line is difficult because of packaging problems caused by required in competition rules empty area template – red box in Fig. 6.18). The differences in stiffness of mounting the rack and the control arms may cause steering angle changes under side forces while cornering. Ensuring that the steering rack is located in indicated areas it will be more likely to obtain understeering in this situation rather than oversteering, which is safer, taking into consideration vehicle stability.

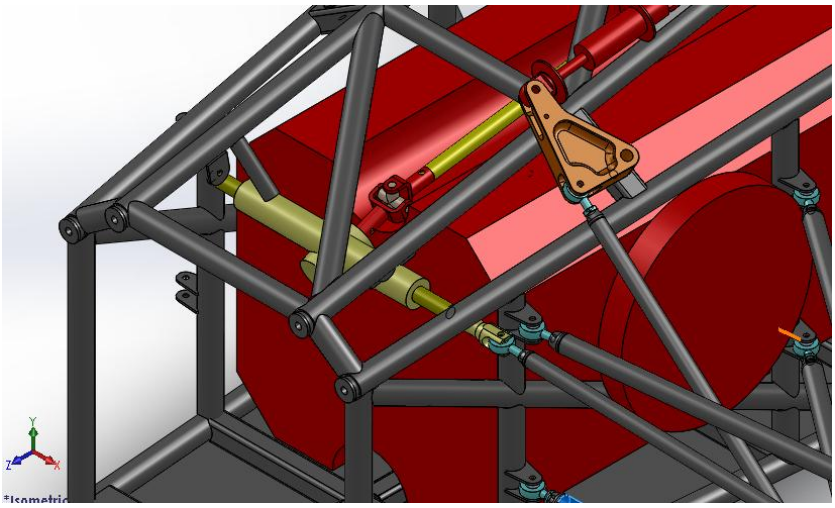

Fig. 6.18. Single Cardan's coupling and the steering rack located in front of and above front axis. Red extrusion is the empty area template required in the competition.

In order to obtain these changes a double Cardan's coupling should be applied to solve packaging issues around empty area template. Additional benefit would be also elimination of angular velocity pulsation, which appears on passive shaft when a single coupling of this type is used.

6.3. SIDE VIEW GEOMETRY ANALYSIS

6.3.1. Anti features

The advantages of high values of anti features is decreasing vehicle's pitch while accelerating and braking. Designing full anti features however is not usual or even impossible because of several reasons. Full anti features are subjectively undesirable and the requirements for achieving them may conflict with those for good handling or braking.

According to source [2] the typical values for anti-squat are between 60% to 80% and anti-dive 60% to 70% (according to [4] seldom more than 50%). Other example values are presented in Fig. 6.19. 40% to 50% for anti-squat and 40% to 60% for anti-dive.

It is important to remember that as anti features are related to instant centers of rotation their values change with suspension travel and should lay within desired limits for all the wheel position range.

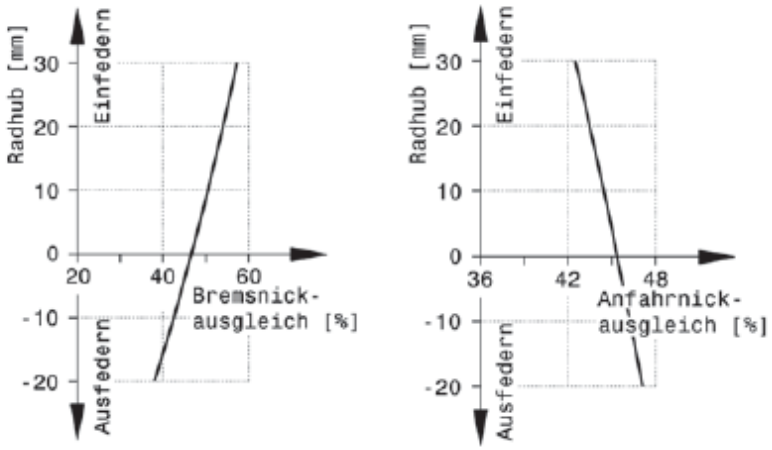

Fig. 6.19. Example acceptable values of anti-dive (left) and anti-squat in bump travel [1].

6.3.2. Results analysis - anti features

For analyzed formula student vehicle anti-dive values for front and rear axle stay between 33% and around 35% within whole bump travel (Fig. 6.20). These values are lower than any of the sources advices.

The value of anti-squat (Fig. 6.21) (only for rear axle – front axle is non-driven and does not produce anti-squat forces) change from almost 50% in rebound to less than 40% in compression and can be considered correct according to some of the sources.

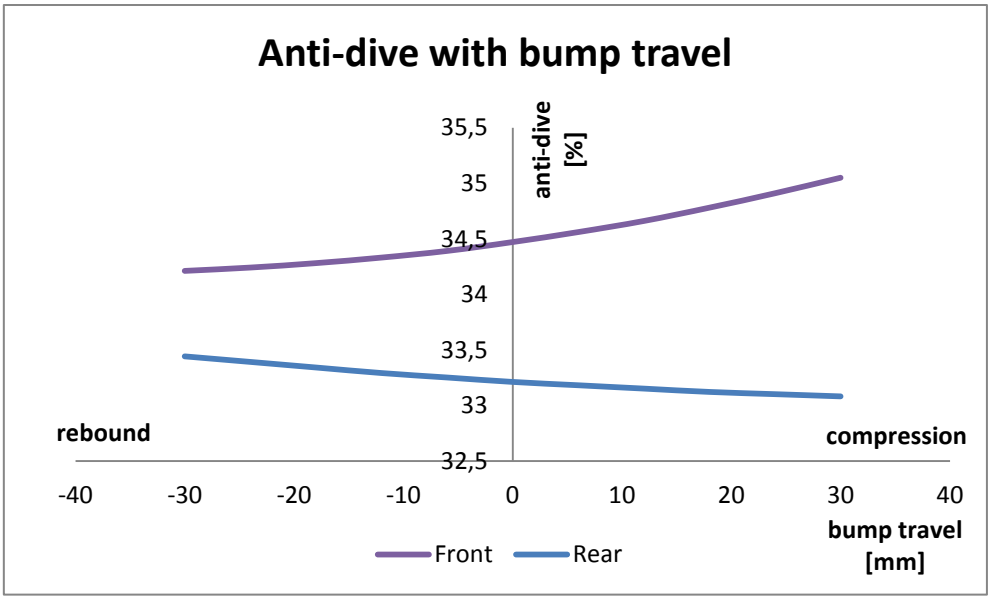

Fig. 6.20. Analyzed vehicle's anti-dive values for front and rear axle changing with bump travel.

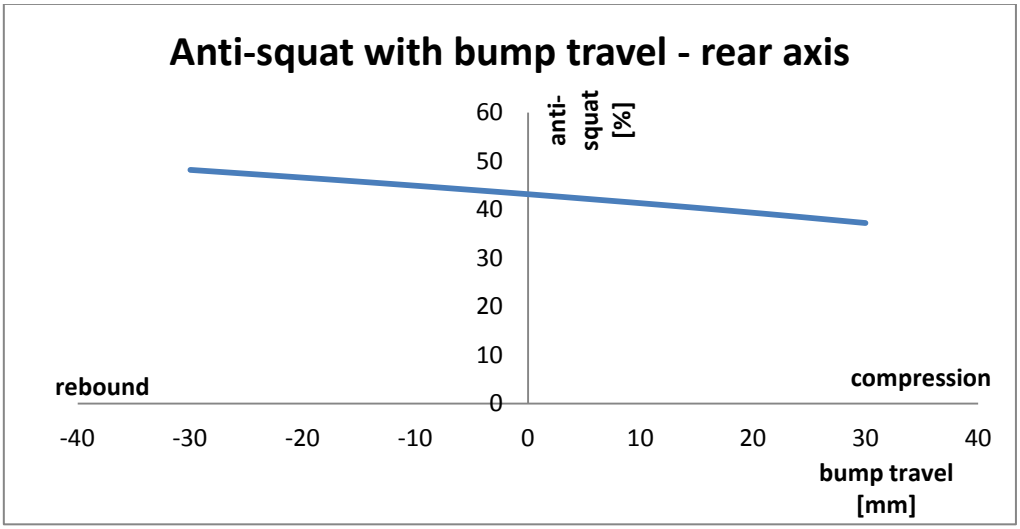

Fig. 6.21. Analyzed vehicle's anti-squat value (rear axle) changing with bump travel

6.3.3. Conclusions

It is advised to increase values of anti features of the analyzed vehicle, especially anti-dive. The design process presented in the beginning of this work suggest starting the side view geometry for front axle with following steps:

- Deciding on desired anti-dive value. With given braking force distribution, % front braking, center of gravity height, h and wheelbase, l, angle ϕ (tanϕ) can be calculated according to Eq. 3.4. For 50% anti-dive and 60% of braking force on front axis:

$$tan\phi = \frac{50\% * 250mm}{60\% * 1493{,}33mm} = 0{,}14 \quad \text{(Eq. 6.3)}$$

$$\phi = 8° \quad \text{(Eq. 6.4)}$$

- Deciding on shortest practical svsa in order to locate IC on the line determined by angle ϕ (Fig. 4.3).

For rear axis a compromise between anti-dive and anti-squat will be required as after locating side view IC for rear suspension, their values will be calculated according to different force diagrams (look Fig. 3.24 for anit-dive and Fig. 3.25 for anti-aquat) and equations (Eq. 3.5 for anti-dive and Eq. 3.6 for anti-squat).

7. FRAME PERFORMANCE TESTS AND GOALS

According to [7] the loads that a vehicle's frame is subjected to during normal exploitation can be simulated with four different tests that all together, if passed with positive result guarantee it's correct performance. These tests are:

- Longitudinal torsion
- Vertical bending
- Lateral bending
- Horizontal lozenging

Longitudinal torsion takes place when two oppositely directed forces act on corners of the car, generating torque along the longitudinal axis of the car. Vertical bending is caused by weight of passenger and car's components installed on the chassis. The magnitude of these forces can by increased in comparison to static situation, when vertical accelerations appear. Lateral bending appears when the car is subjected to side forces related for example to side wind or centrifugal acceleration while cornering. Horizontal lozenging takes place when differences in longitudinal forces appear between tires on opposite sides of the car, making the chassis distort into parallelogram shape. These four loading schemes can also happen simultaneously.

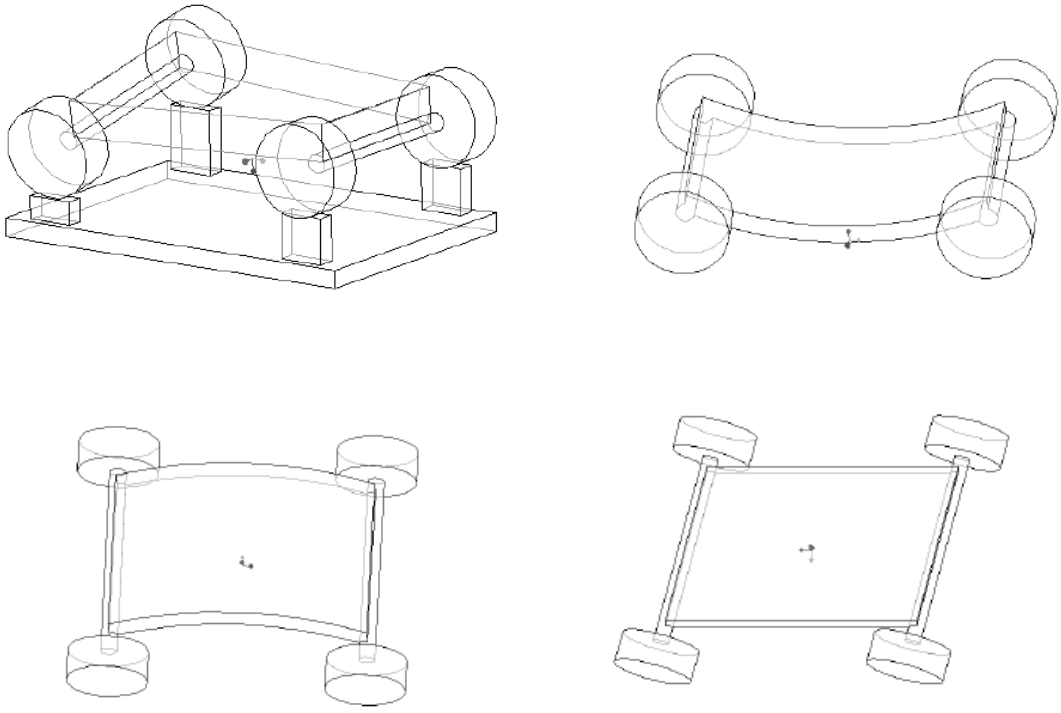

Fig. 7.1 Chassis deformation modes [7]

Usually, and in this paper too, the attention is focused on the test of longitudinal torsion and the frame's performance in it is considered the primary factor when the structure is assessed. This is caused by the fact that frame's deformations under torsional loads can influence handling performance, by changing roll angles of axis and load distribution on tires [8].

For this kind of test design's performance can be expressed as torsional stiffness in Nm per degree, which is torsional torque related to twist angle that it causes. On this basis a design goal can be set. Although there is no specific value that can be considered an optimal one and

the only objective way to asses overall frame's performance are track tests, the design teams usually assume that the chassis's stiffness should be one order magnitude greater than either spring, wheel or tire rate [7]. If a theoretical situation, when all the chassis elements except for shock absorbers (springs and dampers) are perfectly stiff (frame, control arms, push rods,… and all the joints and bearings) is imagined, the goal can be also set as follows: The chassis torsional stiffness must constitute 90% of the perfectly rigid case [7]. The last approach was applied in this paper and all the required calculations are performed in following part.

In addition to the usual analysis of the frame, some more attention will be paid to its behavior around joints of suspension's control arms too. Their location, in some distance from nearest frame's nodes, could be considered a disadvantage of a design, that increases suspension system's compliance. It can change critical suspension's point's (the same as were introduced to LSA model) relative location and influence steering performance because of it. Strategic location of suspension support points is also a target for a rigid chassis design [9].

8. RIGID CHASSIS CASE

To calculate the chassis torsional stiffness for a theoretical, perfectly rigid frame a simple mathematical model presented in Fig. 8.1 will be used. It consists of frame and four springs placed in its corners, that represent the suspension. Three of them are fixed to the ground. On the fourth one there is a vertical force acting upwards. That model is analogical to a situation when three wheels of a car are located on a flat, horizontal surface and the fourth is on a bump. The forces that keep the three wheels at the ground are the loads coming from the car's weight [7].

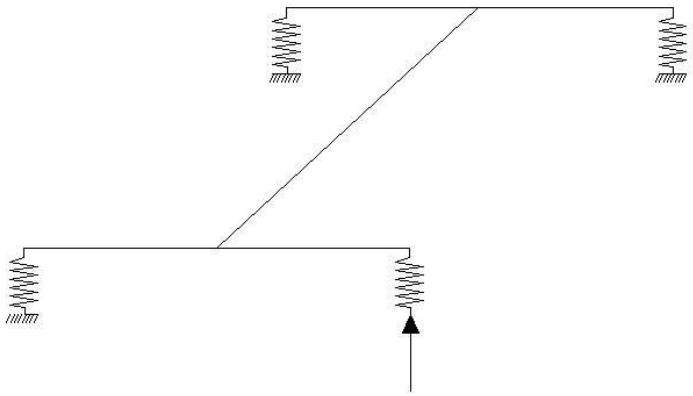

Fig. 8.1 Mathematical model for torsional stiffness calculations for rigid chassis case

Under the force the system will change its position to presented in Fig. 8.2. The rear left and front right springs will rebound and the other two will be compressed. Moreover the spring that is not fixed to the ground will move upwards. For this calculations it will be assumed that only vertical deflections and translations appear.

The twist angle of chassis in this situation, that will be needed to calculate torsional stiffness, is the angle that the line connecting bottom ends of the front springs creates with the ground. It is the same angle that this line creates with analogical line drawn for the rear springs, whose ends remained on the ground. If the system is presented with the frame instead of the ground as reference, as in Fig. 8.3, this angle can be easily related to springs vertical deformations.

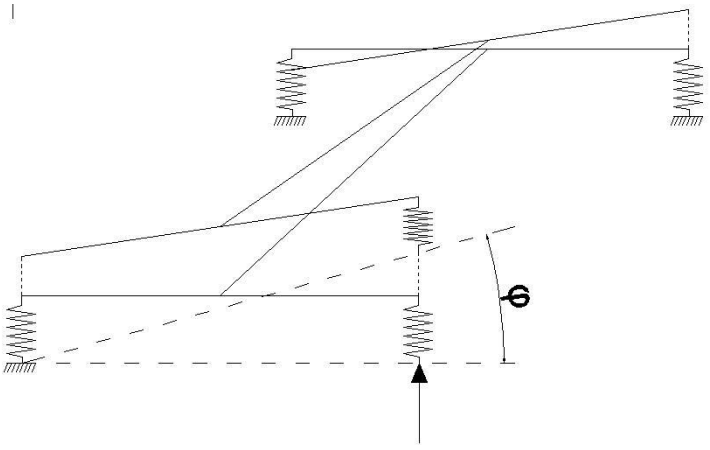

Fig. 8.2 Systems position under the force acting with the ground as reference

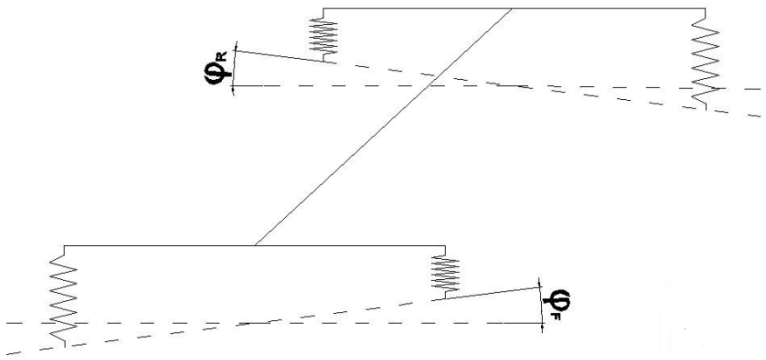

Fig. 8.3 Systems position under the force acting with the frame as reference

This angle will be therefore the sum of inclinations of the lines connecting bottom ends of lines in front and rear relatively to their initial positions and can be calculated as follows:

$$\varphi = \varphi_F + \varphi_R \quad \text{Eq. 8.1}$$

$$\varphi_F = arctan\left(\frac{dy_{FR} - dy_{FL}}{t_F}\right) \quad \text{Eq. 8.2}$$

$$\varphi_R = arctan\left(\frac{dy_{RR} - dy_{RL}}{t_R}\right) \quad \text{Eq. 8.3}$$

where: ϕ – chassis twist angle
ϕ_F, ϕ_R – inclination of front/rear line connecting bottom ends of springs
dy – vertical deflection of front/rear right/left spring
t_F, t_R – front/rear track

Solving the free body diagram of the system for a force of 1000N acting on one of the front springs gives the reaction force of 1000N on the other front spring and 1020N at rear springs. The torque T acting on the frame is:

$$T = 1000N * t_F = 1000N * 1282mm = 1282Nm \quad \text{Eq. 8.4}$$

Springs in this model represent wheel rates of the vehicle. To calculate the deflections then the spring stiffness has to be multiplied by installation rate squared, that can be read from LSA data. The program however gives the values as spring ratio, that have to be inverted to be used in Eq. 8.7 and Eq. 8.8. Fig. 8.4 presents on a simple model how the installation rate determines relations of both forces and displacements/deflections, what makes it necessary to square it.

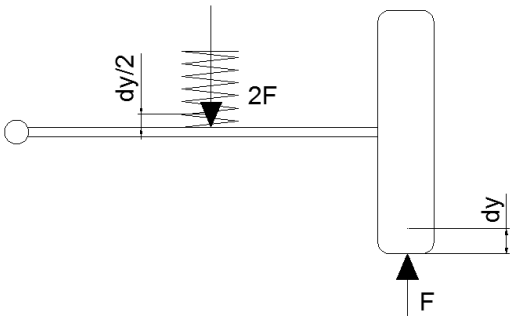

Fig. 8.4 Force and displacement relations between wheel and spring

The simplified model depicts a suspension with single wishbone and a spring attached in half of its length. From the equilibrium of moments it can be concluded that the force acting on the spring is twice the force at the contact patch of the tire. From geometrical relations the spring's deflection equals half of the tire's vertical translation as long as small angles are considered. The value given by LSA takes into consideration, except for rocker's ratio, also corrections related to angles which the spring and push rod create with it. As this angles change constantly with bump travel, rounded values for ride height were used in calculations.

The spring stiffness is given on them by producer in pounds per inch, so in N/mm they are:

$$k_{springF} = 650lbs/inch = 650 * \frac{4{,}45N}{25{,}4mm} = 114N/mm \quad \text{Eq. 8.5}$$

For front and

$$k_{springR} = 850lbs/inch = 850 * \frac{4{,}45N}{25{,}4mm} = 149N/mm \quad \text{Eq. 8.6}$$

for rear.

The wheel rates k_F for front and k_R for rear are then:

$$k_F = k_{springF} * i_F^2 = 114N/mm * 0{,}83^2 = 78{,}5N/mm \quad \text{Eq. 8.7}$$

$$k_R = k_{springR} * i_R^2 = 149N/mm * 0{,}67^2 = 66{,}9N/mm \quad \text{Eq. 8.8}$$

The deflections of the model's springs or in other words wheels' vertical displacements are therefore:

$$-dy_{FL} = dy_{FR} = 1000N/k_F = \frac{1000N}{78{,}5N/mm} = 12{,}74mm \quad \text{Eq. 8.9}$$

$$dy_{RL} = -dy_{RR} = 1000N/k_R = \frac{1020N}{66{,}9N/mm} = 15{,}25mm \quad \text{Eq. 8.10}$$

The twist angle can be now calculated according to Eq. 8.1, Eq. 8.2 and Eq. 8.3.

$$\varphi = \arctan\left(\frac{12{,}74mm+12{,}74mm}{1282mm}\right) + \arctan\left(\frac{15{,}25mm+15{,}25mm}{1240mm}\right) =$$

$$= 0{,}0445\text{rad} = 2{,}55° \quad \text{Eq. 8.11}$$

And with torque calculated in Eq. 8.4 gives the torsional stiffness

$$K_{rigid} = \frac{1282Nm}{2{,}55°} = 502{,}75Nm/° \quad \text{Eq. 8.12}$$

For the case with compliant chassis the torque T will cause twist angle ϕ related to shock absorbers' deflections and additional twist in chassis, related to its limited stiffness, that will be determined in virtual and laboratory tests. Dividing the torque by sum of these angles will give the compliant case's torsional stiffness. These deflections are therefore treated as for springs in series, so the final stiffness can also be calculated as follows:

$$\frac{1}{K} = \frac{1}{K_{rigid}} + \frac{1}{K_{chassis}} \quad \text{Eq. 8.13}$$

Fig. 8.5 presents a mathematical model with compliant chassis and results of calculations done by far. There is a torsional spring placed in the middle of the chassis, that subjected to torque T lets the chassis twist by angle $\varphi_{chassis}$ along its longitudinal axis.

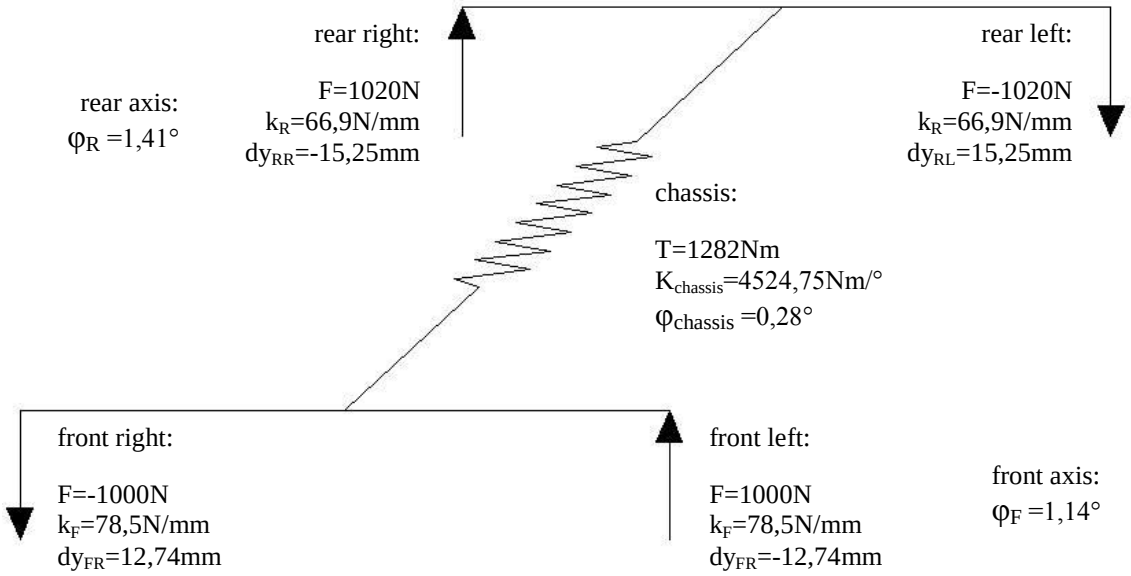

Fig. 8.5 Mathematical model of case with compliant chassis

If torsional stiffness of rigid chassis is known and the goal for compliant frame is set as 90% of it, then the demanded chassis stiffness can be calculated on basis of Eq. 6.14.

$$\frac{1}{0{,}9*502{,}75N/mm} = \frac{1}{502{,}75N/mm} + \frac{1}{K_{chassis}} \qquad \text{Eq. 8.14}$$

$$K_{chassis} = 4524{,}75Nm/° \qquad \text{Eq. 8.15}$$

This value, if compared to Table 10.5, turns out to be very high. None of the frames mentioned there for benchmarking could meet the goal of 90% (452,47 Nm/°) of the rigid case stiffness with that suspension's torsional stiffness value. The most rigid frame of 2711,64Nm/° would result with barely 84%. Note, that because of character of Eq. 6.13 this percentage is an asymptotic function of chassis stiffness and with values getting closer to 90% a substantial growth in chassis stiffness is needed for it to grow another percentage point (Fig. 8.6). That means that springs chosen for the suspension are very stiff and revision of their selection process is recommended. That has to be taken into consideration when results of the tests are analyzed.

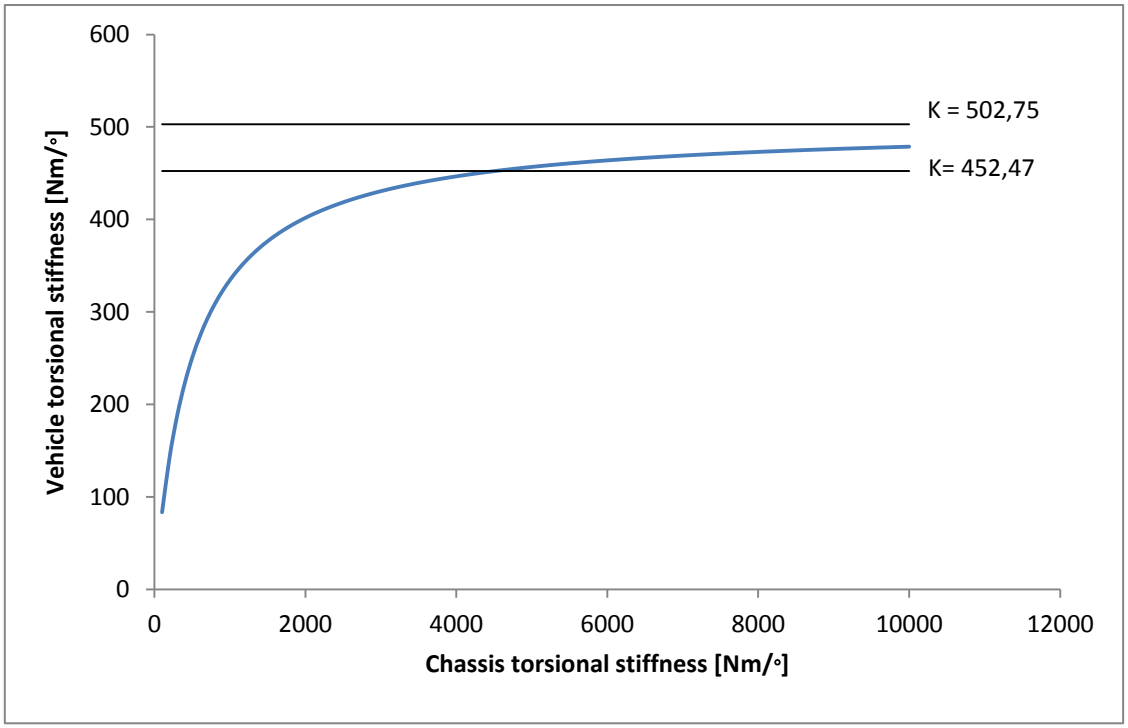

Fig. 8.6 Relation between chassis and full vehicle torsional stiffness for suspension torsional stiffness K=502,75 Nm/°

9. TESTS PROCEEDINGS

The following part of the report contains description of methodologies and results of several virtual and experimental tests. To make the flow of them and relations between them clear, they are presented in Fig. 9.1.

Although in all the tests the structure is in longitudinal torsion, there are important differences between one another. Except for obvious division between virtual and experimental tests we can differentiate tests run for only the frame, without suspension, and tests of full chassis assembly. Except for determining the torsional stiffness in these tests, which was the main goal, also the values of stress were checked. Therefore stiffness and stress tests can be distinguished too.

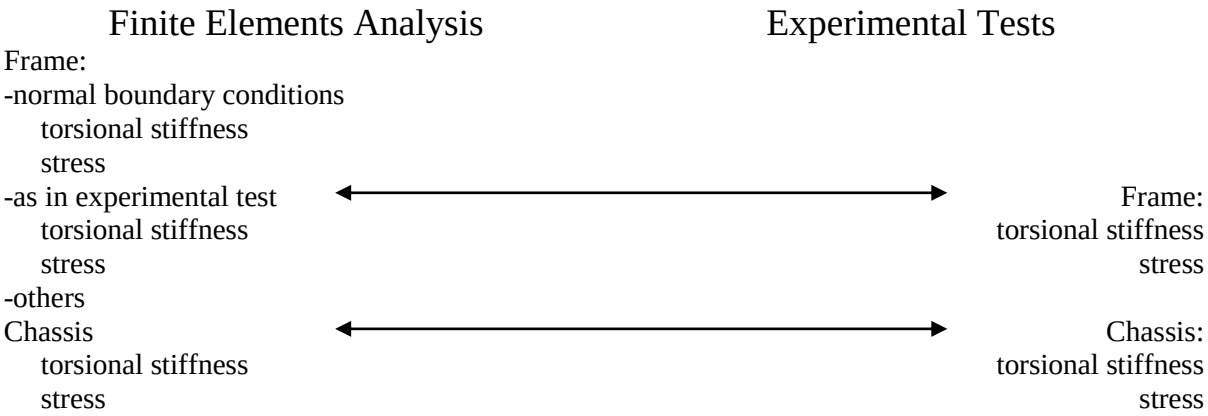

Fig. 9.1 Tests proceedings

The experimental tests were run to verify and validate the virtual ones. If considerable discrepancies appeared, that would mean the model does not represent the reality properly, of course as long as no mistakes are made in experimental tests. The model however is always some kind of simplification of reality and reaching exactly the same results as in experiments is not possible. Reaching close results in both virtual and experimental approach then will validate the virtual one and make it possible to further use it, for example to predict stiffness gains due to improvements proposed. It will also show how accurate the results that the model delivers are and what change can be expected from the real chassis.

What was already mentioned and will be explained more profoundly later, the car was still undergoing adjustments in the period when the experiments were run. The current state of the vehicle made it impossible to set boundary conditions, fixtures, the same way they were planned for software analysis. For that reason additional FEM analysis that copied the boundary conditions possible for test in laboratory were run. They could be then directly compared to practical experiments. The changes regarded mounting the engine and placing the supports in the rear of the car.

As in literature and practical use many methods of fixing the frame, that are different than the one chosen here, are common, they will also be considered. Minor attention however will be paid to them.

10. FINITE ELEMENTS ANALYSIS

10.1 MODEL CREATION

The virtual SolidWorks manufacturing model, previously prepared by design team, was used to prepare model for simulations. It required first of all introducing all the changes between the model and the welded frame that appeared during manufacturing as a result of design teams decisions. The example changes appeared in side of the frame, next to the seat and are presented in Fig. 10.1 together with the original model of the frame delivered for virtual tests.

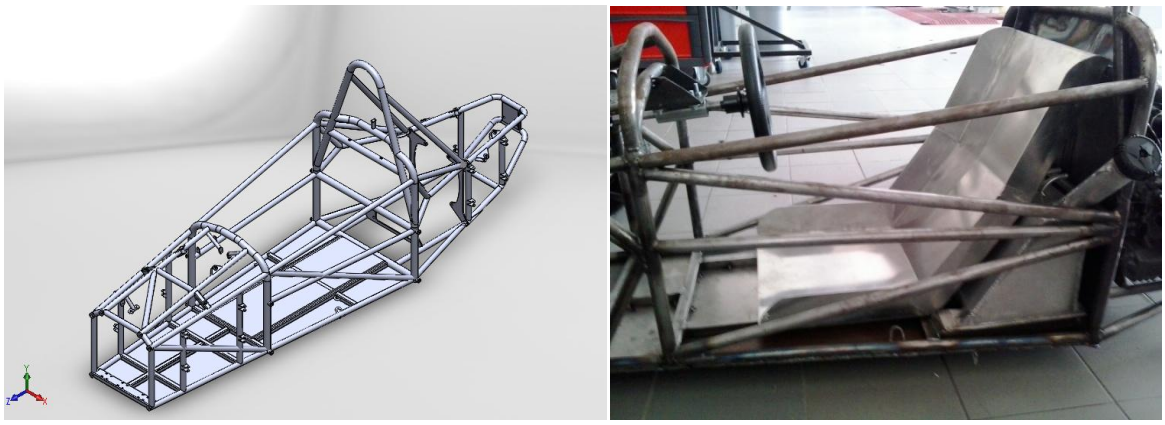

Fig. 10.1 Original frame model and example change made during manufacturing

The manufacturing model turned out not to be well prepared for virtual tests. In spite of much time being spent on adjusting it for this purpose, problems with meshing kept occurring. Because of it, the decision was made to make a new model, dedicated specifically for the analysis. Therefore the model initially delivered, welded frame check for differences and few measurements were the basis for creating a new model. It used the technique of three-dimensional sketch which is the basis for locating in space structural members of defined cross-sections.

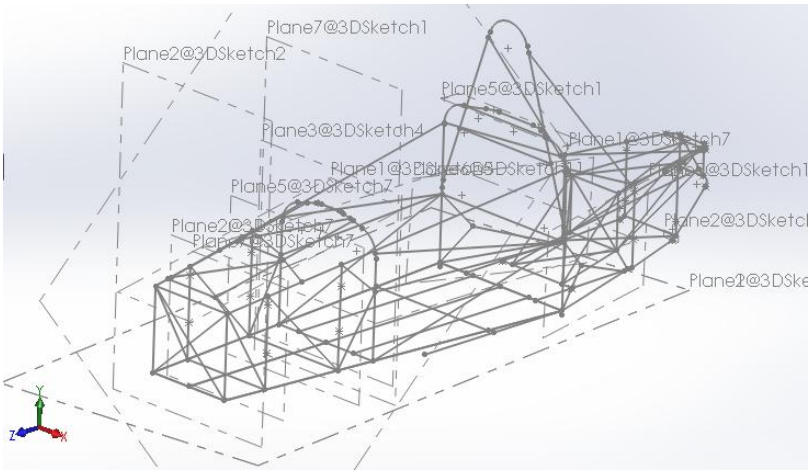

Fig. 10.2 3D sketch for the simulations model

Basing on source papers [7, 10] and SolidWorks online resources [11] dedicated for Formula SAE, it was decided that beam elements model will provide results accurate enough. Most of the elements were therefore treated as beams, transferring forces and moments in all

directions, except for suspension elements, that were treated as trusses, transferring only longitudinal forces. That very easily simulated ball joint connections of control arms. The full mesh is presented in Fig. 10.4. The trusses can be distinguished from the beams, as they are single, long elements not further divided into smaller ones.

At that point it was necessary to decide what kind of elements, except for the frame itself, should be considered in the simulations, as they could influence the results and what kind of simplifications can be applied in order for the program to be able to perform the calculations. It is worth mentioning, that frame model should be subjected to virtual torsional stiffness test in the phase of design, between following iterations. For that reason creating a simple model, that goes through the program's calculations fast can make it easy to test and assess any adjustments introduced and save time. Following the same approach in this work will provide results that can be a point of reference when a frame for next season is designed. As the laboratory tests will be performed too, it will reveal how close to the actual, real chassis torsional stiffness they are too.

Mountings of other systems were not included in the model, neither were thin plates below the frame and behind the driver's back or side safety structures. Engine however, together with gearbox in this case, considerably increases frame's stiffness and in a good, lightweight design should be considered a structural element [10]. Also the front plate was considered in the analysis, as it prevents the front hoop of the frame from deforming.

In order to keep the model consist exclusively of beam elements, those two parts were simplified and replaced with simple, stiff beam structures, that increased the frames' rigidity in specific areas [7, 10]. The chassis' simplified version designated for analysis, together with beam structures representing engine, gearbox and front plate can be seen in Fig. 10.3.

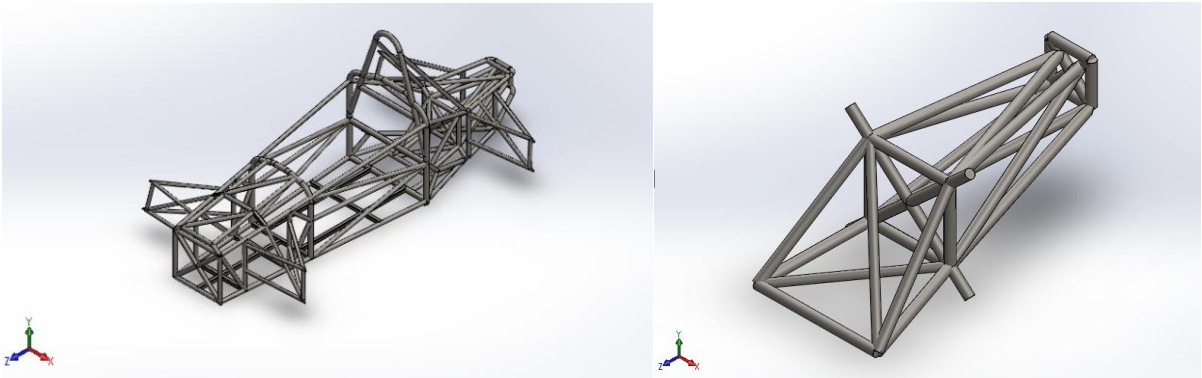

Fig. 10.3 Chassis model prepared for tests and beam structure replacing engine and gearbox

Another simplification regarded removing rocker from suspension and connecting the push rods directly to the frame. That will change loads distribution in this area. It should not however significantly change the final result of torsional stiffness.

It can be noticed that beams in the model prepared for tests are not trimmed in the connections with one another and intersect. It was decided to do so, because of the algorithm that the software follows to create mesh. The initial three-dimensional model is a base for creating set of nodes (Fig. 10.4), which the beam elements are extended between. Such a limited treatment of pipes' connections gave better final result.

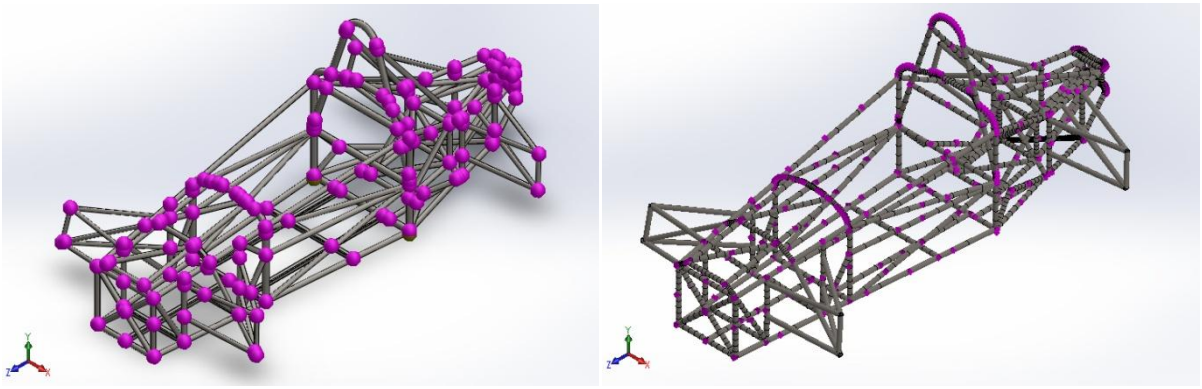

Fig. 10.4 Model represented with its nodes (pink spheres; left) and meshed with beam/truss elements

10.2 FIXTURE AND LOAD APPLICATION

During normal exploitation of a vehicle loads are transferred to the frame through suspension system. That implies a frame test, without suspension mounted, will never provide the same loads distribution, that the car is subjected to on the track. For that reason it is important to be careful when different concepts of fixture and load application are considered, as the results they lead to may vary. In this case, in order to present these differences, the virtual test was run for different boundary conditions, presented in Fig. 10.5 to Fig. 10.7 and the case of engine fully and partially mounted.

What was already pointed out before, the analyzed structure has suspension mounts located in some distance from the nearest frame's nodes and it is demanded to investigate how this fact influences the structure's performance. For that reason the different boundary conditions include both fixing the model at suspension mounts themselves and at the nearest frame nodes, the second option being a theoretical situation, when suspension is mounted in frame nodes. These variations will be referred to relatively as S – suspension mounts and N – frame nodes.

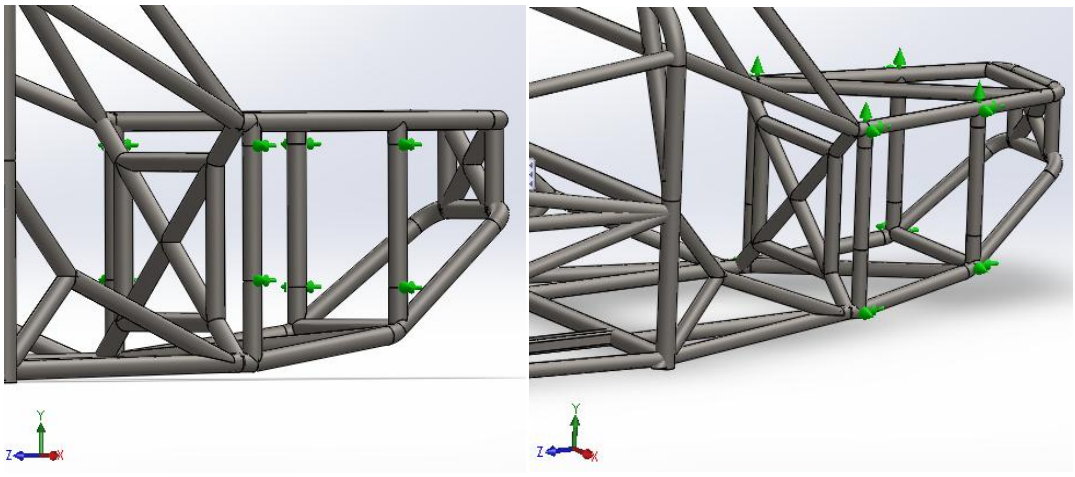

Fig. 10.5 Rear suspension bay fixed at suspension mounts and at frame nodes

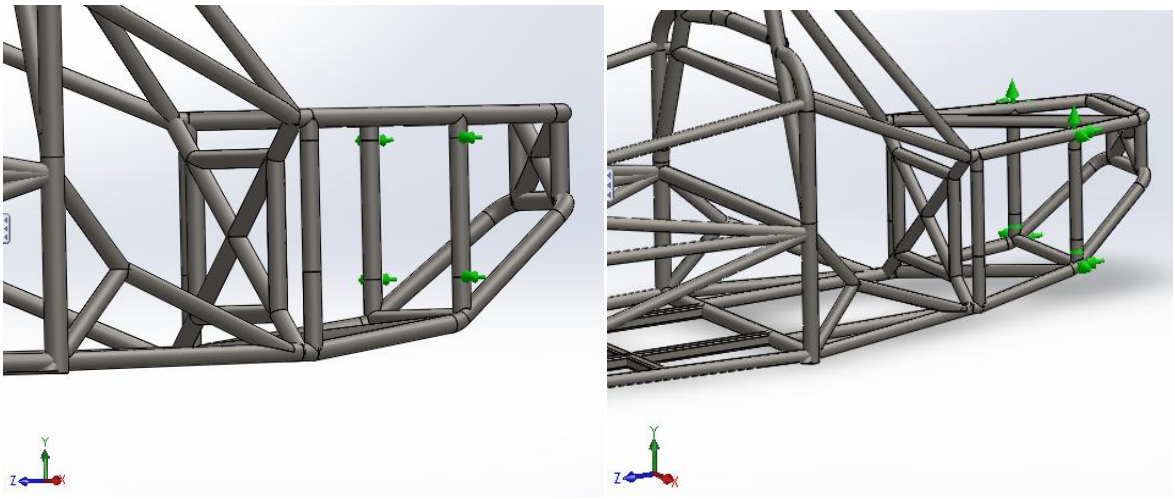

Fig. 10.6 Single plane of rear suspension bay fixed at suspension mounts and at frame nodes

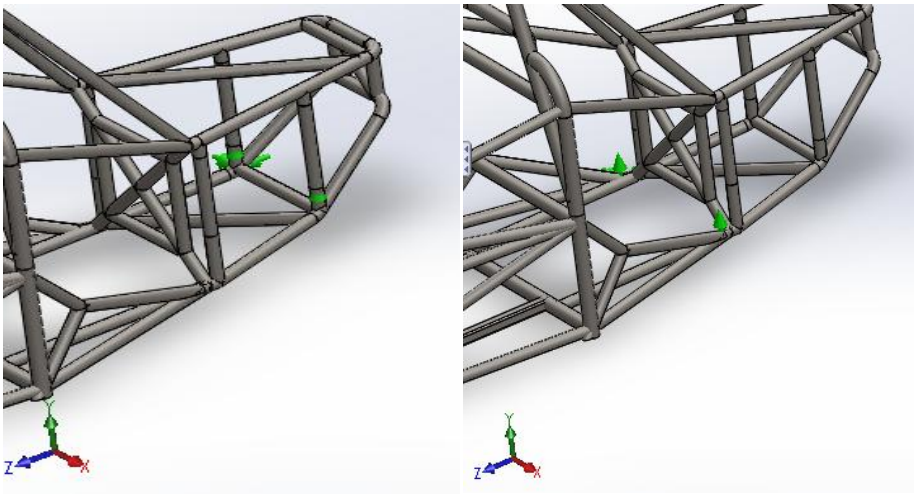

Fig. 10.7 Single line of rear suspension bay fixed at suspension mounts and at frame nodes

The concept referred to as “rear bay” assumes that all the mounts of rear control arms are totally fixed for translations, with free rotations and can be often found in other papers. This however assumes, that suspension mounts do not change their location in relation one to another, which does not have to be true, especially in the case, when no proper triangulation is provided in the area of suspension mounts. On the other hand suspension, if mounted, also provides some support to suspension mounts, when compared to situation, when only the rear mounts of rear bay are supported (referred to as “single plane of rear bay”) and the other mounts are free to translate.

It also should be assumed that top and bottom suspension mounts can move relatively. Even with stiff pipes installed instead of shock absorbers, the suspension is still a truss structure and changes its position without generating any moment counteracting frame deformations.

Another fixture concept then, with frame fixed at the bottom rear of rear suspension bay, locks dislocation of only two points and allows all the others to move. Running test with these boundary conditions will include rear suspension bay’s compliance effects in the results. It is also the closest to the conditions that can be provided for the laboratory test, which will be explained in following part of this paper. For this reason it was chosen for more profound analysis.

It can be concluded that the real value of torsional stiffness, the one, that characterizes chassis on the racing track, lays somewhere between the limits set with the values gained from the tests described.

No matter which of the fixture concepts is considered, it should be later verified, being compared to results from full chassis test.

Analogical considerations could be conducted for force and fixture application in the front of the car. For having a clear way of calculating the torque however, and what follows determining a value of torsional stiffness unequivocally, the structure was introduced in torsion with a single force and fixture in vertical and side directions. They were applied either on the bottom front line of front suspension bay or, for the simulation of test run in workshop, in the further front bottom pipe (Fig. 10.8).

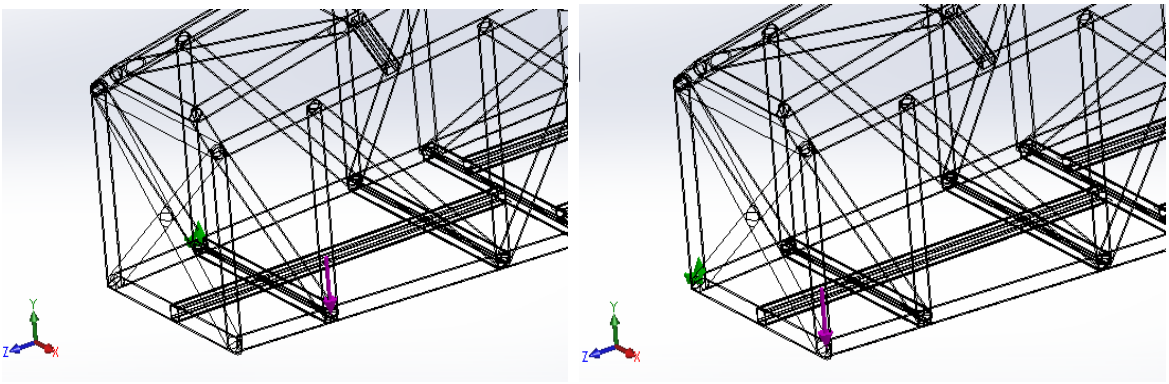

Fig. 10.8 Fixture and load application in front of the car

For full chassis assembly the tests were run with bottoms of three uprights fixed for translations. Rear right in all three directions, rear left for vertical direction and front right for side and vertical direction. The force was applied downwards at the fourth upright (Fig. 10.9).

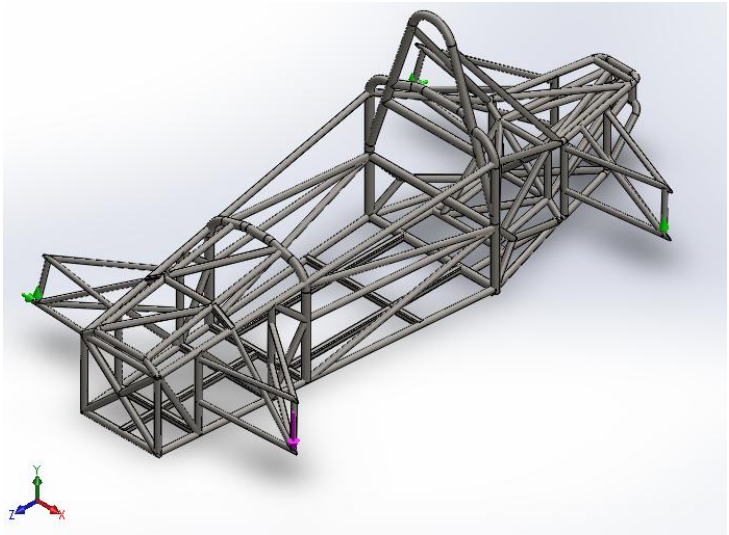

Fig. 10.9 Fixture and load application for full chassis assembly test

10.3 VIRTUAL FRAME TEST

Table 10.1 presents results of the virtual tests for all the boundary conditions concepts, while Fig. 10.10 and Fig. 10.11 depict vertical dislocations for two most important cases: single line fixed with mounted engine, which was considered the correct way of running the test and the case with the same boundary conditions as in experimental test.

Table 10.1 Virtual frame tests results

				engine fully mounted			engine NOT fully mounted		
fixture	force [N]	L [mm]	Torque [Nm]	dy [mm]	angle [°]	K [Nm/°]	dy [mm]	angle [°]	K [Nm/°]
suspension bay N	1000	394	394	0,73	0,11	3737,07	0,75	0,11	3616,36
suspension bay S				0,81	0,12	3352,78	0,84	0,12	3242,82
single plane of suspension bay N				1,00	0,14	2717,26	1,10	0,16	2458,60
single plane of suspension bay S				1,11	0,16	2438,69	1,20	0,17	2265,37
single line of suspension bay				1,369	0,20	1979,09	1,63	0,24	1660,16
as in lab test		364	364	1,016	0,16	2276,07	1,06	0,17	2191,94

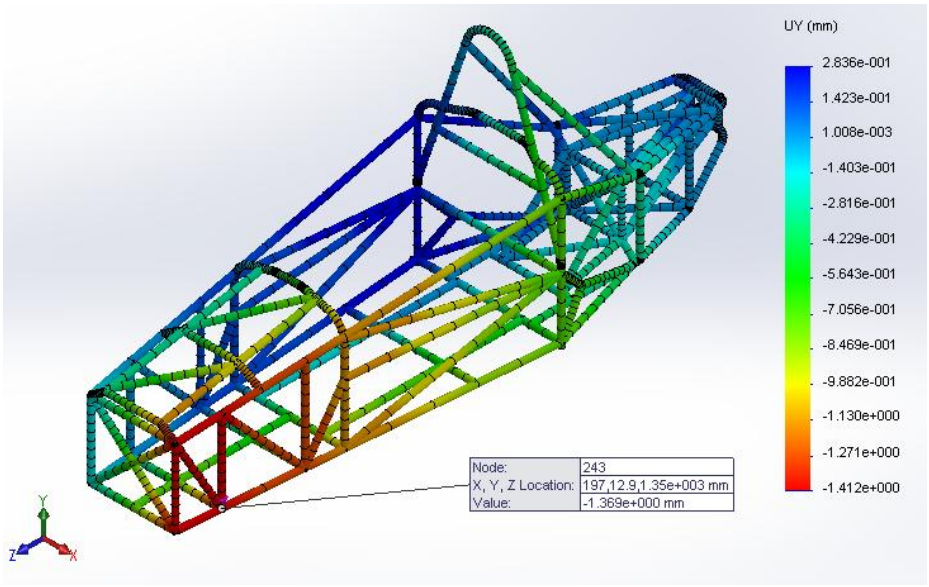

Fig. 10.10 Vertical dislocations for single line fixed and engine fully mounted

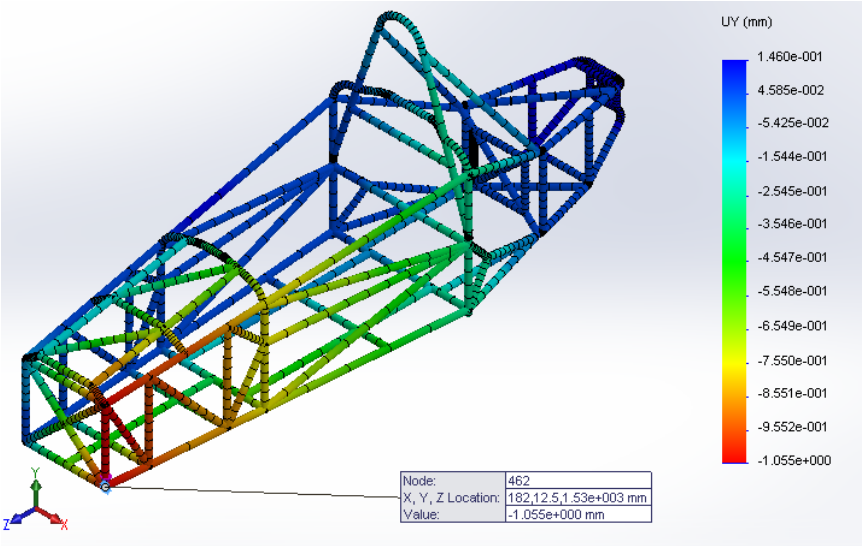

Fig. 10.11 Vertical dislocations for experimental test's boundary conditions

Using virtual tests it was possible to easily calculate torsion angle not only for a frame as a whole, but also for specific compartments along Z axis, which the frame is divided into by vertical pipes. Dislocations dy_1 and dy_2 along Y axis were read for two points in the end of each compartment. Knowing the distance x between them the angle φ was calculated with simple trigonometry relations. The angle was calculated for top and bottom line as presented in Fig. 10.12. The results are gathered in Table 10.2. The twist angle analysis was conducted for the fixtures in one line of rear bay.

Table 10.2 Twist angle analysis for virtual frame test (single line of suspension bay fixed)

		z [mm]	-927	-732	-473	0	862	1016	1349	1534
		x [mm]	120	260	354	620	476	448	392	362
upper line	engine fully mounted	dy_1 [mm]	0,032	-0,005	-0,251	-0,711	-1,129	-1,180	-1,301	-1,352
		dy_2 [mm]	0,100	0,004	0,129	0,280	0,139	0,089	-0,006	-0,076
		φ [°]	0,032	0,002	0,062	0,092	0,153	0,162	0,189	0,202
bottom line		dy_1 [mm]	0,033	0,000	-0,252	-0,708	-1,129	-1,186	-1,307	-1,350
		dy_2 [mm]	0,100	0,000	0,131	0,278	0,140	0,093	0,000	-0,077
		φ [°]	0,032	0,000	0,062	0,091	0,153	0,164	0,191	0,201
upper line	engine NOT fully mounted	dy_1 [mm]	0,051	-0,008	-0,399	-1,054	-1,470	-1,521	-1,643	-1,693
		dy_2 [mm]	0,086	0,008	0,226	0,482	0,211	0,137	-0,006	-0,104
		φ [°]	0,017	0,004	0,101	0,142	0,202	0,212	0,239	0,252
bottom line		dy_1 [mm]	0,051	0,000	-0,403	-1,055	-1,472	-1,529	-1,650	-1,694
		dy_2 [mm]	0,085	0,000	0,229	0,479	0,212	0,142	0,000	-0,104
		φ [°]	0,016	0,000	0,102	0,142	0,203	0,214	0,241	0,252

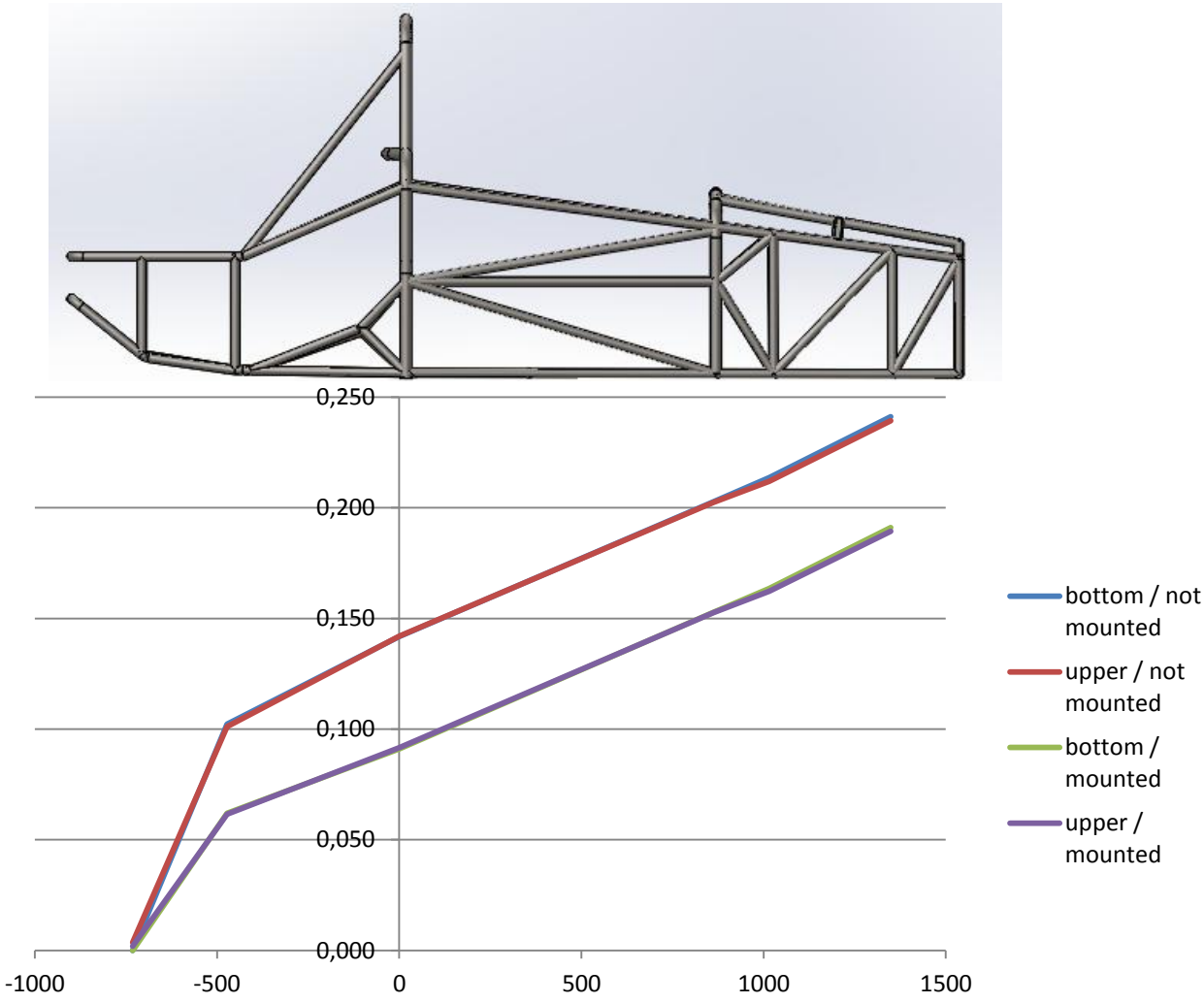

Fig. 10.12 Twist angle value along longitudinal axis of the vehicle in frame test

From analysis of the results presented above following conclusions can be drawn.

Results of tests run with different fixture concepts are significantly different. They vary from 1979,09 Nm/° to 3737,07 Nm/° for the case with mounted engine and from 1660,16 Nm/° to 3616,36 Nm/° with engine partially mounted. Moreover the compartment of the rear bay, where the load distribution is directly influenced by these concepts appears to be critical, as it can be seen in Fig. 10.12. To assess which of the fixture concepts considered is the most accurate, the results will be later verified with full chassis assembly test.

Fixing the frame at its nodes instead of the suspension mounts also changes the resulting torsional stiffness substantially. A theoretical case in which the suspension is mounted in the nodes of the frame in comparison to mounting it outside the nodes increases the stiffness for engine mounted from 3352,78 Nm/° to 3737,07 Nm/° (11,5%) for whole bay fixed, and from 2438,69 Nm/° to 2717,26 Nm/° (11,4%) for single plane fixed. For engine partially mounted the stiffness increases from 3242,82 Nm/° to 3616,36 Nm/° (11,5%) and from 2265,37 Nm/° to 2458,60 Nm/° (8,5%) respectively. That indicates also a problem other than just loss of torsional stiffness. Compliance at control arms' mounts, which appears in this case, results in changes of relative location of suspension points and in its behavior different than designed. Special attention should be paid to ensuring rigidity in that area. Deformation of left rear pipes which the control arms are mounted to can be seen in Fig. 10.13.

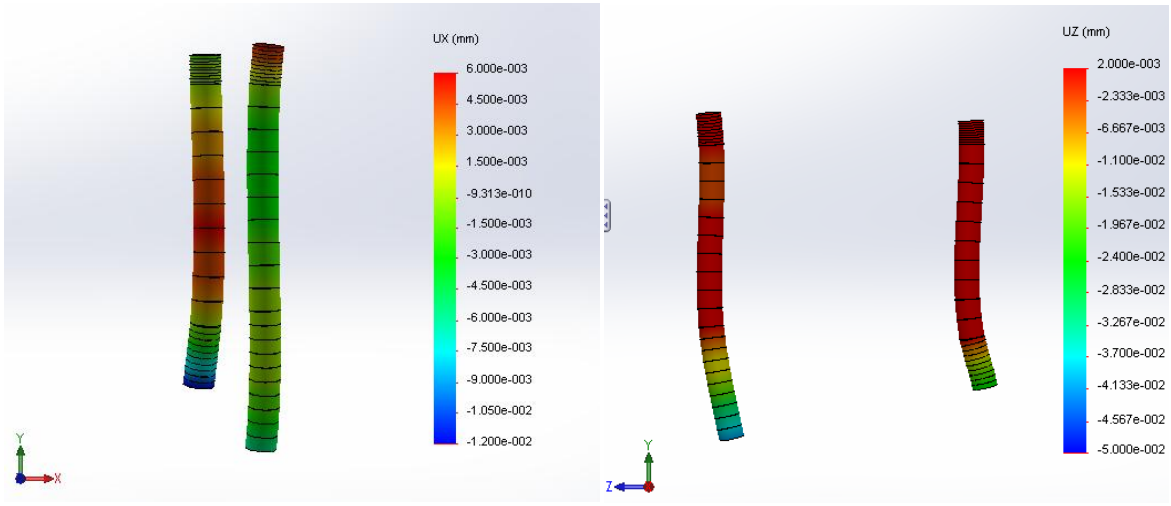

Fig. 10.13 Pipes deformation under suspension support. Displacement along X (sideways; on the left) and Z (fore/aft; on the right) axis.

Comparing the torsional stiffness for the cases with fully and partially mounted engine a growth of 3,3% to even 19,2% can be observed with higher values for less restrained cases. The stiffness is improved mostly in the suspension bay (Fig. 10.12) and to some extent in the following compartment, where the slope drops from 8,36 x 10^5 to 6,14 x 10^5 for the bottom surface of frame. The less significant influence on torsional stiffness in that compartment is caused by the fact, that it already has better triangulation than the suspension bay and did not cause so much deflection even without the engine. Engine mounts in this compartment however are not located in frame nodes and pipes there bend easily. Better use of engine for chassis' stiffness could be expected if the mounts of engine were properly triangulated.

The points of maximum stress (axial and bending) in the structure were indicated at connections of beams of the floor in the front of the vehicle and reached the maximum of almost 33 MPa. Due to the fact that the metal sheet already welded to the floor of the frame tested in the laboratory could to some extent change the stress values other points of high stress were chosen to compare results of virtual and laboratory test. These points, at the hoop in front of the driver, are presented in Fig. 10.14 and they reach values of 22,57 MPa and 18,66 MPa.

It is necessary to explain, that in the figure the values indicated refer to the maximum stress in the beam elements pointed. The exact location of the maximum stress within them can be found with the help of the legend for colors.

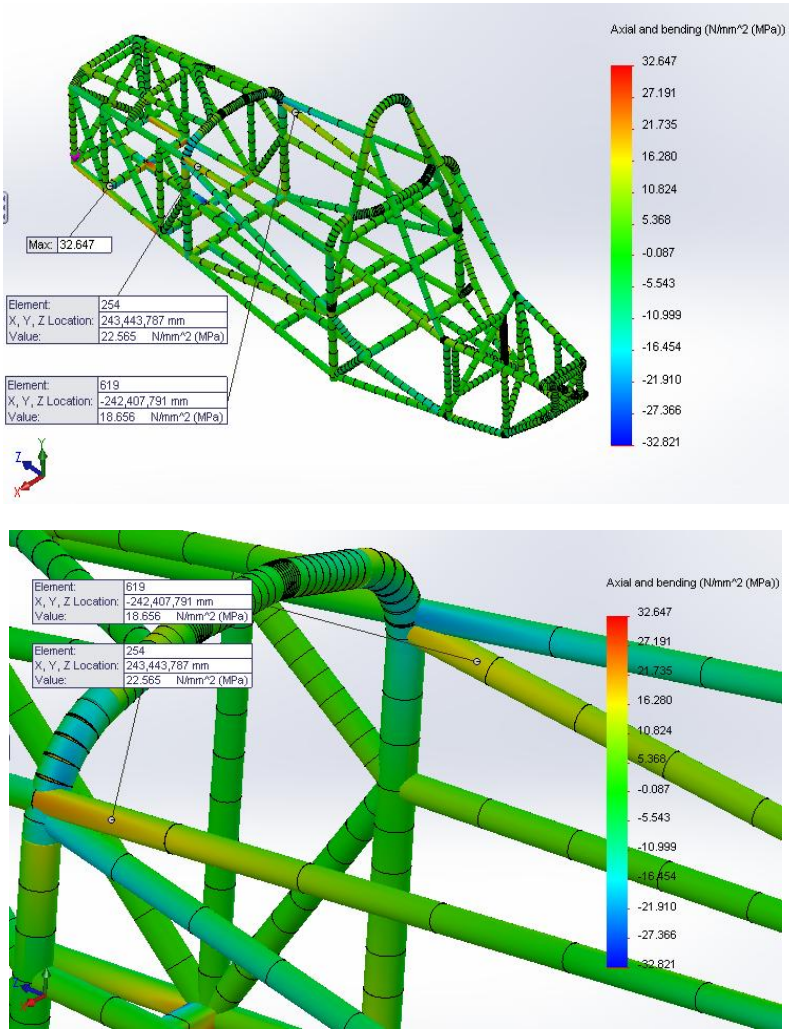

Fig. 10.14 Points, where stress values were measured

These information were used to choose locations of strain gauges in laboratory test. They had to be placed in some distance from the weld beads though and for that reason finer mesh was used to find stress values in these places (Fig. 10.15). The new values were 19,7 MPa and 17,0 MPa.

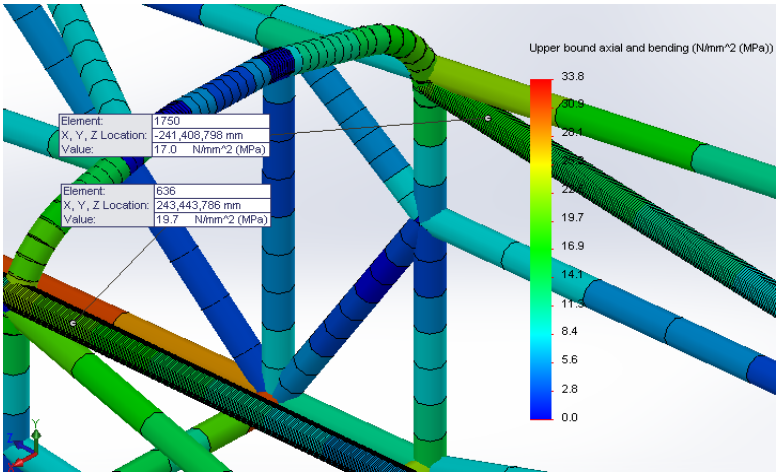

Fig. 10.15 Points for measuring stress value after placing strain gauges

10.4 VIRTUAL CHASSIS TEST

The results for full chassis assembly, presented in Table 10.4 are 1960,3 Nm/° for engine fully mounted and 1850,1 Nm/° for engine partially mounted. That is a decrease comparing to most results of frame test, caused by additional deflection in suspension elements. For a single line fixed in the rear bay however the frame test results were even lower and for that reason should be assessed as irrelevant to describe frame behavior in real working conditions. Omitting them, the case with fixtures in frame nodes, which was purely theoretical and the virtual simulation of laboratory test, which excluded the rear bay completely, the frame torsional stiffness lays between 2265,37 Nm/° and 3352,78Nm/° in virtual tests.

The screens from SolidWorks presenting vertical translations in the chassis are presented in Fig. 10.16 and Fig. 10.17

Table.10.4 Virtual chassis test results

			Engine fully mounted			engine NOT fully mounted		
force [N]	L [mm]	torque [Nm]	d [mm]	angle [°]	K [Nm/°]	d [mm]	angle [°]	K [Nm/°]
1000	1266	1266	14,27	0,646	1960,29	15,12	0,684	1850,09

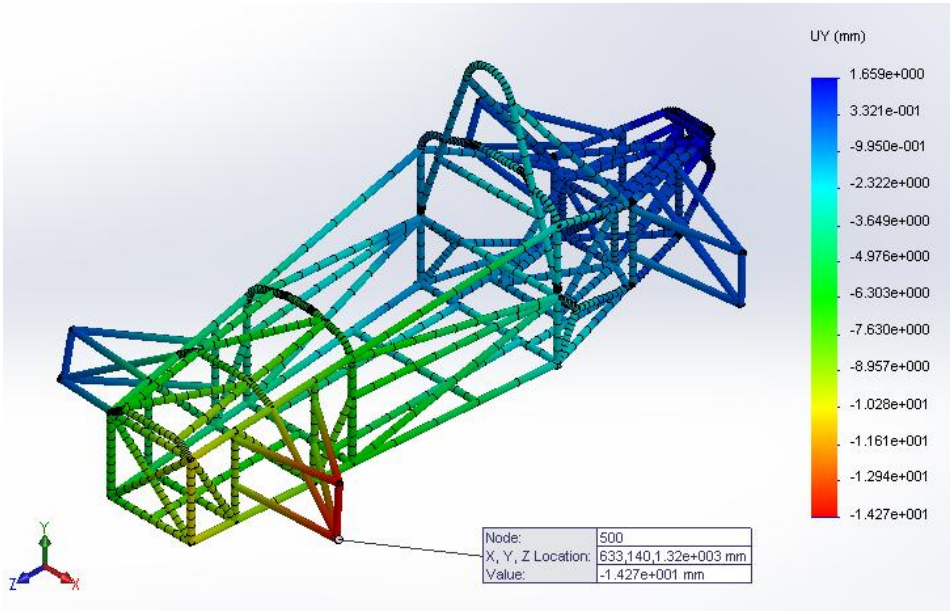

Fig. 10.16 Vertical translation diagram for fully mounted engine case

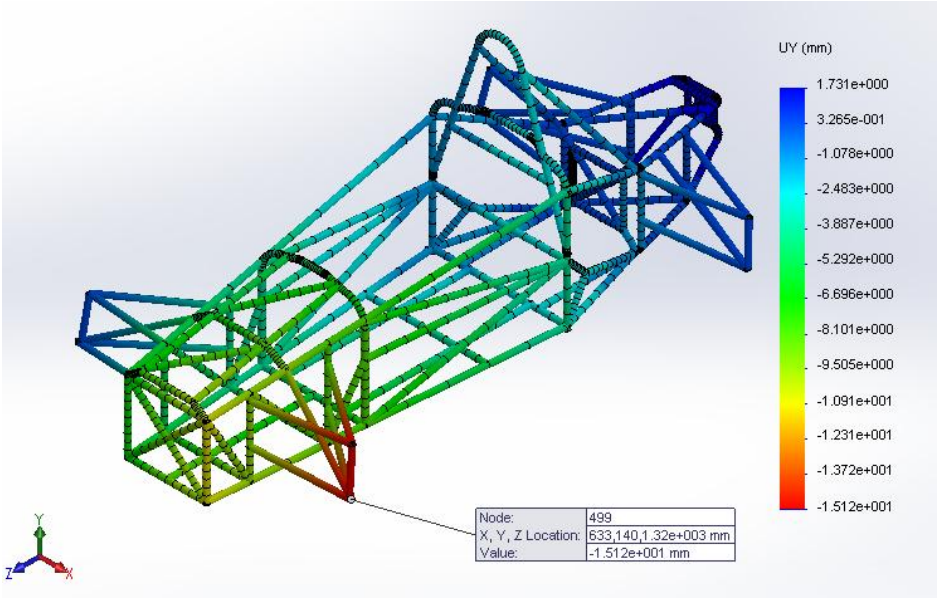

Fig. 10.17 Vertical translation diagram for partially mounted engine case

These results used in Eq. 6.11 show that the goal of 90% of torsional stiffness of theoretical rigid case is not met and the chassis stiffness is barely 79,62% of it. Remembering the relation between chassis stiffness and overall stiffness of the car from Eq. 8.13 and Fig. 8.6 and value of 4524,75Nm/° that is needed to meet the goal, the chassis stiffness would have to grow 2,3 times. That result is unsatisfying and means that whenever the vehicle is subjected to torsion the suspension's work will be substantially affected.

On the other hand if the result is compared to stiffness of other example Formula Student designs (Table 10.5) it is not much worse than them, being 94% of the average value. The source of the problem therefore should be found in very stiff springs used in vehicle being analyzed.

Table 10.5 Chassis torsional stiffness of Cornell University designs for Formula SAE [7]

Year	Stiffness [Nm/°]	Mass [kg]	Stiffness per kg [Nm/°/kg]
1999	2169,31	26	83,90
1998	2169,31	26	83,90
1997	2169,31	26	82,46
1996	1898,15	27	69,74
1995	1355,82	27	49,82
1993	2711,64	23	119,56

Table 10.5 presents also the mass of particular designs of frames and relates torsional stiffness to it. As frame has to be not only stiff, but lightweight too, this method represents how efficiently the beams were used in a structure.

The mass of the analyzed frame was read from model's mass properties in the software. Before that the structures simulating engine and front plate were removed and all the beams were trimmed, to make sure extra length of pipes was not influencing the results. The mass however does not include weld beads or any kind of mounts.

The analyzed frame has mass of 49,5 kg, what results in 39,6 Nm/°/kg. In comparison to frames from Table. 10.5 it is the heaviest and with the lowest stiffness per kg of mass.

First conclusion that comes from the analysis of diagram of twist angle along the chassis (Fig. 10.18) is that the rear bay compartment turns out not to be critical. Forces acting on the frame along control arms are directed accordingly, inboard or outboard, depending on the side of the car, and do not let the frame get into significant torsion in this area. For this reason the frame test with one plane of rear bay fixed does not present the frame behavior correctly either, despite providing the overall result close to torsional stiffness measured in chassis test for twist angle between the front of front bay and rear plane of the rear one. This section twisted 0,46° in chassis test under 1266Nm, giving 2728Nm/° of torsional stiffness, while the result of frame test was 2439Nm/°.

The other conclusion is that the top and bottom line deflect differently in that compartment, which confirms that suspension behavior will be disturbed by compliance effects.

Table 10.6 Twist angle analysis for virtual chassis test

		z [mm]	upright	-732	-473	0	862	1016	1349	upright
		x [mm]	1240	260	354	620	476	448	392	1266
upper line	engine fully mounted	dy1 [mm]	0,131	0,708	-0,384	-2,970	-6,963	-7,645	-9,015	-13,750
		dy2 [mm]	0,119	0,964	0,056	-1,022	-3,716	-4,248	-5,457	-0,221
		fi [°]	-0,001	0,056	0,071	0,180	0,391	0,434	0,520	0,612
bottom line		dy1 [mm]	0,000	0,000	-0,399	-2,966	-6,961	-7,666	-9,020	-14,270
		dy2 [mm]	0,000	0,966	0,070	-1,025	-3,713	-4,253	-5,461	0,000
		fi [°]	0,000	0,213	0,076	0,179	0,391	0,436	0,520	0,646
upper line	engine NOT fully mounted	dy1 [mm]	0,141	0,764	-0,395	-3,244	-7,424	-8,141	-9,581	-14,580
		dy2 [mm]	0,123	0,998	0,066	-0,970	-3,895	-4,466	-5,763	-0,231
		fi [°]	-0,001	0,051	0,075	0,210	0,425	0,470	0,558	0,649
bottom line		dy1 [mm]	0,000	0,000	-0,411	-3,242	-7,422	-8,163	-9,586	-15,120
		dy2 [mm]	0,000	1,000	0,082	-0,980	-3,891	-4,471	-5,767	0,000
		fi [°]	0,000	0,220	0,080	0,209	0,425	0,472	0,558	0,684

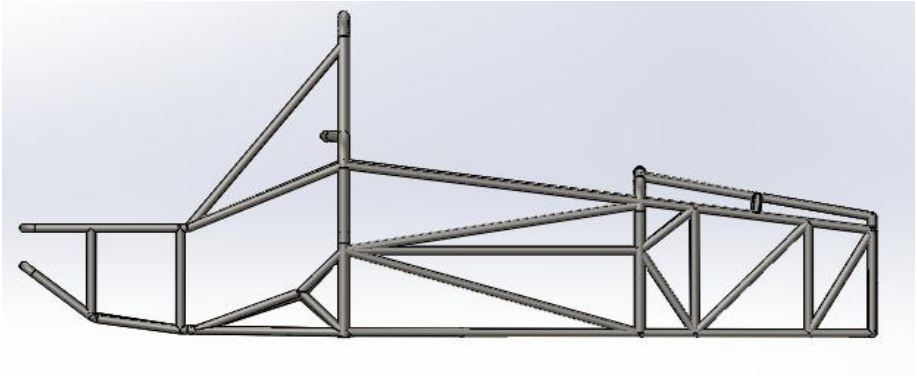

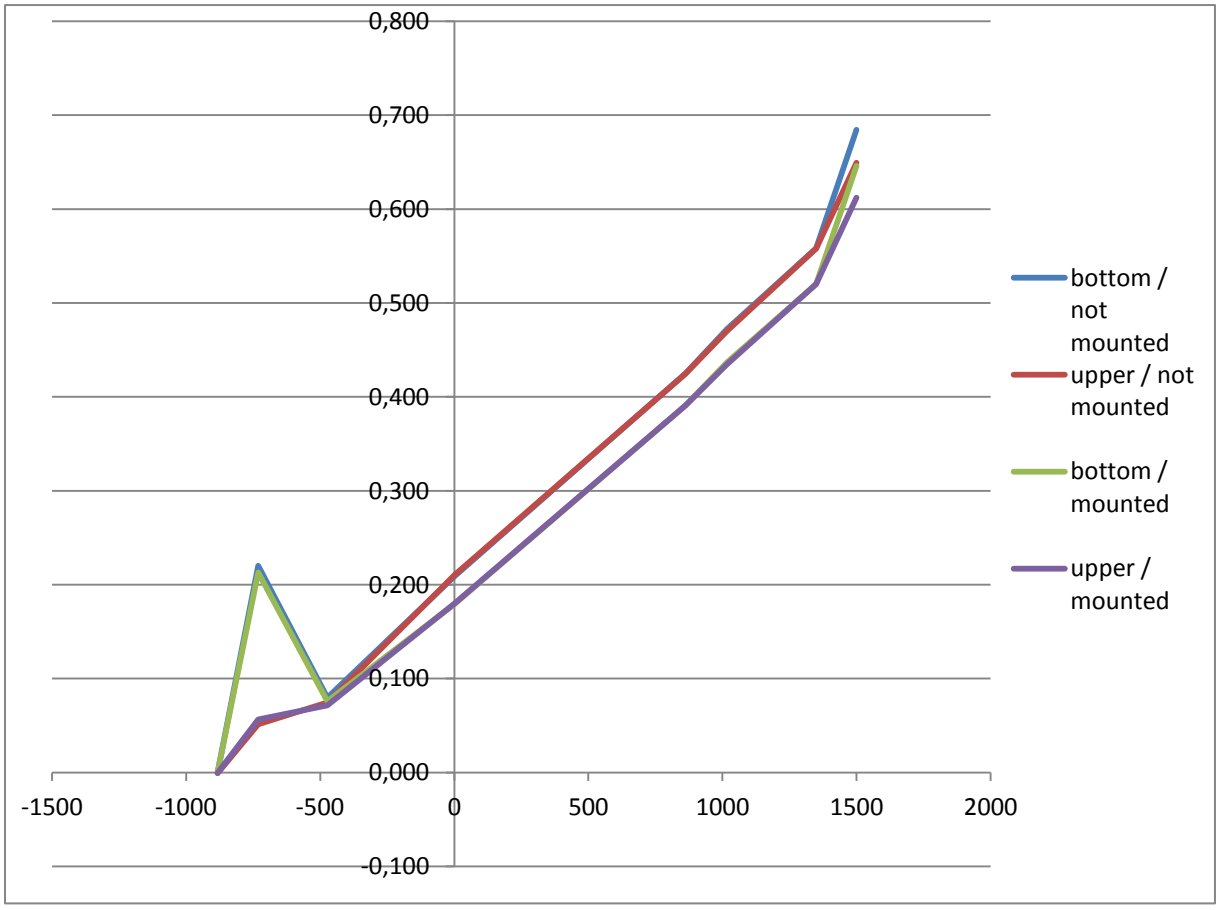

Fig. 10.18 Twist angle value along longitudinal axis of the vehicle

As the rear suspension bay turns out not to be a critical part, and moreover is characterized by low torsion angle, the full mounting of engine influences rather the next compartment and is not as important in overall torsion as it was for some of the frame tests.

The maximum stress appeared in the place where rear left push rod is attached to a frame and had the value of over 103 MPa (Fig. 10.19). Note that for simplification the rocker that is normally placed there was not modeled, what probably influences the result. Stress in the places previously chosen for comparison with experimental tests for frame also in this case are characterized by fairly high values of 73,6 MPa and 63,6 MPa as in Fig. 10.20.

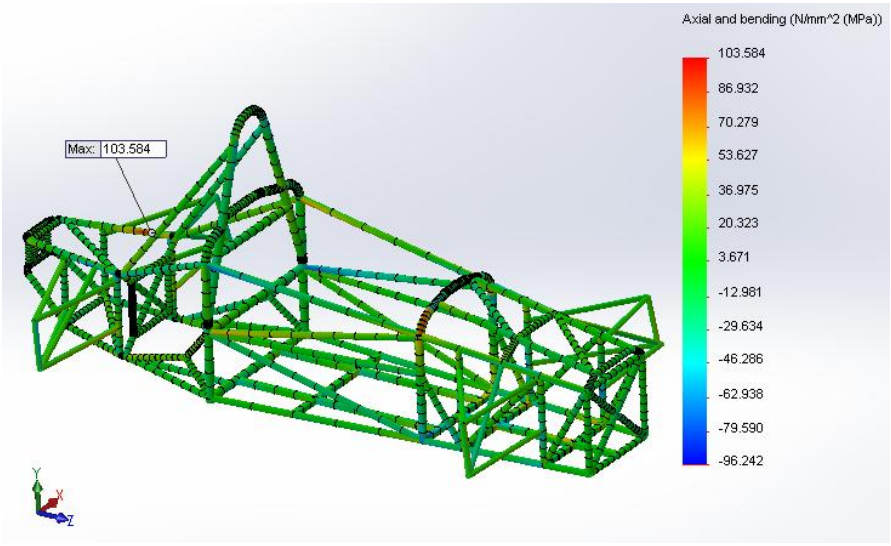

Fig. 10.19 Maximum stress in chassis longitudinal torsion test

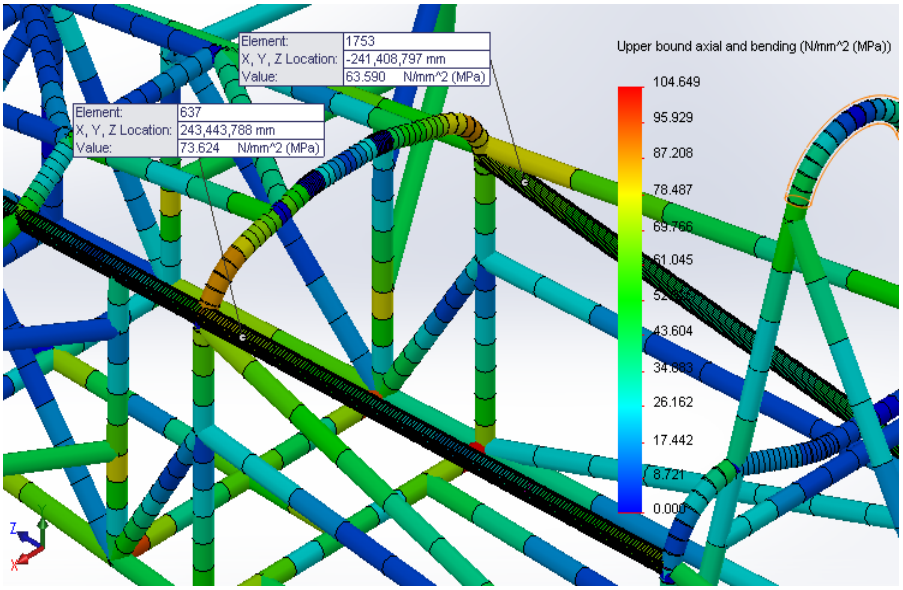

Fig. 10.20 Points for measuring stress value after placing strain gauges – chassis test

10.5 CHASSIS IMPROVEMENTS

After the tests were run for the model and structure in the laboratory some changes were proposed to increase its torsional stiffness. According to many literature sources structures supported with diagonal beams guarantee better torsional stiffness than the ladder type – with beams either parallel or perpendicular to central plane of the car. This type of structure joins ends of a single compartment (compartments as in twist angle analysis) at a certain angle and makes the beams in this area more likely to act for tension and compression than for bending (Fig. 10.21). In other words the improvements proposed guarantee proper triangulation in areas that lacked it before.

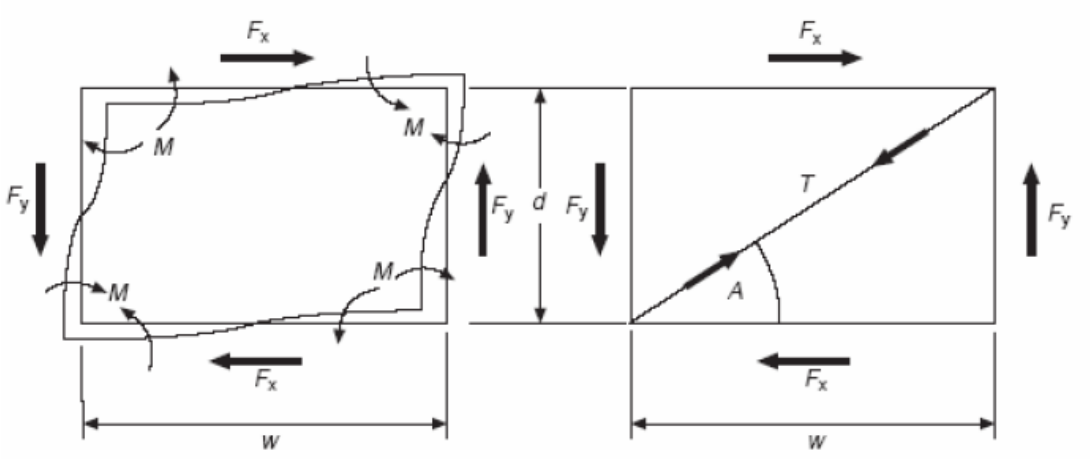

Fig. 10.21 Forces and/or moments in triangulated and non-triangulated structure.

Areas were chosen, where the changed or added beams do not collide with other elements and where they could cover possibly long part of vehicle's length. First of them was the floor under the seat, where longitudinal and transversal beams were exchanged for two diagonal ones (Fig. 10.22). The other was over the engine, where diagonal beams were added, joining the hoop behind the driver and upper engine mounts.

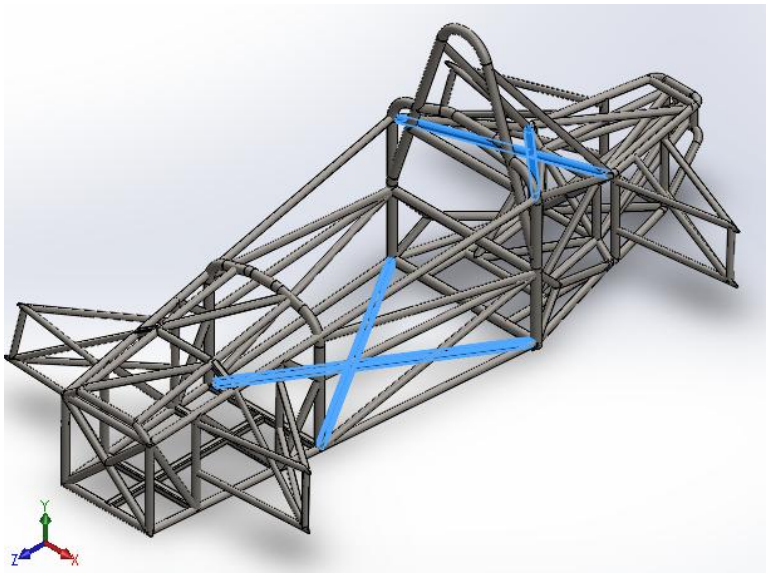

Fig. 10.22 Improvements for torsional stiffness of chassis

The vertical displacement for longitudinal torsion test of that improved chassis are depicted in Fig. 10.23. The end of control arm which the force is applied to dropped by 13mm.

In Table. xx results for changed chassis – with changed floor and with both improvements – can be compared to the original one. The first changed saved 0,4 kg, bringing 5,31% growth in stiffness. Introducing the other one made the new frame 1,1 kg heavier, but resulted in 9,60% growth in stiffness, comparing to original design.

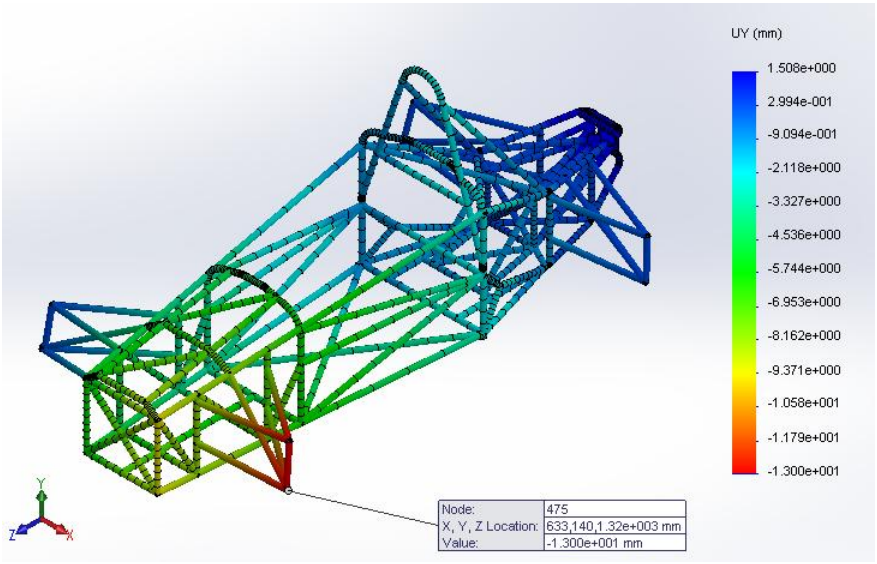

Fig. 10.23 Vertical displacements for chassis with improvements

Table. 10.7

force [N]	L [mm]	moment [Nm]	dy [mm]	angle [°]	K [Nm/°]	stiffness growth	Mass change [kg]	Mass [kg]	Stiffness per kg [Nm/°/kg]
1000	1266	1266	14,27	0,646	1960,29	-	-	49,5	39,60
			13,55	0,613	2064,46	5,31%	-0,4	49,1	42,05
			13,00	0,589	2148,49	9,60%	1,1	50,6	42,46

11. EXPERIMENTAL TESTS

11.1 TORSIONAL STIFFNESS TEST

The practical test run in laboratory was based on fixing three points in the corners of the vehicle and applying load to the fourth one in order to cause torsion of the chassis. Knowing the load and location of fixtures and measuring deflection in four corners of the chassis it was possible to calculate the torsional stiffness.

The test was run for frame and for full chassis assembly.

Note that during the tests the vehicle was undergoing adjustments. Engine was not fully mounted (Fig. 11.1) what has to be taken into consideration when the results are assessed and when laboratory and virtual tests are compared. For that reason extra virtual tests, that present better the influence of not fully mounted engine were performed too. This way it will be possible to compare virtual and laboratory tests and predict to some extent what would be the results of laboratory test with the engine fully mounted. The changes made to the model in order to run these extra tests can be seen in Fig. 11.2.

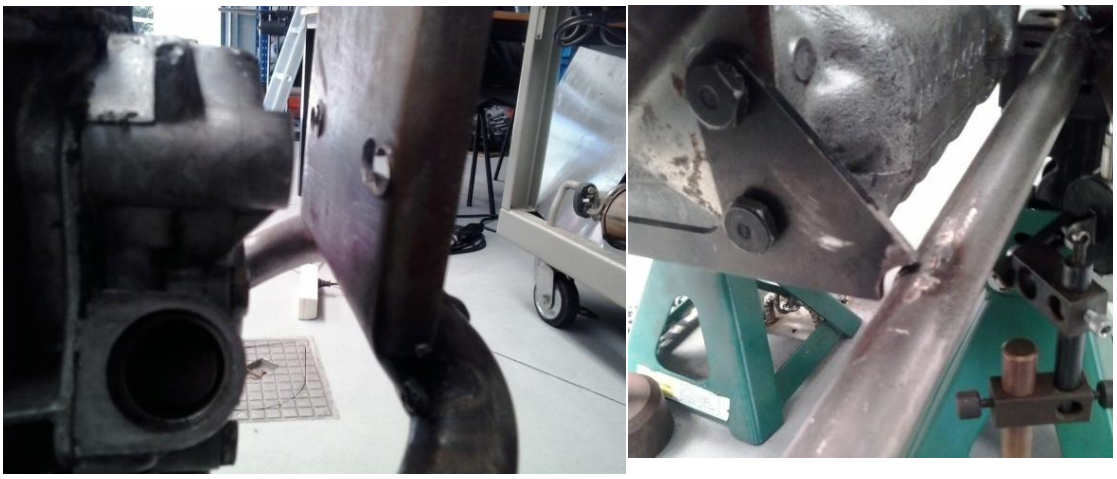

Fig. 11.1 Engine mounts that were either not welded or not bolted

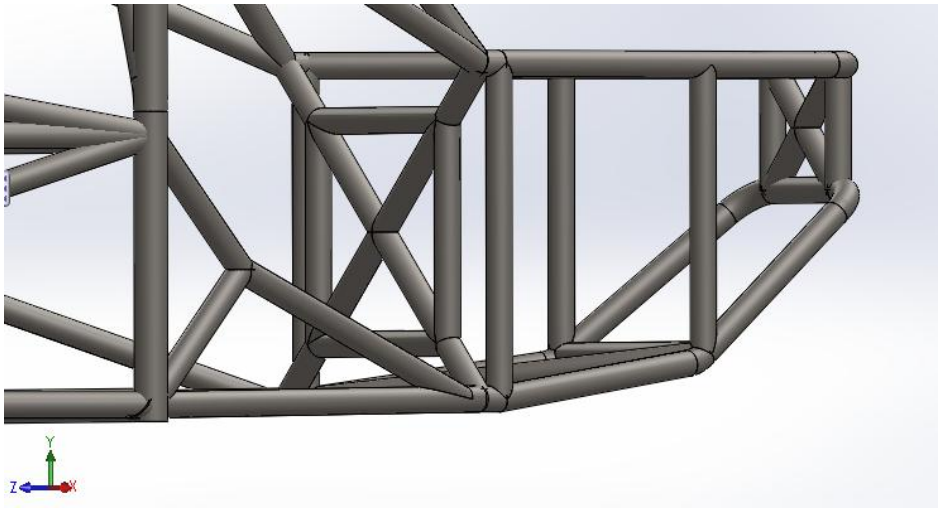

Fig. 11.2 Rear part of the model representing engine not fully mounted

The supports were realized with three jacks. The corner located opposite to the one where loads were applied, was additionally fixed with a chain preventing it from being lifted (Fig. 11.3). Because the jacks were equipped with rubber pads, located directly where the vehicle was supported, deflections in all these points were expected. For that reason dial gauges measuring dislocations in vertical direction were placed in all four corner of the vehicle.

Because of the possibility of engine not being properly fixed even on its middle mounts due to deformations after welding required by recent adjustments, the supports were placed in front of it. In case of full chassis assembly the jacks were placed under the uprights. In order to load the structure plates of around 10kg each were gradually hung in the free corner. The exact mass of the plates was taken into consideration when calculating torque acting on the structure.

Fig. 11.3 Rear and front of the car prepared for frame laboratory tests

After collecting all the data, the calculations were conducted according to following equations.

$$K = \frac{T}{\varphi} \quad \text{Eq. 11.1}$$

$$T = m * g * L_F \quad \text{Eq. 11.2}$$

$$\varphi = \varphi_F - \varphi_R \quad \text{Eq. 11.3}$$

$$\varphi_F = \arctan\left(\frac{dy_{FL} - dy_{FR}}{L_F}\right) \quad \text{Eq. 11.4}$$

$$\varphi_R = \arctan\left(\frac{dy_{RL} + dy_{RR}}{L_R}\right) \quad \text{Eq. 11.5}$$

where: K – frame/chassis torsional stiffness
ϕ – frame/chassis twist angle
T – torque acting on the frame
m – mass of the weight plates
g – gravitational acceleration
L_F – distance between support (jack) in the front and point of load application
L_R – distance between supports (jacks) in the rear
ϕ_F, ϕ_R – front and rear axis inclination
dy – vertical translation in front/rear left/right corner

The symbols can be compared with schemes from Fig. 11.4 (frame) and Fig. 11.5 (chassis). Each of them depicts front (on the left side of figure) and rear part of the car supported on rubber pads of jacks (checked rectangles) with weights placed in the front left corner. Attention should be paid to directions of displacements dy, which explain plus and minus signs in Eq. 11.4 and Eq. 11.5.

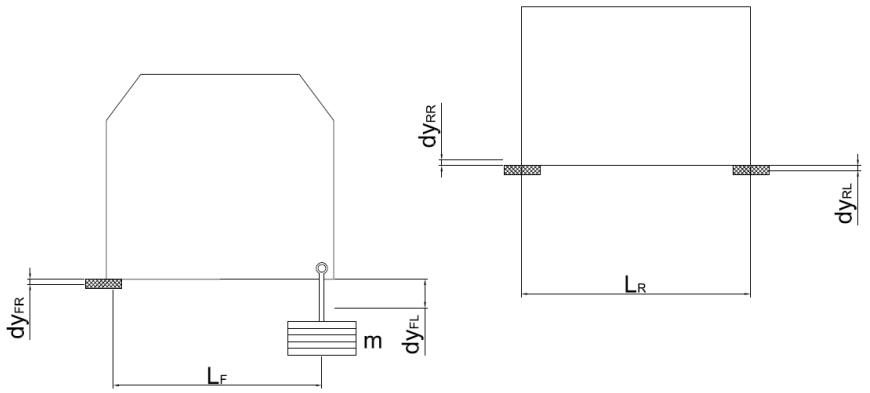

Fig. 11.4 Scheme of supports loads and displacements in laboratory frame test

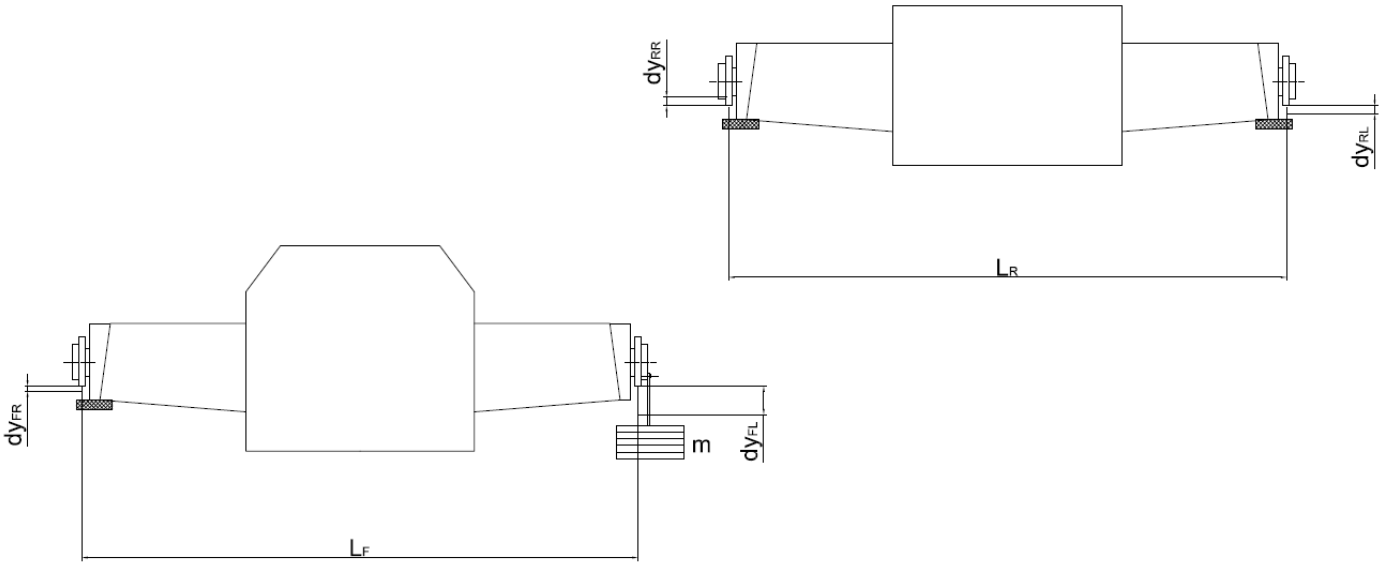

Fig. 11.5 Scheme of supports loads and displacements in laboratory chassis test

11.2 STRESS TEST

Simultaneously with the torsion test stress values in the structure were supposed to be checked to be later compared with the virtual tests' results. For that purpose strain gauges were placed in two points previously chosen on the basis of SolidWorks simulations (Fig. 11.6).

Fig. 11.6 Strain gauge and digital indicator used in the tests

The stresses were indicated by the software in the mode of Axial plus Bending. That means the values stood for sum of tension along beams' axis caused by axial forces and tension in the walls of pipes related to bending. In order to measure the same kind of stress in the laboratory experiment, only one strain gauge was installed on each of the pipes chosen for test, along their axis and connected into a circuit of a quarter bridge.

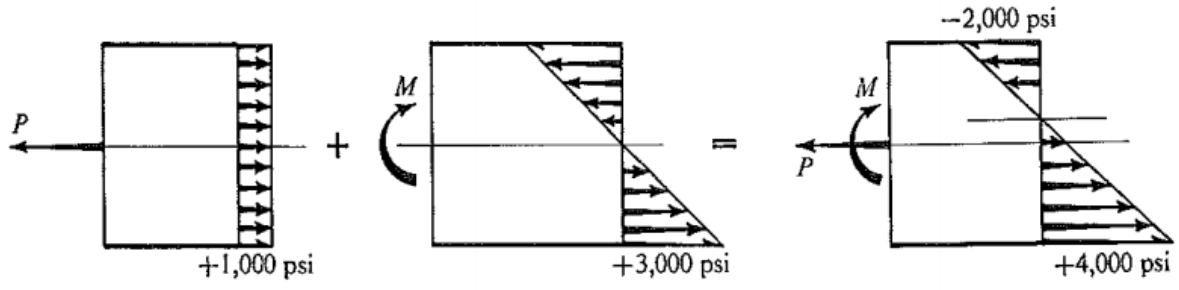

Fig. 11.7 Combined tension of axial forces and bending in a beam [12]

The strain gauges had resistance of 350 Ω ± 0,30% and gauge factor of 2,04 ± 1%. The correct connection with quarter bridge connection scheme from the indicator is presented in Fig. 11.8.

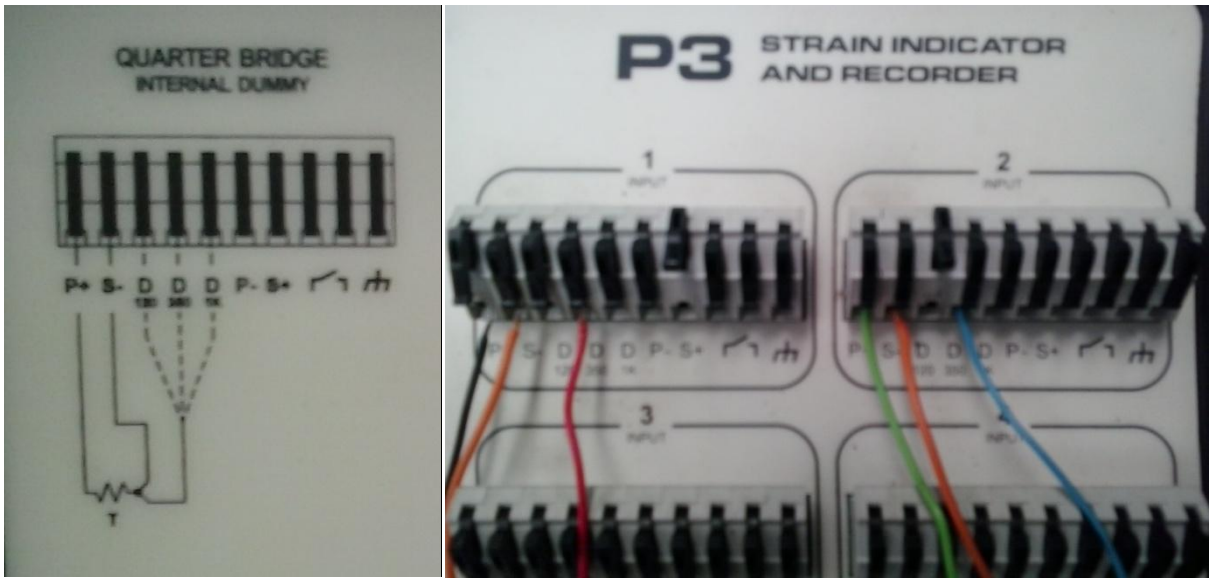

Fig. 11.8 Quarter bridge scheme from digital indicator and strain gauges connection

The stress values could be calculated later as follows.

$$\sigma = E * \varepsilon \qquad \text{Eq. 11.6}$$

where: σ – stress
E=210 GPa – elasticity modulus for steel
ε – strain indicated

As the indicator was displaying microstrain, με, the readings had to be multiplied by 10^{-6} in order to obtain strain, ε. Stress, σ in MPa is therefore:

$$\sigma = E * \mu\varepsilon * 10^{-6} = 2{,}1 * 10^{5} MPa * \mu\varepsilon * 10^{-6} = 0{,}21 * \mu\varepsilon \; MPa \qquad \text{Eq. 11.7}$$

11.3 EXPERIMENTAL FRAME TESTS RESULTS

Table 11.1 gathers average results of frame laboratory test for both torsion angle and stress values in two points. They are represented in graphic form in Fig. 11.9 to Fig. 11.10. As the relations they represent are linear, the trend lines intersecting the origin of coordinate system were plotted for every graph.

Table 11.1 Results of frame laboratory test

No. of plates	mass [kg]	torque [Nm]	Displacement [mm]				Angle [°]			Microstrain		Stress [MPa]	
			Rear		Front								
			Left	Right	Left	Right	Rear	Front	Total	Ch 1	Ch 2	Ch 1	Ch 2
0	0,00	0,00	0,000	0,000	0,000	0,000	0,000	0,000	0,000	0,0	0,0	0,00	0,00
1	9,90	35,06	0,058	0,013	0,340	0,180	0,009	0,025	0,016	7,6	7,8	1,60	1,64
2	19,74	69,91	0,144	0,028	0,783	0,452	0,023	0,052	0,029	15,4	15,2	3,23	3,19
3	29,44	104,26	0,238	0,038	1,290	0,778	0,037	0,081	0,044	22,8	23,0	4,79	4,83
4	39,16	138,68	0,348	0,048	1,811	1,112	0,053	0,110	0,057	30,2	30,4	6,34	6,38
5	48,92	173,25	0,448	0,064	2,287	1,392	0,068	0,141	0,073	38,4	37,6	8,06	7,90
6	58,74	208,02	0,558	0,081	2,765	1,670	0,085	0,172	0,087	45,6	45,2	9,58	9,49
7	68,84	243,79	0,680	0,101	3,290	1,980	0,104	0,206	0,102	53,6	53,0	11,26	11,13
8	78,60	278,35	0,808	0,122	3,738	2,232	0,124	0,237	0,113	61,0	60,4	12,81	12,68
7	68,84	243,79	0,790	0,105	3,529	2,174	0,119	0,213	0,094	53,6	53,2	11,26	11,17
6	58,74	208,02	0,740	0,086	3,249	2,048	0,110	0,189	0,079	45,4	45,2	9,53	9,49
5	48,92	173,25	0,694	0,067	2,914	1,876	0,101	0,163	0,062	38,0	37,6	7,98	7,90
4	39,16	138,68	0,576	0,051	2,537	1,666	0,083	0,137	0,054	30,8	30,4	6,47	6,38
3	29,44	104,26	0,486	0,039	2,076	1,386	0,070	0,109	0,039	22,8	22,6	4,79	4,75
2	19,74	69,91	0,384	0,028	1,547	1,038	0,055	0,080	0,025	15,6	15,4	3,28	3,23
1	9,90	35,06	0,256	0,018	0,938	0,632	0,036	0,048	0,012	7,8	8,0	1,64	1,68
0	0,00	0,00	0,120	0,007	0,289	0,204	0,017	0,013	-0,003	0,0	0,0	0,00	0,00

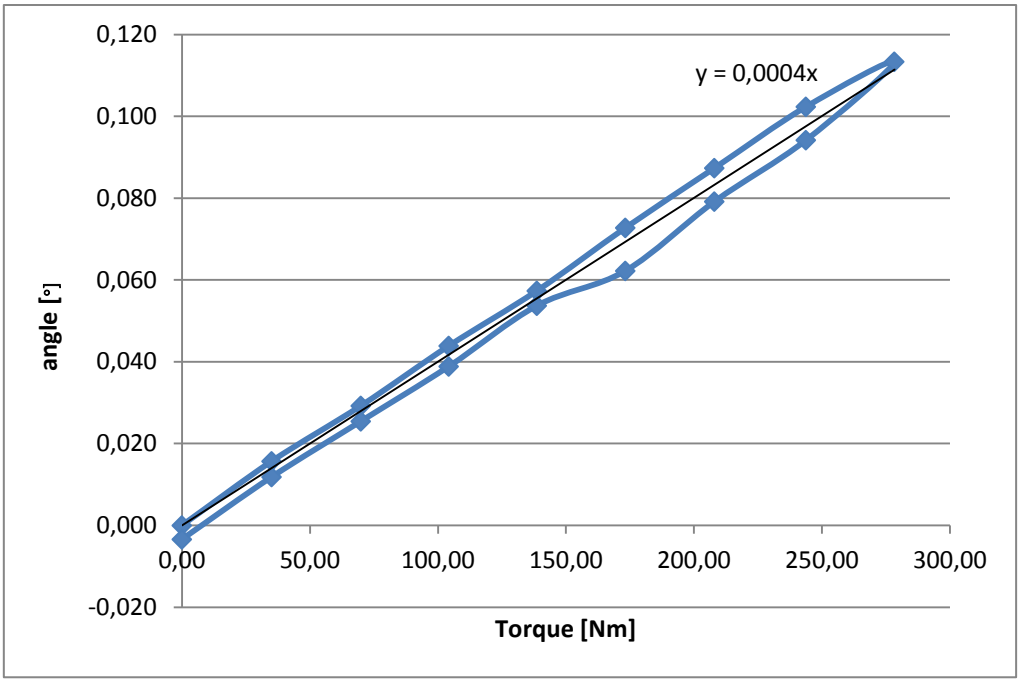

Fig. 11.9 Angle and torque relation in laboratory frame test

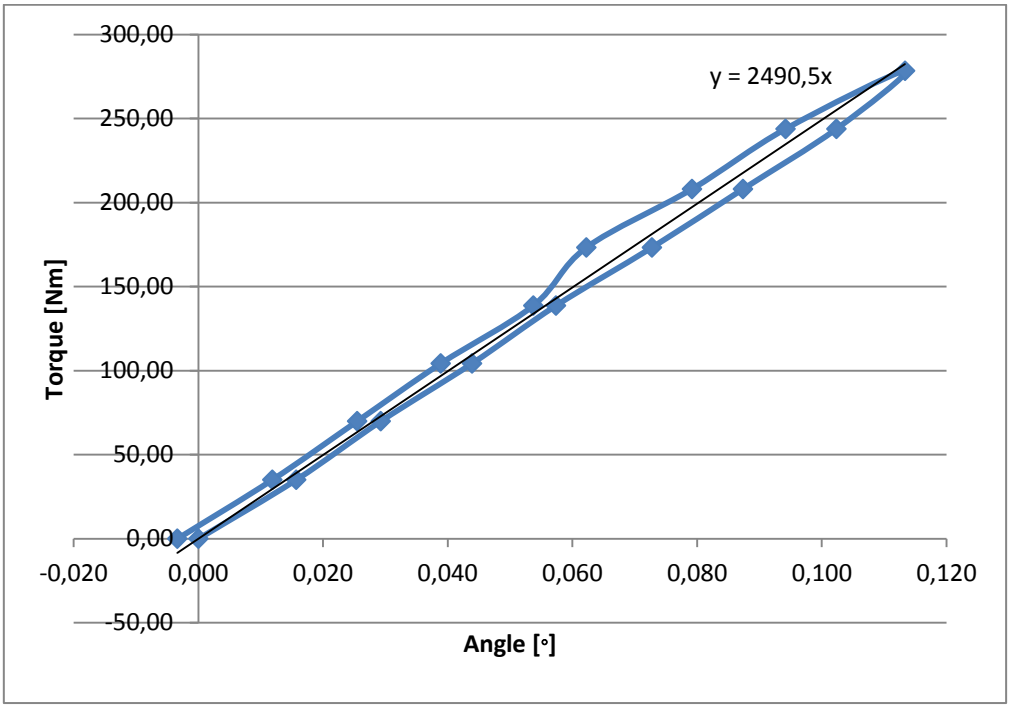

Fig. 11.10 Torsional stiffness determined from torque-angle relation

Longitudinal torsional stiffness determined this way is 2490,5 Nm/° and constitutes 113,6% of the value of 2191,9Nm/° determined in virtual test (boundary conditions as in experimental test).

At that point it is worth referring again to the considerations about boundary conditions and influence of the engine. The laboratory test was run with the engine only partially mounted and only for one certain set of fixtures and load application. The result of 2490,5Nm/° should

therefore not be treated as exact one. This value will increase when the engine is properly mounted. In virtual test the torsional stiffness grew by 3,8%.

Even bigger differences could be observed if the frame was supported on jacks behind the rear suspension bay as it is normally done in such tests, as in virtual tests it caused drop by 24,3%.

Nevertheless the laboratory test shows that the real values of torsional stiffness should be expected to be higher than the ones determined in virtual tests.

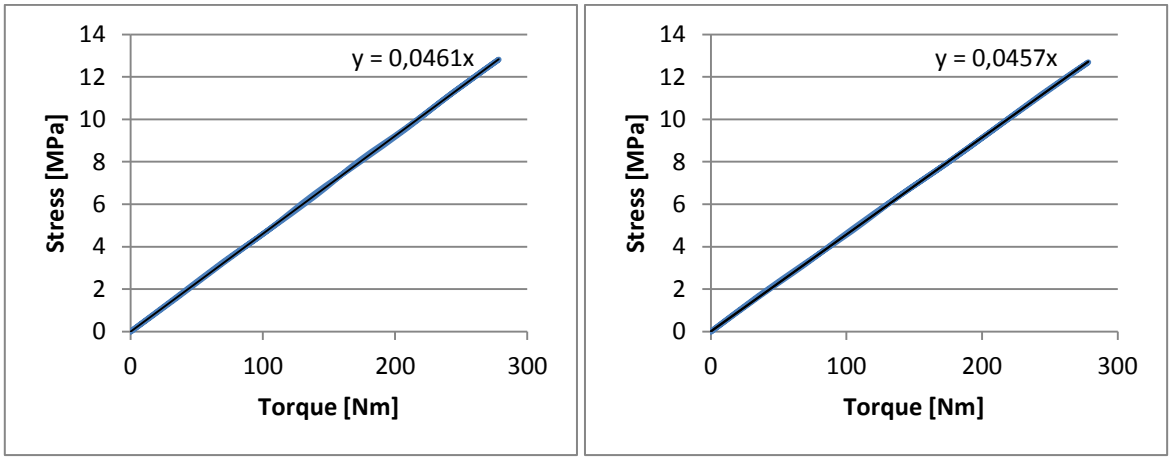

Fig. 11.11 Stress-torque relations in two chosen points of frame

The relations between stress in indicated previously points and the torque from Fig. 11.11 are respectively 0,0461 MPa/Nm and 0,0457 MPa/Nm. For 364 Nm applied in virtual test it gives 16,8 MPa and 16,6 MPa. The real values are then 85,2% and 97,9% of the ones predicted with the software, which proves the tests were plausible and the maximum value of 33 MPa in the frame found with software should not be exceeded.

11.4 EXPERIMENTAL CHASSIS TESTS RESULTS

The results of laboratory torsional stiffness test, presented in Table 10.7 and Fig. 11.12 and Fig. 11.13 gave the result of 1437,3 Nm/°, which is 22% less than in virtual tests (partially mounted engine). Taking into consideration that the test for frame gave opposite results – the result gained with the experimental approach was higher - and that the discrepancy is so high, the source of that result may be the engine mounted badly after the chassis went through adjustments. Four bolt connections were deformed after welding and the bolts could not be fastened properly. It might have not ensured rigid connection between two parts of frame. In frame test this connection was already behind the supports and did not influence the results.

If that value is used in Eq. 8.13 it results with just 74,12% of the rigid case's stiffness. A bit higher value can be expected when the engine is mounted.

Table 11.2 Results of frame laboratory test

No. of plates	mass [kg]	torque [Nm]	Displacement [mm]				Angle [°]			Microstrain		Stress	
			Rear		Front								
			Left	Right	Left	Right	Rear	Front	Total	Ch 1	Ch 2	Ch 1	Ch 2
0	0,00	0,00	0,000	0,000	0,000	0,000	0,000	0,000	0,000	0,0	0,0	0,00	0,00
1	9,90	133,05	0,106	0,036	2,251	0,034	0,006	0,093	0,087	33,4	31,6	7,01	6,64
2	19,74	265,30	0,205	0,100	4,754	0,108	0,013	0,194	0,181	67,4	63,2	14,15	13,27
3	29,44	395,66	0,315	0,164	7,180	0,198	0,021	0,292	0,271	98,6	93,8	20,71	19,70
4	39,16	526,30	0,425	0,246	9,628	0,280	0,029	0,391	0,362	132,2	125,0	27,76	26,25
3	29,44	395,66	0,367	0,210	7,576	0,286	0,025	0,305	0,280	99,2	93,8	20,83	19,70
2	19,74	265,30	0,277	0,162	5,349	0,242	0,019	0,214	0,195	66,6	63,0	13,99	13,23
1	9,90	133,05	0,160	0,102	2,716	0,166	0,011	0,107	0,095	33,4	31,8	7,01	6,68
0	0,00	0,00	0,036	0,012	0,127	0,048	0,002	0,003	0,001	0,6	0,2	0,13	0,04

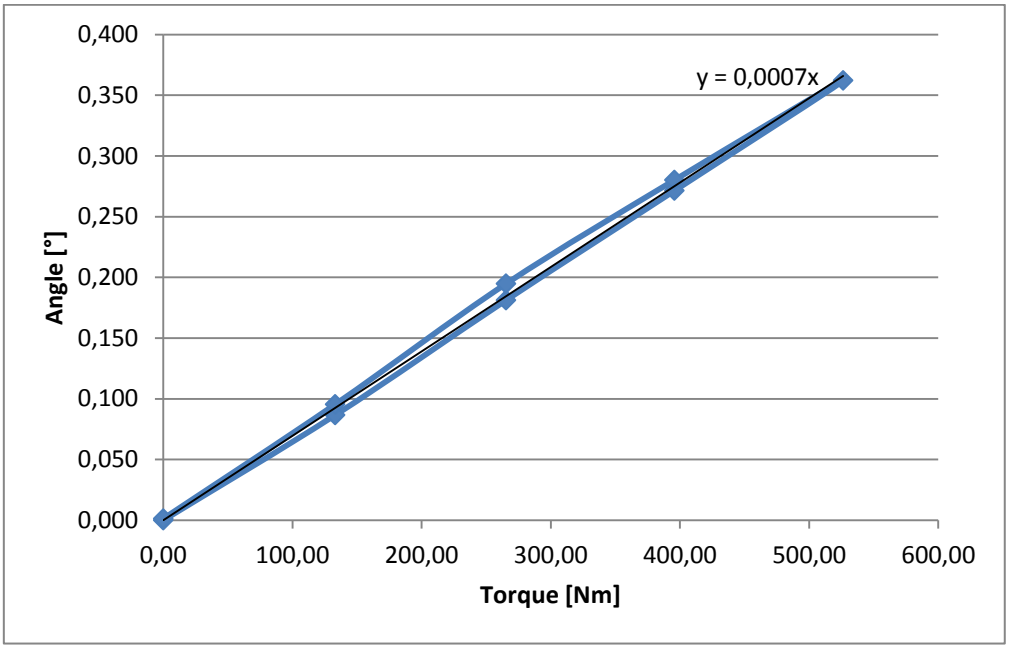

Fig. 11.12 Angle and torque relation in laboratory frame test

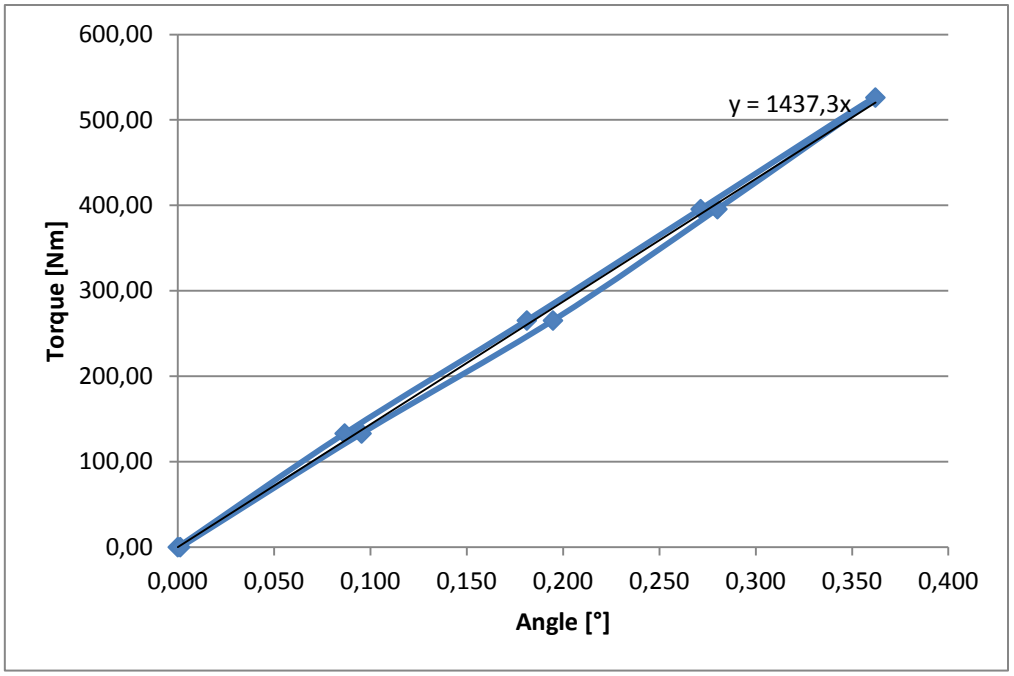

Fig. 11.13 Torsional stiffness determined from torque-angle relation

The readings from strain gauges (Fig. 11.14) gave relations of 0,0527 MPa/Nm and 0,0499 MPa/Nm, which for 1266 Nm used for virtual tests results in 66,7 MPa and 63,2 MPa and is 90,7% and 99,3% of results from virtual tests respectively. It can be assumed that this validates the virtual test and the maximum stress value of 103 MPa obtained in it.

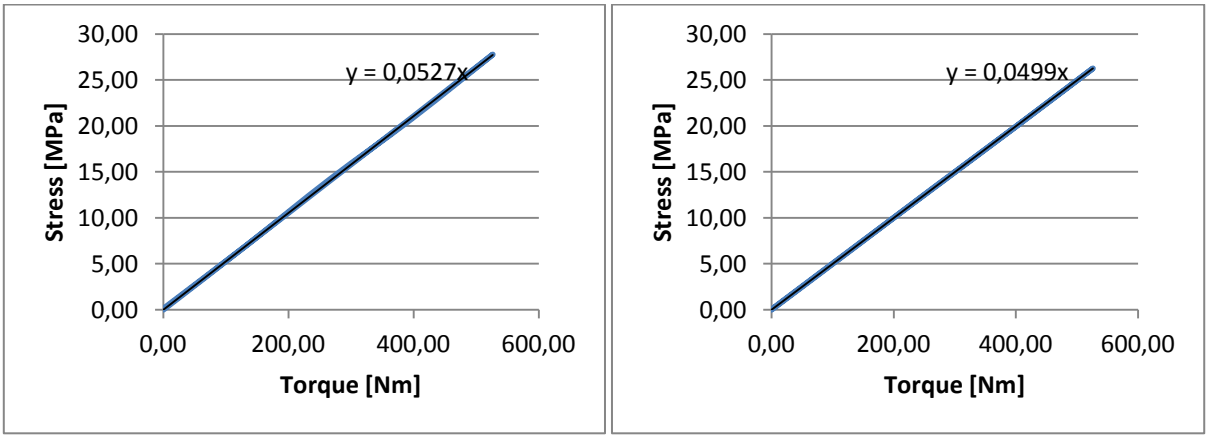

Fig. 11.14 Stress-torque relations in two chosen points of frame for chassis test

12. CONCLUSIONS

The work presented analysis of chassis of a Formula Student racing car. It included virtual analysis of suspension geometry and longitudinal torsion tests run with the finite elements method for frame and full chassis assembly. The results of longitudinal torsion test were verified with experimental test too. The results gathered were compared with goals set on the basis of literature research and changes, that can be taken into consideration when a new car is designed were suggested.

The suspension geometry test revealed that several modifications should be introduced to the design. First of all front view control arms configuration should be modified the way, that roll centers are lowered and stay within values suggested. Changes proposed to front view geometry will also increase camber gain beneficially and help obtain desired camber curve in body roll.

Attention should be paid also to wheel packaging. Incompatible hub and rim mounting holes resulted in longer scrub radius than primarily desired. Another selection of these parts can help keep the scrub radius and kingpin inclination within values suggested.

The structural analysis showed that the suspension supports on frame do not provide enough rigidity. They are not located in frame's nodes, what causes bending under forces transferred through control arms, and can disturb suspension's work. The design process of a frame should start only when the suspension geometry is already designed. The designer can then focus on providing enough rigidity to suspension bays.

The torsional stiffness determined in virtual tests proved that the chassis is not stiff enough and with 1960,29 Nm/° reaches barely 79,62% of the theoretical case of perfectly rigid chassis (while the goal was 90%, reached with 4524,75 Nm/°). It was however noticed that the value determined is only a bit lower than average value of other frames, whose data was collected for benchmarking. The reason of the low percentage is the fact that springs installed in the vehicle are very stiff. It is recommended to revise selection of them. Structural improvements, that increased stiffness by 9,60% to 2148,49 Nm/°.

The frame, with 49,5 kg is very heavy too. Benchmarking showed that the same or even higher stiffness can be reached with steel frames of less than 30 kg.

The result of chassis torsional stiffness determined in experimental test turned out to be lower than the one obtained with software. Even though in frame test the result was opposite and real frame was more rigid than virtual. The results of chassis test might have been disturbed by engine mounted badly after the chassis went through adjustments. It is advised to run full chassis longitudinal torsion test again, when the frame is complete.

Analysis of twist angle along longitudinal axis of the car in frame test showed, that the rear suspension bay is the least rigid compartment of the frame. Despite the fact, that in full chassis test the twist angle was low there, it is important to take care of better triangulation of this area, because it directly affects control arms and work of suspension.

The tests compared also different concepts of fixing the frame for torsion tests. It turned out that none of the concepts ensured the same behavior of the frame as in full chassis test, which is considered to better represent the real conditions. It is also important to run the tests, treating engine as structural element, as it can positively influence the torsional stiffness.

Measurements of stress values in frame during laboratory tests verified the results of software tests, reaching between 85,2% and 99,3% of their values.

13. REFERENCES

[1] Trzesniowski, Michael. Rennwagentechnik: Grundlagen, Konstruktion, Komponenten, Systeme. Wiesbaden, Vieweg+Teubner Verlag, 2012. ISBN 978-3-8348-2209-3 (eBook)

[2] Heiβing, Bernd; Ersoy, Metin. Chassis Handbook: Fundamentals, Driving Dynamics, Components, Mechatronics, Perspectives. Wiesbaden, Vieweg+Teubner Verlag, 2012. ISBN 978-3-8348-0994-0

[3] Milliken, William F.; Milliken, Douglas L. Race Car Vehicle Dynamics. Warrendale, PA, Society of Automotive Engineers, Inc., 1995. ISBN 1-56091-526-9

[4] Gillespie, Thomas D. Fundamentals of Vehicle Dynamics. Warrendale, PA, Society of Automotive Engineers, Inc., 1992, ISBN 1560911999 (ISBN13 9781560911999)

[5] Gaffney III, Edmund F.; Salinas, Anthony R. Introduction to Formula SAE® Suspension and Frame Design. University of Missouri – Rolla, 1997

[6] Theander, Adam. Design of a Suspension for a Formula Student Race Car. Stockholm, Royal Institute of Technology, 2004

[7] Riley, William B., George, Albert R. Design, Analysis and Testing of a Formula SAE Car Chassis, Warrendale, PA, Society of Automotive Engineers, Inc., 2002 ISSN 0148-7191

[8] Pang Shu-yi;Guan Xin;Zhan Jun, Research of chassis torsional stiffness on vehicle handling performance, State Key Laboratory of Automobile Dynamic Simulation, Jilin University, Changchun, China, 2010

[9] Thompson, Lonny L., Raju, Srikanth, Law, E. Harry, Design of a Winston Cup Chassis for Torsional Stiffness, Warrendale, PA, Society of Automotive Engineers, Inc., 1998

[10] Abrams, Ryan, Formula SAE Race Car Analysis: Simulation and Testing of the Engine as a Structural Member, The University of Western Ontario, Canada, 2008, F2008-SC-005

[11] Dassault Systèmes SolidWorks Corporation, SolidWorks Education SAE Frame Analysis, http://www.youtube.com/user/solidworks (accessed 05.03.2014)

[12] Popov, Egor P., Introduction to Mechanics of Solids, Prentice-Hall, 1968, ISBN 0134877693